ANALYSIS AND CONTROL OF FAN NOISE WITHIN A CONVERGING DUCT SECTION OF LIMITED LENGTH

XI QIANG

Ph.D

The Hong Kong Polytechnic University

2015

THE HONG KONG POLYTECHNIC UNIVERSITY

DEPARTMENT OF MECHANICAL ENGINEERING

Analysis and Control of Fan Noise within a Converging Duct Section of Limited Length

XI Qiang

A thesis submitted in partial fulfillment of the requirements for the

Degree of Doctor of Philosophy

December 2014

CERTIFICATE OF ORIGINALITY

I hereby declare that this thesis is my own work and that, to the best of my knowledge and belief, it reproduces no material previously published or written, nor material that has been accepted for the award of any other degree or diploma, except where due acknowledgement has been made in the text.

(Signed) _____

XI Qiang

Abstract

The objective of this study is twofold. One is to identify the noise sources of hairdryer system and investigate the corresponding noise generation mechanisms, and the other one is to use the panel with low mass to strength ratio and with micro-perforation to reduce the sound radiation from the fan which is installed in the duct with low aspect ratio. The proposed device will be adopted into the hairdryer to improve the sound quality of the product.

Hairdryer is a typical example of the domestic product of simple ducted-fan system with low aspect ratio. A series of acoustical measurements and sound source identification approaches are conducted to search for the dominant sound sources and their characteristics in the spectrum of the hairdryer provided by Kenford Industrial Co., Ltd. The noise is found mainly in the low-to-medium frequency range. In addition, the aerodynamics pattern and aeroacoutics features can be found by computational fluid dynamics (CFD) study. It is found that the maximum vortex occurs at the tip clearance regime and there is unsteady inlet flow due to the irregular structure at the inlet. Different level of the roughness is introduced at the inlet surface of hairdryer and hence the broadband noise at the low frequency regime can be reduced. In order to understand the physics behind, the aerodynamic pattern is also investigated by using particle image velocimetry (PIV) tests which can show the flow field variation at the inlet of the hairdryer. It is found that the rough surface can provide a more uniform inlet flow. However, there is a trade-off enhancement of the noise at the first and second blade passage frequencies.

A passive noise control strategy is proposed with a micro-perforated panel (MPP) housing device. It shares the feature of drum-like silencer with MPP covering on the two side-branch cavities but the working principles are different and the source is placed at the centre of the device. The mechanism to control noise by MPP housing is to undergo sound cancellation supplemented with sound absorption instead of sound reflection by drum silencer or plate silencer. To realize it into the real application, the proposed device is to be designed in compact configuration compared with the traditional silencer and muffler in the market.

To investigate the performance of the proposed device, a two-dimensional theoretical model for MPP device housing a dipole source is established. The vibro-acoustic interaction is studied in detail to understand the coupling between the panel vibration induced by the dipole source and the sound fields of a duct and backed cavities. With the aid of finite element method (FEM), the analytical model is validated and the device attenuation performance is studied. To optimize the design, parameters such as structural properties of the panel, perforations property of MPP and configuration of the cavities are to be investigated. To conduct the experimental validation, a small speaker is used to simulate the axial fan with dipole nature. It is found that there is good agreement among experiment, analytical model and finite element method. For the real application in the hairdryer, the MPP housing device with a compact geometry can successfully reduce noise at the blade passage frequency. The sound quality of the product will be improved by the utilization of MPP housing device as the loudness has been reduced in the dominant noise frequency region.

To further improve the performance of the proposed MPP housing device, a non-uniform section hollow tube with a Herschel-Quincke nature (MPPHQ) is introduced to tackle the drawback of passband in low frequency to acquire a wider stopband. The optimization of the shape, configuration and location of the hollow tube is processed. The optimal performance can be achieved with a compact housing geometry. The hybrid MPPHQ housing maintains the performance of proposed MPP housing device and at the same time, the passband regime which is originally contributed by MPP housing device is released. In addition, the sound attenuation performances of MPP housing device with partitioned cavity to control different nature of sound sources have also been examined, numerically and experimentally. It is found that when the partitioned cavity is properly designed, the performance of MPP housing device can be significantly improved without any enlargement of geometry size. It can be beneficial for the design of silencer in the future.

ACKNOWLEDGEMENTS

I would like to express my deepest appreciation to my chief supervisor, Dr. Choy Yat-Sze, for her creative thoughts and professional guidance throughout my past four years' study. I am also deeply grateful to my two co-supervisors Prof. Cheng Li and Prof. Tang Shiu-Keung, for giving me the invaluable enlightenment and encouragement. Special thanks go to Kenford Industrial Co., Ltd which provides funding to the project and a number of specimens needed through the research process. I thank them for giving me the opportunity to learn so much at The Hong Kong Polytechnic University, and continuously giving encouragement and generous help. This thesis would not be successful without their guidance and support.

I would also like to thank Mr. Michael Keong, Dr. Liu Yang, Dr. Wang Chunqi, Dr. Wang Xiaonan, Ms. Chiang Yankei, Mr. Wang Zhibo and Mr. Wang Tiangang for their kind assistance and discussions during my study. I would also like to express my sincere thanks to all the staff and technicians in the laboratories and offices for their support.

Finally, I am grateful to my parents for their understanding and support. Special thanks go to my wife, Shi Junli, for all of her love, help and understanding during my PhD study.

Table of contents

Figures and tables

Nomenclature

Symbol	Description
A	Cross section area of the plate
A_1	Cross section area of straight duct before HQ-tube (upstream)
A_2	Cross section area of HQ-tube
A_3	Cross section area of straight duct in the section of HQ-tube (middle)
A_4	Cross section area of straight duct after HQ-tube (downstream)
a	Radius of a cylindrical duct
a_n	Acceleration of membrane vibration
B	Bending stiffness
C_1,C_2	Coefficients
c_0	Sound speed
c_n	Model phase speed
d	Diameter of the hole
F	Force exertion of the dipole source
F_s	Sound suppression factor
f	Frequency

f_1	Lower band limit of the *IL* spectrum in low frequency
f_2	Higher band limit of the *IL* spectrum in low frequency
f_3	Lower band limit of the *IL* spectrum in medium frequency
f_4	Higher band limit of the *IL* spectrum in medium frequency
f_r	Frequency ratio of stopband
H	Upper width of HQ tube
h	Duct height
h_c	Cavity height
I	Area moment of inertia
$\vec{I}$	Sound intensity vector
I_j	Modal coefficient of the incident wave
i	Imaginary unit
IL	Insertion loss
IL_{cr}	Criterion level of insertion loss
IL_d	Insertion loss for the dipole radiation
IL_{up}	Insertion loss directly from raw data, upstream
IL_{dn}	Insertion loss directly from raw data, downstream
k,k_0	Wave number, defined as $k=\omega/c$

k_n	modal wave number
L, L_c	Cavity length
L_{dn}	Duct length before the chamber, left-hand side, upstream
L_{total}	Total length of the silencer
L_{up}	Duct length after the chamber, right-hand side, downstream
l_2	Length of HQ-tube
l_3	Length of main duct in the segment of HQ-tube
M	Mach number
m	Mass ratio of the plate
N	Number of blades
$\vec{n}$	Normal direction of the surface
n	Integer
n_1	Integer
n_2	Integer
p	Acoustical pressure
p_{cav}	Sound pressure radiated to the cavity
p_d	Sound pressure radiated by the dipole source
p_{di}^{+}	Amplitude of the dipole sound source transmitted to left

p_{di}^{-}	Amplitude of the dipole sound source transmitted to right
p_{dn}	Measured pressure of the downstream side by microphone
p_L	Pressure at the left side of duct end
p_m	Sound pressure radiated by the monopole source
p_{out}	Sound pressure at the outlet of duct
p_R	Pressure at the right side of duct end
p_{rad}	Sound pressure radiated to the duct
p_{ud}	Dipole extracted pressure of the downstream of duct outlet
p_{up}	Measured pressure of the upstream side by microphone
q	Dipole source strength
R_j	Modal radiation coefficient of *jth in-vacuo* mode
r_{far}	Distance between microphone and the far-side duct
r_{near}	Distance between microphone and the near-side duct
rpm	Rotation speed of fan
S_1	Cross section area of the main duct of expansion chamber
S_2	Cross section area of the expansion chamber
SPL	Sound pressure level
t	Thickness of the panel

u	Maximum velocity in the fluid field
V_j	Vibration amplitude of *jth in-vacuo* mode
V_{Re}	Volume of the resonator
V_{rms}	Turbulence fluctuation
v_0	Particle velocity of fluid in the holes
v_p	Velocity of plate vibration
W	Side width of HQ tube
$W_{outlets}$	Sound power at the outlets of silencing device
W_s	Sound power radiated by a source in different configurations
W_{str}	Sound power of source in a straight duct
x, y, z	Cartesian coordinates
Z_{cav}	Cavity modal impedance
Z_{open}	Impedance of duct open-end
Z_{rad}	Duct model impedance
$Z_{i,react}$	Acoustic reactance
$Z_{i,resist}$	Acoustic resistance
ρ_0	Air density
Δt	Time step size in the CFD simulation

Δx	Smallest mesh size
μ	Coefficient of viscosity
ω	Angular frequency
δ_{0n}	Kronecker delta function
σ	Perforation ratio
η	Displacement of plate vibration
ψ_n	Modal velocity potential
λ	Wavelength
β	Reflection coefficient
ζ	Damping ratio
ξr	Sound radiation efficiency

Chapter 1 Introduction

1.1 Background

Noise is undesirable or unwanted sound to human beings. Considering the scientific effect of noise on the society has been one of the important design factors for many products. Fans and blowers are commonly used in domestic products for delivering ventilation air or in large machinery to satisfy industrial process requirements, for example, the driving fan in the ventilation system or the cooling fan in computers or the turbo-fans in aircrafts. Rotor of the fan will receive energy from a rotating shaft and transmit the energy to the air, which is pressurized to overcome the resistance induced by duct walls' surface, dampers, or components from other parts in a ducted-fan system. The issue of ducted-fan noise among the above applications is not new, but it increasingly becomes a critical concern for the demanding of higher quality life with quieter products.

Fans or propellers are mostly implanted inside a cylindrical shroud or duct for a great many merits (Abrego and Bulaga, 2002). The ducted-fan would be more efficient in producing thrust compared to a conventional propeller by reducing propeller blade tip losses, especially with a low speed but high static thrust level. Besides, the air velocity can be easily adjusted by the designer through shaping the ductwork appropriately, in order to allow the fan operating more efficiently with a higher air speed than a propeller. In addition, the diameter of a ducted-fan will be smaller than a free propeller for the same static thrust, and ducted-fans usually are much quieter than propellers, for they cover the blade noise. Besides, the tip speed

and tip vortex intensity will be smaller, both of the two parameters contribute to the major noise production. Last, but certainly not the least, ducted-fans will enhance the safety level on the ground. However, the ducted-fans also have several disadvantages, including that clearances between the blade tips and the duct will be smaller to achieve good efficiency requirements, rotation speed of the fan blade will be higher, the design of the duct configuration will be more complex, and the weight of ducted-fans will be increased even if they are made of advanced composites. In general, the application of ducted-fans is inclusive for numerous advantages although it may increase the difficulty of design and manufacturing.

The hairdryer is a typical sample of a ducted-fan system with low aspect ratio. It is designed to blow cool or hot air over wet hair so that the evaporation of water particles will be accelerated and the wet hair will become dried much faster. At the same time, the consumer can utilize the hairdryer to control the shape and style of hair themselves through adjusting the flow speed or the temperature of the air flow, or even the temporary hydrogen bonds inside. Therefore, the hairdryers are gradually more popular in modern life for its convenience of use and powerful functions. However, the noise radiation is an annoying problem, which will potentially influence the emotion and satisfaction of the consumers. In this regard, the current study was motivated preliminarily by the research collaboration project supported by Kenford Industrial Co., Ltd. It included noise identification of hairdryer provided by the company and developing effective noise control method in ducted-fan system with limit length that can be applied for hairdryer.

1.2 Review of noise control methods

The noise control measures can be employed at the source, at the receiver and in the propagating path. Controlling at the source is the most effective way while the most common noise abatement method is adopted in the propagating path. The devices used fall into mainly two categories: active and passive control device.

1.2.1 Active control method

The concept of active noise control (ANC) was introduced in 1930s (Lueg, 1938) and had been implemented with the rapid development of electronic and computer technology. Modern active noise control takes use of digital signal processing or analog circuits to design the adaptive algorithms (Kostek and Franchek, 2000) which are utilized to control the actuators to generate sound with an anti-phase relationship for cancelling the perceivable noise through destructive interference, with reference sensors providing feedbacks to the controller. The number of reference sensors and actuators is determined according to specified sound field. Multiple microphones for detection and secondary sources were employed in Tyler and Sofrin's (1962) model to eliminate the higher modes of ducted-fan noise. A ring formed by 48 microphones as the reference sensors and 12 control drivers in a duct were used by Gerhold (1997) to control the tone noise of ducted-fan. The ANC technique for controlling the fan noise has been developed rapidly with a number of successes. Quinlan (1992) obtained attenuation of 12 dB for the fundamental BPF noise and 10 dB for the A-weighted sound power level by the application of active control to the problem of axial fan tonal radiation. MacGillivray *et al.* (1995) achieved a 20 dB reduction for BPF tone, a 15 dB decrease at the second harmonic, and a 7 to 8 dB noise level reduction at the third

harmonic of BPF. The remarkable point in the work of MacGillivray *et al.* (1995) was that the fan unit itself functioned as the control source in the ANC scheme, by modulating the unit with a shaker in the axial direction. Nauhaus *et al.* (2003) generated the anti-phase sound field superimposed destructively on the primary source by additional small flow obstructions around the blade tips, achieving 20.5 dB of BPF noise reduction. Wong *et al.* (2003) integrated passive and active method in a hybrid device to attenuate the broadband and high level low frequency discrete fan noise respectively, obtaining an overall attenuation of 6 dBA. The infra red device was fresh employed as a reference signal source to eliminate the acoustic feedback. In Wang and Huang's (2006) study of active noise control from a small axial fan, two pairs of 90° phase difference loudspeakers were used to construct the rotating dipole to suppress the primary source, resulting in a 13 dB noise reduction of sound power for both closed and open-loop ANC schemes.

Although a great many successful active noise control cases have been reported in laboratory experiments, the range of long term commercial applications is still small (Hansen, 1997; Hansen, 2004) due to the cost, maintenance and complexity of technical requirements. For example, the active muffler for automotive exhausts designed by Kim *et al.* (1998) and the ANC system for controlling ducted-fan developed by Gerhold (1997) included a number of microphones. The proposed ANC systems work effectively to cancel the primary source, but the additional sensor and actuator will result in relatively high cost. Another concern of high cost is the labor component associated with expertise in understanding of the principles of active noise control including acoustics, electronics, signal processing, automatic control, and so on. Furthermore, for the requirement of avoiding mode

spillover due to mismatch of the mode compositions (Gerhold, 1997) and stability concerns of the whole system, the practical application of the active noise control remains in question. Besides, active noise control systems are essentially limited to the control of plane wave propagating in ducts and to control single or multiple tonal noises with rather narrow stopbands. For future development of ANC systems, implementation of algorithm with high correlation between reference signal and the unwanted noise (Chen *et al.*, 2015), and more stable systems with proper actuators and sensors while keeping cost low, and obtaining wider effective bands are the main trends.

1.2.2 Passive control method

Passive noise control refers to the noise attenuation by sound isolating materials such as sound-absorbing, insulation materials, or a muffler. Passive noise control measures will be more effective at higher frequency ranges and often provide an adequate solution for noise radiation problems without the usage for active control device. Regarding the noise abatement mechanism of dissipation or reflection, passive noise control can be further divided into dissipative and reactive control methods.

1.2.2.1 Dissipative noise control

Dissipative noise control refers to the usage of fibrous or porous sound-absorbing materials (Allard, 1993) to attenuate sound. The noise abatement mechanism can be driven from two aspects: one is the conversion of acoustic energy to heat caused by friction between the oscillating air and fibers of porous material, and the other is the energy dissipation due to the viscous damping of the air particles in the voids of porous material.

Duct lining with porous sound absorbing materials was developed rather mature and reliable in last century to attenuate the medium-to-high frequency noise (Mechel and Ver, 1992; Ingard, 1994). A well-designed dissipative silencer can provide good sound attenuation over medium-to-high frequency range. However, there are several concerns about porous or fibrous absorbers. The first one is acoustical. Low frequency sound radiation attracts more attenuation, for it is more sensitive to human beings, so it is important to consider the low frequency range. Conversely, traditional absorbers are ineffective in the low frequency range, such as 200 Hz (Huang, 2004), and alternative treatments are required. Besides, in order to improve the absorption performance of the absorber, the thickness of the absorption materials is commonly increased or the absorption material is integrated with an air gap behind. Thus, the geometry of the dissipative absorber is usually bulky. Another concern is about hygiene reasons. Porous or fibrous materials themselves are abrasive and usually have low durability, and there is a need to replace the absorbers after a certain period. In addition, it is easy to accumulate dust, and even bacteria which poses a health hazard to humans. The dust is difficult to clean and the cost is rather high for periodic cleaning. Therefore, it is quite necessary to seek an alternative method that can work effectively in low frequency range and solve hygiene problems.

To achieve both objectives, many researchers have adopted membranes and plates in noise abatement. For example, in order to examine the sound absorption characteristics of a membrane-type sound absorber, a theoretical study was carried out by Sakagami *et al.* (1996). A closed-form analytical solution was established for obtaining sound absorption coefficient of a membrane with infinite length integrating a backing air-back cavity. For the application, membranes were utilized

widely as an integrated construction component of the roof and ceiling in the architectural (Takahashi *et al*., 1996), and the room acoustical quality was mainly controlled by the membranes' acoustic properties: the density, thickness, tension, and permeability. Panel materials were also used as alternatives to integrate both sound absorption properties and resonant structural vibration characteristics (Brown, 1964; Ford and McCormick, 1969; Horoshenkov and Sakagami, 1998; Horoshenkov and Sakagami, 2001).

The idea of utilizing the friction in small holes and slots to absorb sound energy had a longer history than using fibers initially. The acoustic behavior of perforated facings was analyzed by Bolt (1947). However, it was thanks to an old Chinese master acoustician (Maa, 1975; Maa, 1987), that micro-perforated absorbers (MPA) were installed for the first time in 1992 to attenuate the noise during the opening of the German Bundestag in Bonn (Fuchs and Zha, 1997). A typical micro-perforated panel (MPP) absorber takes the form of a sheet of MPP in front of backing cavity that can only provide efficient sound absorption in a rather narrow frequency band. This special Helmholtz resonator type absorption is determined mainly by geometrical parameter and the MPP may be made of arbitrary materials. The perforation in the MPP can be reduced to sub millimeter size (diameter from 0.5 mm to 1 mm) and the MPP itself can provide low acoustic mass reactance but enough acoustic resistance necessary for wideband sound absorber, without additional fibrous or porous materials. In order to improve the MPA's performance, additional MPPs have been employed into the backing cavities forming a double-layer MPA (Maa, 1987; Zhang and Gu, 1998; Sakagami *et al*., 2006; Sakagami *et al*., 2009) or even multiple-layer MPA (Lee and Chen, 2001; Lee and Kwon, 2004).

Studies show that the absorption performance has been enhanced indeed by the insertion of extra MPPs. However, the control parameters determining the absorption performance rise, which in turn increase the complexity of the design and optimization process. Despite multiple MPAs, it is possible to reduce the size of perforation (Maa, 1998) or adopt MPP with irregular cavity (Wang *et al.*, 2010) to broaden the effective frequency band, which was investigated theoretically and validated by experiment with normal incidence of sound wave, reporting a wider absorption bandwidth due to the increased vibro-acoustic coupling between the cavity and air motion in MPP. The sound absorption performance of MPP absorber was further examined in a compound array (Wang and Huang, 2011) reporting strong local resonance resulting in resonance absorption, and a periodic array with oblique incidence in diffuse field (Wang *et al*., 2014) detecting break down of parallel absorption mechanism at low frequencies.

With the properties of clean and efficient sound absorption capacity taking place of traditional porous materials, MPPs are finding more and more applications such as in barrier design (Asdrubali and Pispola, 2007), room acoustics (Kang and Fuchs, 1999; Drotleff and Zhou, 2001), and acoustic liners (Chiu and Chang 2008; Dickey *et al*., 1998; Guo *et al*., 2008; Jing *et al*., 2007; Lu *et al*., 2014; Wang *et al*., 2012; Wu,1997). The MPP is regarded as the new generation of fibreless absorption material and the future market for the application of MPP is enormous. Up to present, majority of such studies utilized the absorption property of the MPP assuming the MPP without vibration and focused the effort onto the absorption performance improvement by geometry design.

1.2.2.2 Reactive noise control

Reactive silencers generally consist of a number of chambers and tubes and can attenuate sound by reflection of sound by impedance discontinuities. It is effective in controlling noise at low and media frequency. Typical reactive devices include expansion chambers, Helmholtz resonators and Herschel-Quincke tubes.

1.2.2.2.1 Expansion chamber

Expansion chambers attenuate sound wave by introducing a sudden change in the main duct. There is usually a broadband noise reduction in the designed frequency range, although the attenuation is not that high. The transmission loss is well known as: $TL = 10\log 10[1 + 0.25(\frac{S_2}{S_1} - \frac{S_1}{S_2})^2 \sin^2(kL_c)]$ where S_1 and S_2 are the cross section area of the main duct and the chamber section respectively, k is the wave number, and L_c is the length of the central chamber. The amplitude of transmission loss depends on the expansion ratio which is defined as S_2/S_1. The maximum transmission loss occurs when the chamber length is equal to the quarter wavelength or its odd multiples, and the passband exists at the frequencies where the chamber length is same as half wavelength or its multiples. The acoustic attenuation performance of conventional expansion chambers is affected by geometry of the chamber. Thus, many experiments and investigations are based on the study of the geometry in order to improve noise attenuation efficiency: rectangular cross-section or circular cross-section (Ih and Lee, 1985; Selamet and Radavich, 1997), a single chamber or multi-chambers (Munjal, 2014), with single inlet/double outlets (Wu *et al*., 2008), with inlet and outlet extension (Selamet and Ji, 1999), with integration of perforated facing (Ji, 2010) or with complicated internal configurations (Yu and Cheng, 2015). For the acoustic domain is simple,

it is easy to design and optimize the geometry of expansion chamber. A well designed expansion chamber can perform effectively at desired frequency ranges. The expansion chambers have been extensively used as silencers in the exhaust systems (Munjal, 1987) of internal combustion engines. However, the discontinuity of the duct cross section results in pressure loss, which will cause extra energy consumption. Thus, more noise could be produced through providing additional power to make up the pressure. To eliminate the passband caused by the chamber length, the common way is to extend the device with multi-chambers with different dimensions or very complicated internal configurations (Yu and Cheng, 2015) which will increase the design, optimization and constructing complexity. Besides, high sound attenuation of the expansion chamber requires a high expansion ratio which will make the device very bulky.

1.2.2.2.2 Helmholtz resonators

Helmholtz resonators are widely used in ducts, pipes and many other applications (Munjal, 2014). It is well known that the sound transmission loss of the resonators will be rather high at their resonance frequencies (Ingard, 1953). The stiffness provided by the resonator cavity and the mass of air in the neck will determine the resonance frequency. At the resonance frequency, by the excitation of incident wave, the air in the resonator neck will oscillate strongly. During this process, friction plays a minor role in the oscillation dynamics. Besides, the cavity stiffness is balanced by the air inertia. Such balance will eliminate the acoustic impedance to the incident waves. As a result, a zero pressure will be obtained at the mouth surface of the resonator. Due to the property of narrow bandwidth of Helmholtz resonator, an accurate prediction of its resonance frequency is most important in its design. There are certain corrections of the neck length which is named the

effective length instead of physical length in different studies (Rayleigh, 1945; Chanaud, 1994 and Chanaud, 1997). Regarding the simplicity in the constructing of resonator, the range of the application of Helmholtz resonator is rather wide. In most cases, the resonators are used to attenuate noise in duct-like structures. The scholars investigated various kinds of configurations to improve the sound attenuation capacity of resonators. Multiple array resonators (Li *et al*., 2007; Seo and Kim, 2005) were used to broaden the narrow band characteristics of a resonator in the low-frequency band. In order to push the resonance frequency to a lower frequency region without increasing any volume, Selamet and Lee (2003) designed a concentric circular Helmholtz resonator with an extended neck resulting in resonance frequency shifting down. The effects of shape, length of the neck extension on the resonator behavior were examined, and even the perforation was introduced on the neck extension to improve resonator behavior. The resonance frequency can also be shifted to a lower frequency by lining the resonator with fibrous materials (Selamet *et al*., 2005). Helmholtz resonator integrating with a tapered neck (Tang, 2005) can result in an acoustic impedance reduction, and in turn an increase of the highest sound absorption coefficient will be achieved. Coupled Helmholtz resonators (Xu *et al*., 2010; Tang *et al*., 2012) were formed through the attachment of another cavity to the rear end of a Helmholtz resonator. There was a hole opened for the attachment of the extra cavity produce the additional resonator effect. The newly formed coupled resonator can significantly widen the working bandwidth. However, the cavity volume or the neck length must be very large when the resonators are applied to control the low frequency noise for the cavity stiffness is extremely high. Together with the difficulty of

tuning to the right resonance frequency for the property of rather narrow bandwidth, limitations still exist in the real application.

1.2.2.2.3 Herschel-Quincke tube

The Herschel-Quincke (HQ) tube is another typical reactive noise control device used in ducts. The concept was first introduced by Herschel (1833) who theorized that, "No motion is, strictly speaking, annihilated; but it may be divided, and the divided parts made to oppose and, in effect, destroy each other." The HQ-tube is formed by hollow side-tubes attached on the main duct. The sound cancellation will appear if the path difference between the sound wave in the main duct and that in the side tube is odd numbers of half wavelength. Quincke (1866) validated the theory by experiments and Stewart (1928) improved the theoretical explanation by observing that sound cancellation would also appear when the sum of the path is multiple of wavelength on condition that the path difference is not multiple of wave length. More recently, Selamet *et al.* (1994) extended the study to derive an analytical model without any geometry restrictions on the duct cross-section area and found that broadband sound attenuation can be achieved by removing the geometry restrictions. The limitation of HQ-tube is also the narrow bandwidth.

1.3 Advanced silencing technology in duct

Briefly speaking, active noise control can be very effective at low frequencies when the noise source consists of a small number of discrete frequencies, but the application of the ANC system is limited due to the cost, maintenance and complexity of technical requirement. For the passive treatments, the dissipative absorbers lining with porous materials attenuate the medium-to-high frequency

well, but are ineffective in the low frequency range and cause environment concerns. For the expansion chambers, the attenuation performance is appreciable in the desired frequency range but the pressure loss caused by the discontinuity of the duct cross section is an essential issue. Resonators and HQ-tubes work effectively in the resonance frequency, but the bandwith is rather narrow. So there is a demand to seek a broadband passive noise control device which will work effectively from low to medium frequency range with no pressure drop and "clean" without any porous materials.

Huang (2002) introduced the concept of a drum-like silencer which is formed by an expansion chamber with light membranes covering the side-branch cavities under a fairly high tension. When the sound wave propagates from the upstream of the silencer, then passes over the membrane section, the membrane will be induced to vibrate and radiates sound to both upstream and downstream of the duct. Thus, the part of sound waves traveling to the upstream duct will result in energy flux reduction in the newly formed transmitted wave in the downstream of duct due to the principle of energy conservation law. The air-membrane interaction was analyzed in terms of *in-vacuo* modes through two-dimension model (Huang, 2002) and three-dimension model (Huang and Choy, 2005). Such vibro-acoustic interaction for the purpose of wave reflection was new and unique (Huang, 1999). Experimental validation for the drum-like silencer was carried out without (Choy and Huang, 2002) and with flow (Choy and Huang, 2005). Parameter study has been also carried to optimize the geometry of silencer and the membrane properties. The results show that the drum-like silencer with a rather high tensioned membrane with a length of five times the duct height and the same height of backed-cavity reports a relatively wide stopband from low to medium frequency

range. The performance can even be maintained when the flow speed is small, that is, under 20 m/s. Compared to traditional noise control methods mentioned above, the drum-like silencer is environmental-friendly for it is fiber-free. Besides, no pressure loss will be caused because there is no sudden change of duct cross section area as the membranes are flush-mounted with the duct. Furthermore, regarding the complete separation of gaseous media by the membranes, there is a possibility to employ a low impedance gas, such as helium, to fill the cavity to further enhance the silencer performance (Choy and Huang, 2003) in low frequency range.

To ease the installing process without any machine for exerting force, Huang (2006) replaced the high tensioned membrane with a simply supported, high bending stiffness while relatively low mass plate and took use of the natural bending moment of the plate as the sole structural restoring force. It has been studied theoretically that the eigen-frequency of the second *in-vacuo* mode for plate vibration is changed to four times as much as that of first mode, instead of twice for the tensioned membrane. The change of intermodal relationship results in a wider stopband than the tensioned membrane silencer. The plate silencer works as a low frequency wave reflector which will cover a rather broad frequency band wider than one octave. In the case of both the leading edge and trailing edge clamped, the silencer obtained a stopband of 4.25 from f=0.0353 to f= 0.149 in which the TL was larger than 10 dB with plate properties of mass ration m=1 and bending stiffness B=0.129. To further improve the performance of plate silencer, Wang *et al.* (2007) optimized the plate silencer with clamped support boundary condition, making the implement process of plate easier, and the attenuation

performance of plate with non-uniform mass distribution was also investigated. The optimization study showed that the frequency ratio of stopband could be widened up to 6 with a proper distribution of the bending stiffness along the plate. As the light plate with rather high bending stiffness would bring a wider stopband, the requirement of composite plates would be extremely high. Wang *et al.* (2008) manufactured a sandwich plate to supplement the requirement of plate with low mass but high bending stiffness and the noise attenuation mechanism was investigated (Wang and Huang, 2008). Choy *et al.* (2012) fabricated the reinforced composite plate with light mass and high bending stiffness installed in the two-plate and six-plate silencer, and a lower band limit was achieved with an appreciate stopband.

Membranes or plates covering the side-branch cavities show attractive performance via the sound wave reflection with the elimination of pressure drop caused by the change of cross sectional area (Huang, 2002; Wang *et al*., 2007; Choy *et al.*, 2012). However, there still are limitations which resist the extensive application of such type of silencing devices. For the membrane silencer, the tension requirement is relatively high that it will increase the difficulty in installing and maintaining process. For the plate silencer, the plate should have high strength to mass ratio, but no existing raw material can achieve such strict requirement. In order to widen the stopband of plate silencer, Wang *et al.* (2012) introduced perforations on the plate to contribute to sound absorption, which compensate for the deficiency of the passband due to the insufficient sound reflection resulting in a wider stopband, and to relax the strict requirement of plate bending stiffness. Liu *et al.* (2012) recently introduced a method to suppress the subsonic axial fan noise at

the source position by membrane housing through the interaction between membrane vibration and the sound fields in the duct and cavities via vibro-acoustic coupling, undergoing sound cancellation. In such case of membrane housing the source, the tension needed is rather small.

1.4 Motivations and objectives

This study focuses on the investigation of sound source components of the hairdryer and development of noise control method to control ducted-fan noise. A series of experiments were carried out to measure the noise level of the sample hairdryers and to identify the noise sources in order to determine the dominant noise sources and the properties of the noise sources. Noise control method will be developed to reduce the noise level. Through the previous literature review, the traditional duct linings are ineffective in the low frequency range and porous or fibrous materials themselves are abrasive and usually have low durability. The classical reactive control methods of expansion chambers would cause pressure drops and become bulky when controlling low frequency noise; resonators and HQ tubes are difficult to obtain a wide stopband. For the active control methods, the real application is limited due to the cost, maintenance and complexity of technical requirement. The concepts of drum-like (Huang, 2002), plate silencer (Wang *et al*., 2007; Choy *et al*., 2012) and plate with perforations (Wang *et al*., 2012), can be adopted and thus a broadband and relatively low frequency noise attenuation can be achieved by a rather compact geometry. Due to the limitation of duct length, the silencer would be installed close to the sound source. The newly introduced membrane housing by Liu *et al*. (2012) can control the ducted-fan noise at the source position through sound cancellation mechanism. But the drawback of such

design is still the extra mechanism for the entering tension on the membranes. For the product of hairdryer with fan installed in a short duct, the noise control should be a user-friendly method that is easy to install, maintain and replace, with compact geometry and with wide stopband to cover the first two BPFs of fan noise. Therefore, the MPP with clamped boundaries is utilized integrating both the sound cancellation and sound absorption mechanism, to attenuate the product noise at the desired frequency effectively.

The objectives of current study can be drawn from two aspects. One is the noise source identification of product of hairdryer with fan installed in the duct through the acoustical field, vibration and fluid field measurement and analysis. And the other one is the development of a passive noise control method for controlling sound source radiation directly in sound quality aspects and that will be the major target of current study. The development of noise control method can be further divided into three parts. First, a detail analytical modal of MPP housing the dipole sound source is built for the understanding of full coupling among the fluid fields and the plate vibration, and both the numerical and experimental validation are carried out. The MPP housing device would be installed onto the hairdryer to reduce the noise level of product with dominant fan noise. Second, based on the optimal configuration of MPP housing device, a hybrid device is designed via introducing a hollow tube to improve the device performance validated by the experiments. Finally, the effort is put into further improvement of the device performance through modifying the internal configuration of side-cavities with no enlargement of housing device geometry.

1.5 Outline of the current work

Both theoretical and experimental efforts have been involved in the study. This thesis is consisted of six chapters. Chapter 1 focuses on the background and objectives of the present work including the review of relevant works.

Chapter 2 focuses on the experimental investigation of sound field characteristics and sources identification of hairdryers. The experiments are conducted through acoustical measurement by microphones in an anechoic chamber to investigate the sound field characteristics, and vibration test through accelerometers to look into the effect of motor operation, and fluid field study though PIV (particle image velocimetry) tests to inspect the flow pattern. All the noise components are identified by matching their corresponding peak in the sound pressure level (SPL, hereinafter) spectrum and detailed analysis shows that roughness of the inlet surface is an essential issue for the noise generation.

In Chapter 3, a two-dimensional theoretical model for MPP device housing a dipole source is established. It shares the feature of drum-like silencer with MPP covering on the two side-branch cavities, but it is with a dipole source excitation at the center. An analytical model of the vibro-acoustic interaction is studied to deeply understand the coupling between the panel vibration induced by the dipole source and the sound fields of a duct and backed cavities. With the aid of finite element method (FEM), the analytical model is validated by the numerical results. The sound attenuation performance of the fresh developed MPP housing device will be examined through parametric study and the noise suppression mechanism

of such MPP housing device will be investigated through the modal analysis, radiation suppression and intensity field study.

Chapter 4 focuses on the experimental validation and application of MPP housing device on hairdryer. Perforated balsa wood with relatively high strength to mass ratio is utilized and a loudspeaker is used to function as the dipole source. The spectral peaks and trends of the measured insertion loss are compared with the prediction and good agreement between the two has been achieved. The successful application of MPP housing device on the hairdryer will also be stated in this chapter and results show that, with a compact MPP housing device close to the fan-motor assembly, the BPF noise at 2200 Hz can be inhibited and the total sound pressure level can be lower about 2 dB. From the loudness analysis, the utilization of MPP housing device will improve the sound quality of the product, as the loudness will be much lower from 800 Hz to 3000 Hz, covering two dominant loudness peak regions existing in the loudness curve of hairdryer with smooth enclosure.

Chapter 5 focuses on performance investigation of a hybrid MPPHQ device composed of proposed MPP housing device integrated a non-uniform section area hollow tube. The aim is to supplement the passband issue due to the cavity length to obtain a broadband sound attenuation in the low frequency range. The modeling of the hybrid noise control system is described in detail and the numerical model is established to predict the noise attenuation performance of hybrid device with a finite duct length controlling the dipole sound at the source. Optimization process is implemented through the variation of tube geometry and the numerical results are presented with the comparison between optimal MPPHQ and proposed MPP

housing device with equivalent chamber length. Experiments are carried out for validation and good agreement between the prediction and the measurement has been achieved.

Chapter 6 focuses on the investigation of cavity partition effect on the MPP housing device with different nature sound sources. The influences of modification of cavity internal configuration in the case of incident wave, monopole source and dipole source in the center are studied. The numerical models are setup to look into the pressure field and intensity field variation and to investigate the relationship between the position of partition and the corresponding sound suppression performance. Experiments are carried out to validate the numerical prediction and such useful information would be beneficial to future muffler deigns.

Chapter 7 summarizes conclusions drawn from present work and provides suggestions for future study.

Chapter 2 Noise sources identification of hairdryer

2.1 Introduction

Hairdryer HD768 with a centrifugal fan provided by Kenford Company is the sample for current study. A series of experiments are to be conducted in order to identify different sound sources housed inside the hairdryer and its correlation with the radiated sound from the outlet of the hairdryer. For the hairdryer, with a centrifugal housed in the duct with short length, the noise components are quite complicated. The possible sources are the associated noise due to the inlet flow distortion caused by the inlet of the hairdryer, fluctuating pressure on the rotor blade caused by the unsteady flows, motor noise, tip leakage flow and the possible flow separation from the rotor blades and stationary obstacle. In order to study the characteristics of fan noise and search for noise control method accordingly, all possible noise sources inside the hairdryer due to different mechanisms of sound generation should be identified first by the approach of elimination.

Figure 2.1(a) and Figure 2.1 (b) show the hairdryer provided by Kenford Company with model no. 768 and CAD drawing of its internal components respectively. Based on the specifications provided by the manufacturer, the nominated rotating speed of the fan is around 17000 *rpm*. According to the testing in the lab, the

measured rotating speed of the fan by an optical tachometer is found to be roughly 17000 ± 500 *rpm*.

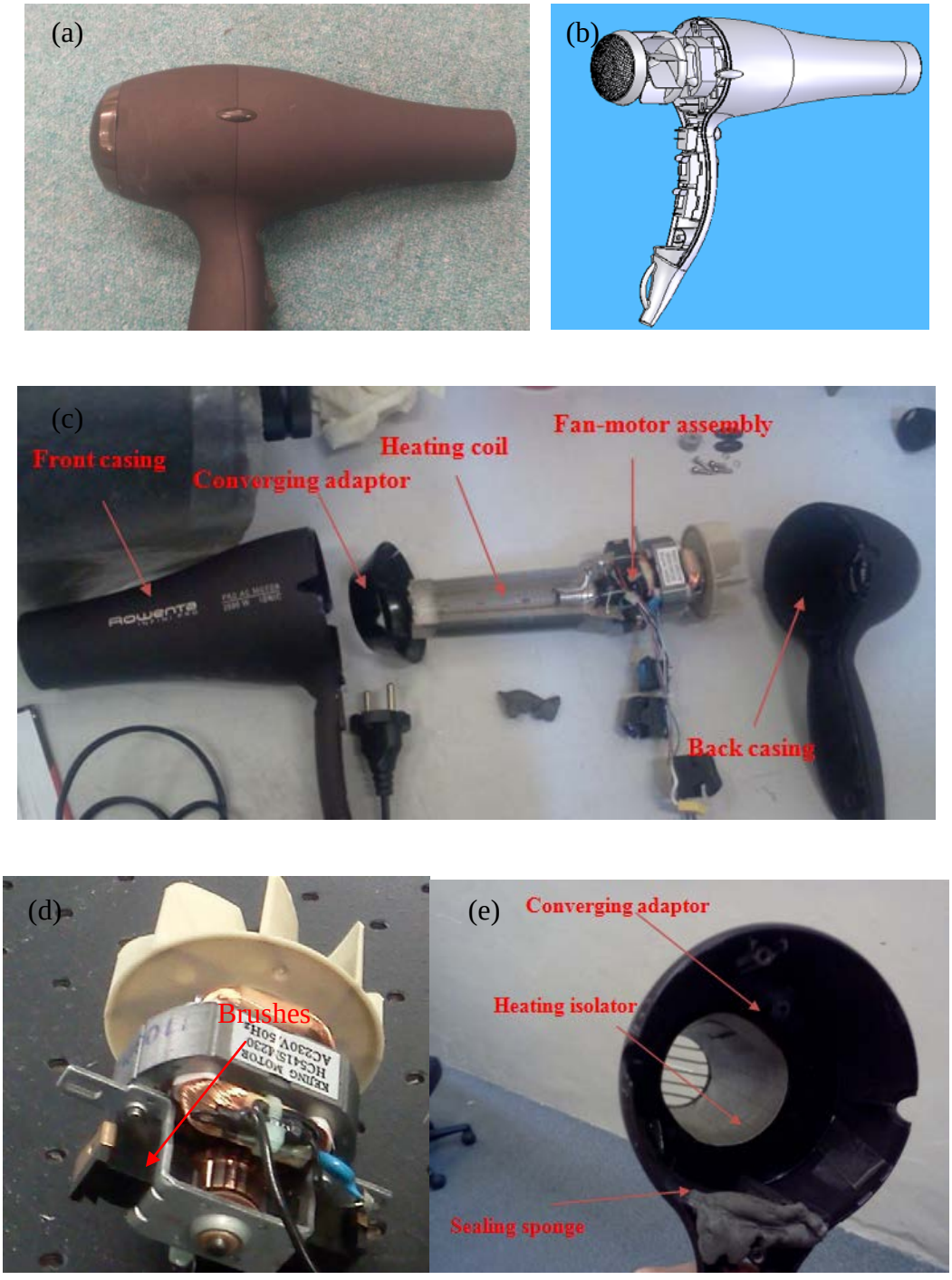

Figure 2.1: Configuration of hairdryer. (a) Hairdryer of model no. 768, (b) CAD drawing showing internal components, (c) photo of hairdryer components and (d) details of motor-fan assembly with brushes and (e) inner part of the front enclosure

All the components inside the casing of hairdryer are shown in Figure 2.1 (c) in detail. It includes a centrifugal fan with 8 blades assembled with motor, heating coil for heating the air as well as converging adaptor for converging the air flow into the regime with the boundary wall of heat isolating paper as shown in Figure 2.1 (e) such that the discharge speed can be increased. The motor used in this special 768 type hairdryer is with brushes as shown in the Figure 2.1(d). It is simple to control, has a low cost while being powerful enough.

2.2 Hair dryer noise mechanisms

Although different fans may cause different types of noises, the noise mechanisms are similar. Generally, they can be separated into vibrational noise, contributed by the structural vibrations such as the motor-fan assembly and noise from the steady/unsteady flows.

2.2.1 Vibrational noise

Vibration is common in the products with rotational fans and mainly caused by the unbalance of operating parts. Main sources of vibration are unbalanced motor operation, unbalance of the fan blades, poor installation of fan blades onto the motor axis and brushes inside the motor. The unbalanced problems are mainly caused by the low accuracy of manufacturing of product components and the low quality control due to the low cost of products. The brushes inside the motor (as shown in Figure 2.1(d)) can be one of the dominant vibrations. Since they have constant friction between the moving and stationary parts, such friction generates a lot of noise. However, if brushes are removed, motors are normally not as powerful as those with brushes.

2.2.2 Steady/Unsteady flow noise

The noise from a rotational fan can generally be classified as discrete pure tones and broadband noise. The tonal noise is also called as rotational noise (Longhouse, 1976) and the frequency is determined by the fan rotation speed. When the fan is rotating at a constant speed, there will be lift force acting on the blade parallel with the inlet flow and drag force in a circular direction against the rotation force. As the fan blades are rotating, an unsteady pattern of flow field relative to the observer will be produced, and such unsteady pattern flow will generate a loading noise, also called the Gutin noise (1936). Apart from this steady loading noise, there will be other unsteady flow noise:

1) The inlet flow can be unsteady because of the existence of the turbulent eddies and will generate noise. One of the sources is the flow passing the protection grid of hairdryer at the inlet and another one is the flow passing the sharp edges with notches located at the upstream position. The noise produced by such turbulence is related to the intensity and the size of the turbulence. In general, this turbulence noise is a broadband noise (Trunzo *et al*., 1981).
2) The tip clearance inside the casing will produce considerable noise. Due to the tip clearance and pressure difference between the pressure side and suction side of a blade, a tip leakage flow over the blade tip will be formed. The leakage flow acts as an unstable shear layer and causes vortices near the tip, and finally these vortices will produce noise. The intensity of the tip-leakage flow and the related tip-leakage vortex depends on the size of the gap and the pressure difference. Such tip-clearance-induced noise is observed in broadband features

and limited narrow band regions and will be increased subsequently with the growth of clearance height (Karstadt, 2010).

3) The interaction of turbulent flow with the blade surface may cause noise, which is the trailing edge noise. Fluid turbulence is utilized to characterize the irregularity of flow of air and other fluids past or through objects. The turbulent flow can be regarded as a continuous series of randomly orientated eddies of various sizes and intensity in a form of energy cascade (Doolan, 2008), and part of the energy would be scattered into sound waves (Ffowcs Williams and Hall, 1970). In addition, such noise from unsteady flow over the blade surface is broadband type in frequency domain (Howe, 1978).

2.3 CFD study of hair dryer

To investigate the characteristics of the hairdryer flow field and the relationship between volume flow rate and the shape of the enclosure, commercial software package of Fluent 6.3 is used to compute the fluid dynamics. The Large Eddy Simulation (LES) approach is applied to solve the three dimensional incompressible Navier-Stokes equations and to capture the vortex dynamic clearly and accurately. For the solver settings, unsteady and second order implicit are chosen. In the calculations, the moving mesh technique has been applied on the fan blade region in order to allow the unsteady interactions between the impeller and the housing. Turbulence is modeled with the WALE subgrid-scale model. The boundary conditions of fan inlet and outlet are set as pressure inlet and pressure outlet, and other solid parts of the fan are treated as stationary wall. The pressure-velocity coupling is calculated through the SIMPLE algorithm. The time step of

the calculations Δt is set to 3.5×10^{-6} seconds, which is related to the Courant–Friedrichs–Lewy condition (CFL condition) to ensure convergence of the simulation. CFL condition is described as $\frac{u*\Delta t}{\Delta x} \leq const$. The CFL constant number used here was 1, where the smallest mesh dimension Δx is 0.25 mm, and u is determined from the steady simulation case about maximum velocity 70 m/s.

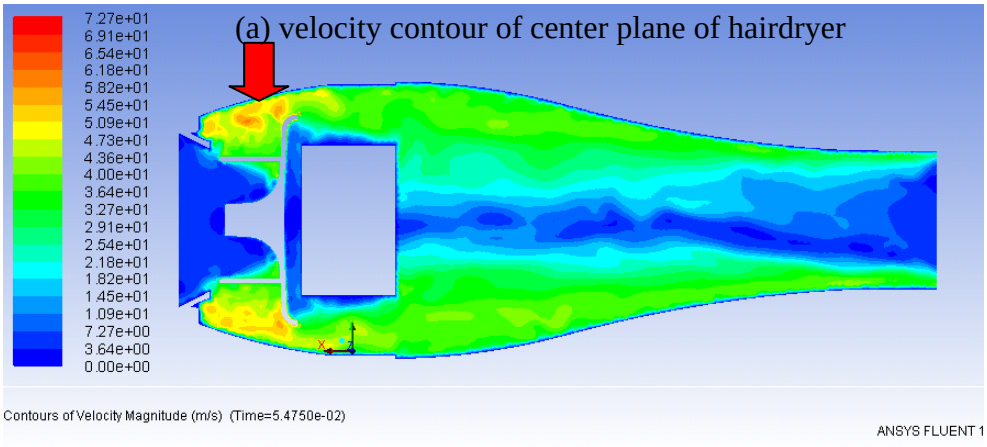

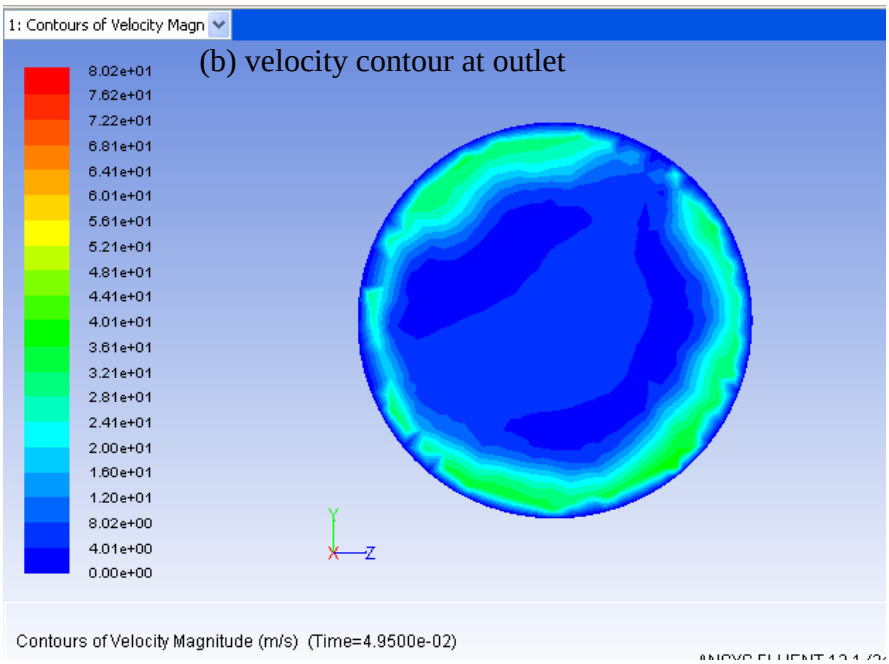

Figure 2.2: The CFD simulation results (a) velocity distribution of *z*-plane and (b) is the velocity magnitude of the outlet surface

Through the CFD study, the information of flow field inside the hairdryer can be captured, such as the velocity contour, pressure distribution, trace line of flow particles, volume flow rate of the product and so on. Figure 2.2 (a) indicates the velocity pattern of plane z and the maximum velocity is observed appearing at the trailing edge of the fan blade near the inlet with the speed about 70 m/s. At the outlet region shown as Figure 2.2 (b), the maximum velocity is around 25 m/s and the velocity at the center is lower than that near the wall. This general trend matches well with the measurement data (which will be shown in later section, Section 2.4.3) and makes sense, as there is a blockage in the center due to the motor. Besides, from the velocity contour it can be found that the maximum velocity gradient, which incarnates the related shear force and vortex, occurs at the tip clearance region. In addition, it seems that the vacancy volume locating at the inlet side has influence to the velocity field. The vortex production or the flow field variation will in turn affect the sound pressure distribution or even induce a major sound source of the product. However, it needs further study to investigate the relationship between this vortex and the enclosure shape design, and the vortex size and frequency which relates to the sound pressure spectrum.

2.4 Experimental study of hair dryer

2.4.1 Acoustical measurement

A series of experiments have been carried out to measure the sound field of the hairdryer in order to identify the noise sources and characteristics. The free field microphone is used in the experiment for data collection and Figure 2.3 depicts the flow chart for the whole data acquisition system. The sound pressure level signals are acquired by microphones (B&K 4189) at the inlet side (upstream) and at the

outlet side (downstream) which are connected to B&K's Nexus with four channels condition Amplifier (B&K 2693). Then the signals are transmitted through a filtering system with high pass filter for the frequency beyond 100 Hz due to eliminating the electronic noise inside the system. Signal from the microphone is digitized by National Instrumental card DAQCard-6062E at the sufficient sampling rate of 25 KHz for 10 seconds. The A/D process is controlled by a MATLAB code developed by the research team of PolyU.

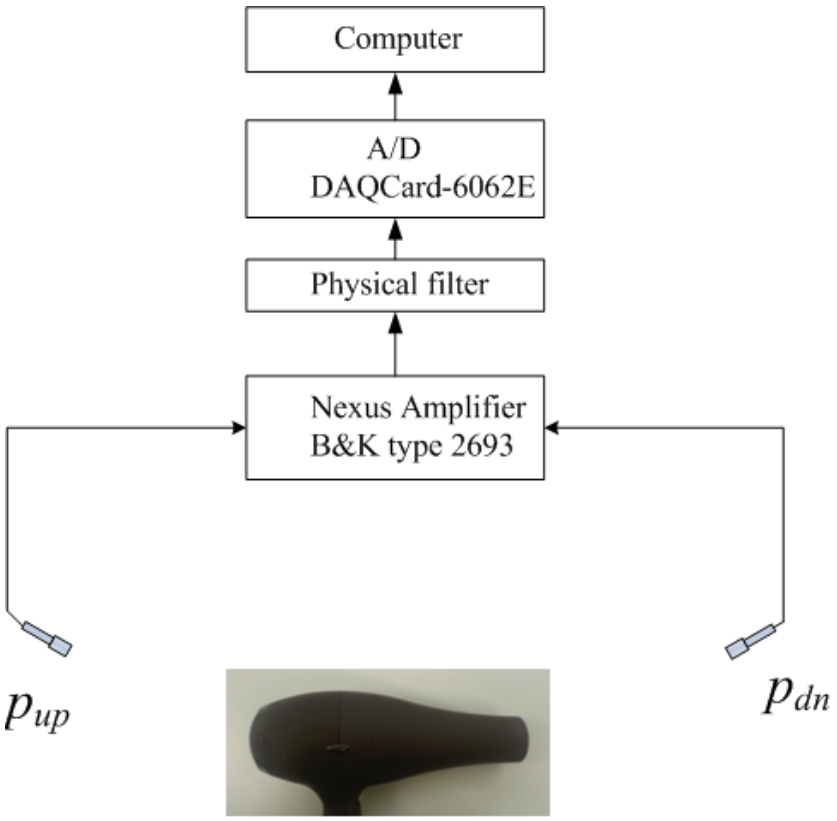

Figure 2.3: Flow chart for the data acquisition system

In order to maintain the rotating speed of the fan to make sure the same operation condition for each measurement, a transformer is employed to control the voltage and the rotation speed of the fan is to be monitored by a tachometer (HT 441) as

shown in Figure 2.4 (a). And Figure 2.4(b) indicates the attachment of the reflective film on the fan blade for tachometer measurement. The rotation speed measurement is essential for it directly relates to the blade passage frequency (BPF) which usually is a dominant fan noise frequency.

(a)  (b) 

Figure 2.4: Equipment for measurement of rotational speed. (a)Digital tachometer HT441 and (b) attachment location of the reflection film

The noise spectrum obtained by the microphones at the upstream and downstream of the hairdryer is shown in Figure 2.5(a) and Figure 2.5(b) respectively. There are several obvious peaks in the spectrum as labelled A, B, C and D. The most dominant peak C at 800 Hz reports a sound pressure level of 68 dB and 61 dB at the upstream and downstream respectively. The users may feel uncomfortable due to such dominant peaks. There are three other tonal noises: peak A at the frequency of 279 Hz, peak B at the frequency of 473.6 Hz and peak D at the frequency of 4482 Hz. Regarding the 8 blades of current rotating fan and its rotational speed about 17000 *rpm*, the corresponding first blade passage frequency (BPF = $rpm \times N/60$) is 2266 Hz, where *rpm* is the rotational speed and *N* is number of the blades. In reality, the rotational speed varies within 500 *rpm* that implies the first blade passage frequency varies from 2200 Hz to 2333 Hz. Consequently, the second blade passage frequency is about 4400 Hz to 4666 Hz. Therefore, the

occurrence of the peak D shown in Figure 2.5 is attributed to the second blade passage frequency. It is clear that the component B has not contributed that much to the total noise compared to the broad component C and even the other two pure tones. Therefore, only the broadband 800 Hz noise and two pure tones of A and D are considered in following investigation.

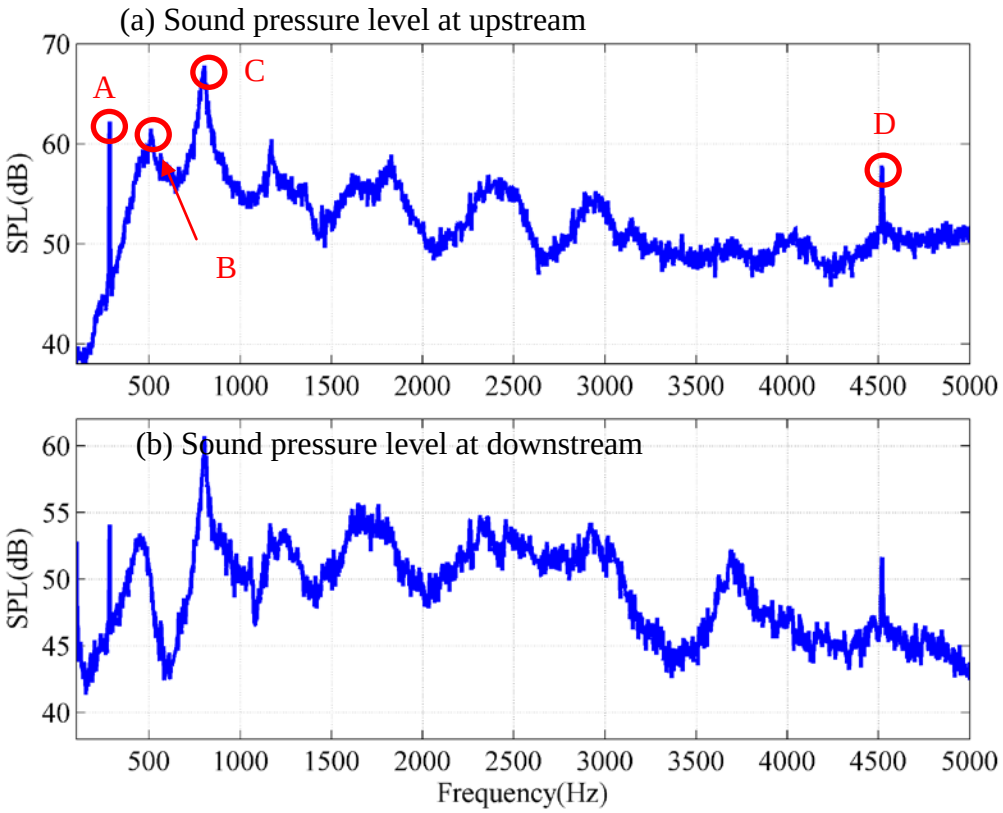

Figure 2.5: SPL spectrum of the 768 type hairdryer provided by Kenford Company (a) upstream and (b) downstream

Noise component C is with a broadband nature and from the noise generation mechanism literature, such broadband noise usually is caused by the unsteady flow of inlet distortion or tip leakage or the trailing edge. From the CFD study, it can be found that the maximum velocity appears at the tip clearance region and it seems that the vacancy volume locates at the inlet side has influence on the velocity field.

Thus, an approach focusing on the noise induced by the unsteady inlet flow is carried out. Figure 2.6(a) to (c) show the original smooth enclosure provided by Kenford Company, enclosure with rough surface at the inlet region of the casing by sticking a thin layer (1 mm thickness) of sandpaper type P60 and enclosure with rubber ring filling at the vacancy volume. The aim of this trial is to investigate whether the inlet flow will be influenced so as to the sound field.

(a)Smooth enclosure (b)Rough surface (c)Rubber ring

Figure 2.6: Different back enclosure at the inlet:(a) Original smooth enclosure (b) Rough surface at the inlet (c) Enclosure with rubber ring at the inlet

Figure 2.7 represents the comparison of the sound pressure level in the frequency range from 0 to 3000 Hz, for back enclosure with smooth surface and rough surface by sticking sandpaper. The measured results demonstrate that the sound pressure level in the frequency range around 800 Hz is significantly decreased both at upstream and downstream. This dominant band at 800 Hz is perceived annoying in the original smooth enclosure and it seems to be reduced by utilization of roughness at the inlet. One thing should be pointed out is that, the key issue in this process is the roughness, not the thickness. Other materials like paper and plastic with smooth surface and identical thickness have been implanted at the same location of back enclosure, but the sound field at 800 Hz has no change. Different types of sandpapers from P180 to P60 with different roughness, the larger number

representing smoother surface, have also been utilized in the experiment, but only the P60 sandpaper has such special effect. The P60 sandpaper owns a rough surface with average particle dimeter of 269 μm. On the other hand, the sound pressure level at the first BPF is drastically increased and it is slightly shifted to lower frequency when there is rough surface on the inlet of the hairdyer. Ultimately, the dominant noise becomes the pure tone of first BPF 64 dB at upstream and 59 dB at the downstream respectively. Nevertheless, the total sound pressure level is decreased from 80.7 dB to 80.2 dB with the effect of rough surface at the inlet of the hairdryer.

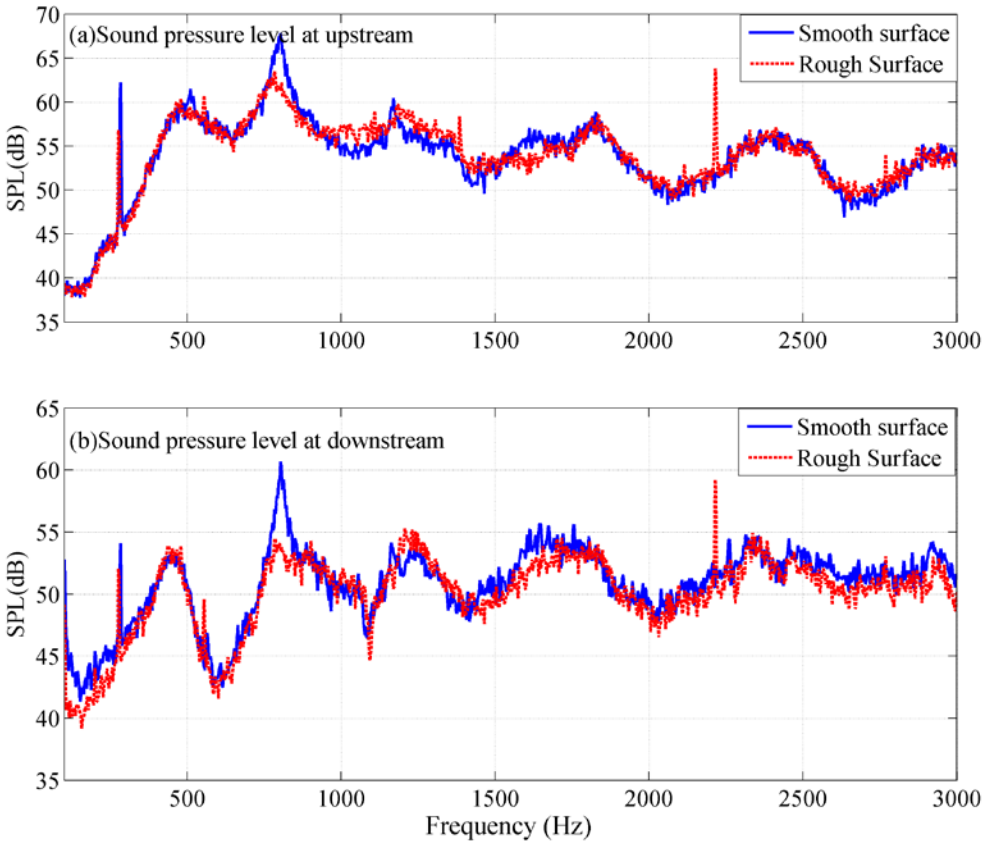

Figure 2.7: Comparison of SPL spectrum of the hairdryer with smooth surface and rough surface at the inlet of the casing for the frequency range of 0-3000 Hz

Sound pressure level change with the usage of a rubber ring at the inlet of casing to cover the small vacancy volume at the inlet is depicted in Figure 2.8. The results show that there is obvious noise reduction at the frequency range of about 800 Hz. Similar to the result of placing sandpaper at the inlet of the casing, the pure tone of first and second BPF are induced at either upstream and downstream at very high magnitude. The results indicate that the application of rubber ring at the vacancy volume will prevent the generation of corresponding turbulence for the 800 Hz noise and the usage of roughness will destroy the turbulence related to the 800 Hz sound. However, the change of flow properties will induce the high frequency pure tone of BPF noise. There should be certain balance between the two, but that is difficult to control.

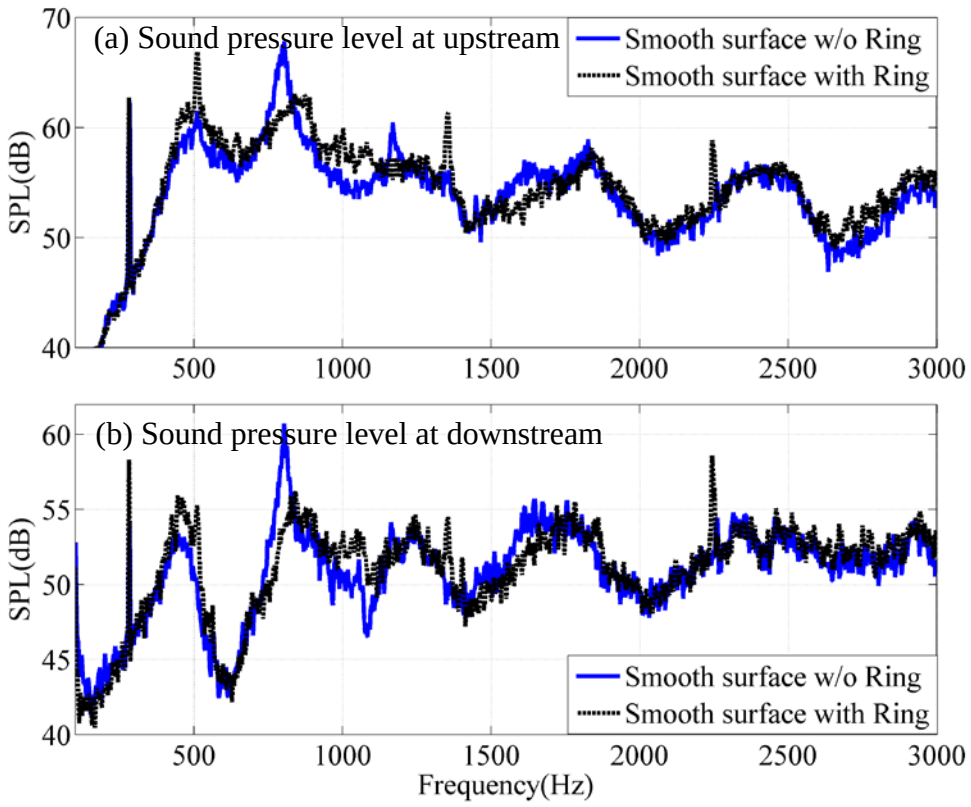

Figure 2.8: Sound prsssure level spectrum change of Hairdryer provided by Kenford Company by the application of rubber ring at the inlet

The sound pressure level of 800 Hz noise is decreased in all directions with different levels by changing the smooth surface to rough surface at the inlet as shown in Figure 2.9 (a). By subtracting all the sound pressure level by a value of 44 dB, the noise reduction will be clearer in all directions as presented by Figure 2.9 (b). It shows that the noise reduction at the upstream (0°) is more significant (5 dB on average) than that at the outlet side (180°) which is about 3 dB. From the shape of SPL contour, it can be also concluded that the 800 Hz broadband noise is more annoying at the inlet side which roughly indicates that the noise generation position is at the upstream, the inlet.

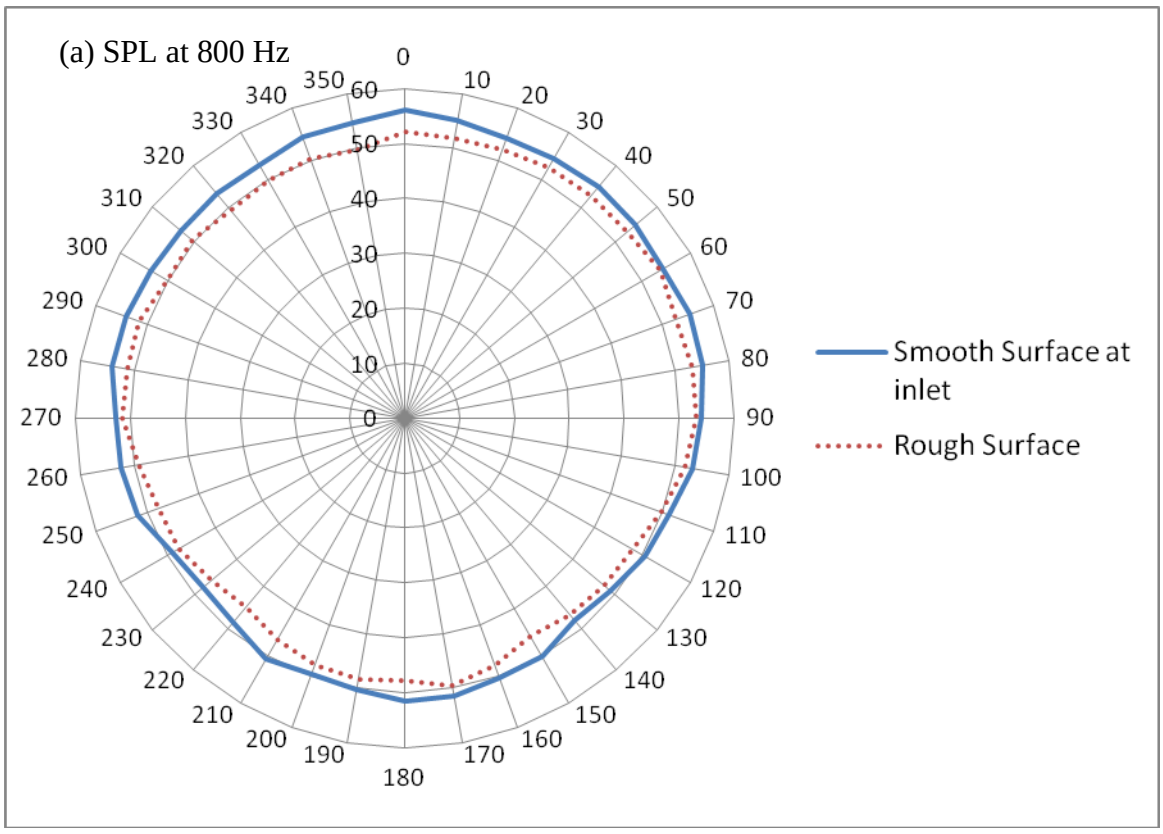

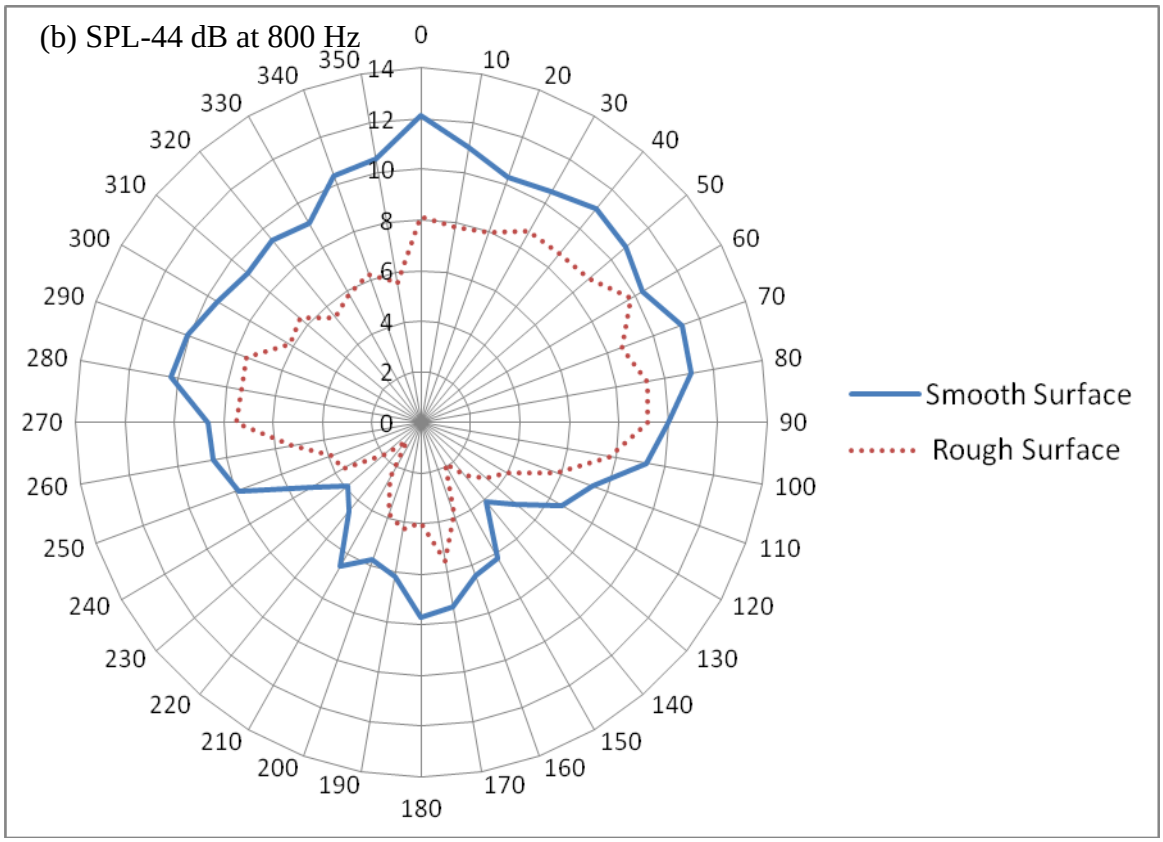

Figure 2.9: Comparison of SPL contour between smooth surface and rough surface at the inlet at frequency 800 Hz. (a) SPL; (b) SPL by deduction of 44 dB

With placing the strip of sandpaper at the inlet of casing, the noise level at first BPF is increased significantly. Figure 2.10 shows the change of sound pressure level of 1st BPF pure tone at different directions with the application of sandpaper. There is an increase of sound pressure level by about 7 dB and 5 dB at upstream and downstream respectively.

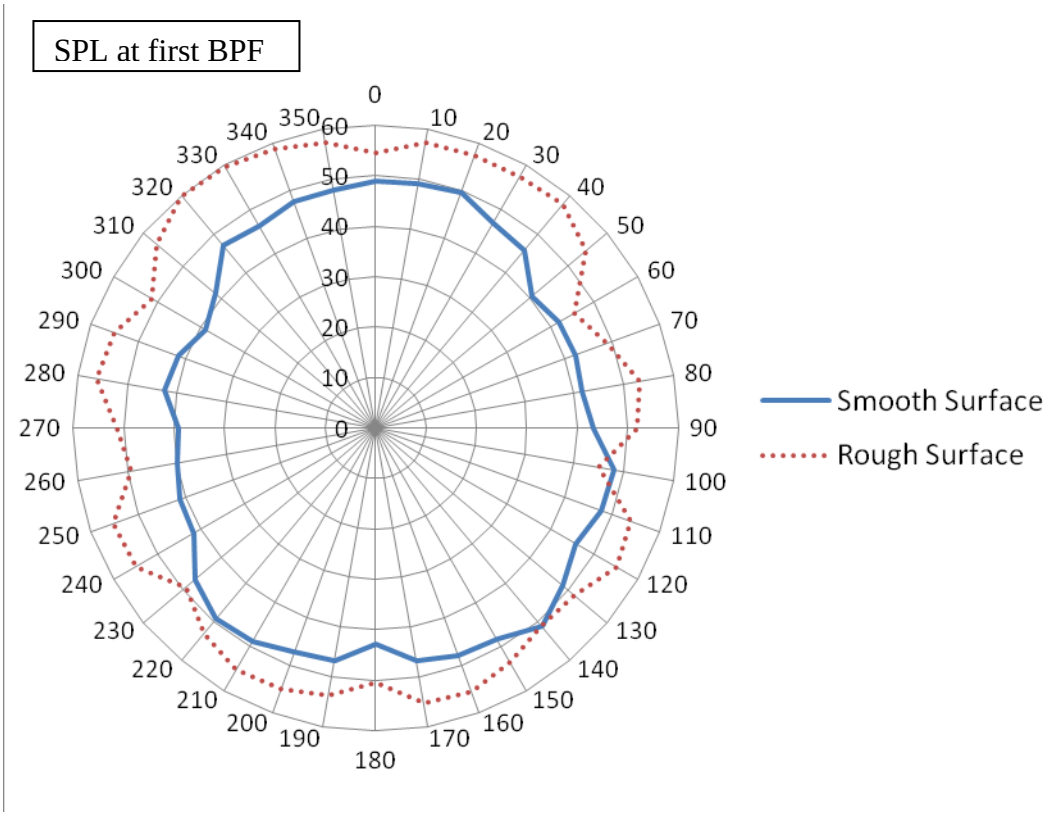

Figure 2.10: Comparison of SPL contour between smooth surface and rough surface at the inlet at frequency of 2241 Hz

In short, by changing the roughness of the back casing at inlet, the sound pressure level of hairdryer at the frequency range of 650 Hz to 850 Hz (broadband noise) is reduced by about 5 dB and 3 dB at the upstream and downstream respectively. On the other hand, the BPF pure tone noise is magnified by about 5 dB at both 1st BPF and its second harmonics. There are two main advantages of adopting the rough surface in the hairdryer. (1) Before the modification, the dominant noise source is around 800 Hz, and this noise will be more sensitive to human ears compared to the 2200 Hz dominant noise. From the equal-loudness contour (ISO 226, 2003) shown in Figure 2.11, when the noise level is about 60 dB to 70 dB, the loudness-level will be higher at the frequency around 1000 Hz compared to that around 2200 Hz. (2) The noise component around 800 Hz can be regarded as low frequency

noise. Actually, it is difficult to control low frequency noise by the existing passive noise control technology in a limited space. Although the noise at relatively high frequency of 2241 Hz is induced, the noise control method to deal with such a high frequency 2241 Hz noise in the limit length of the hairdryer will be easier.

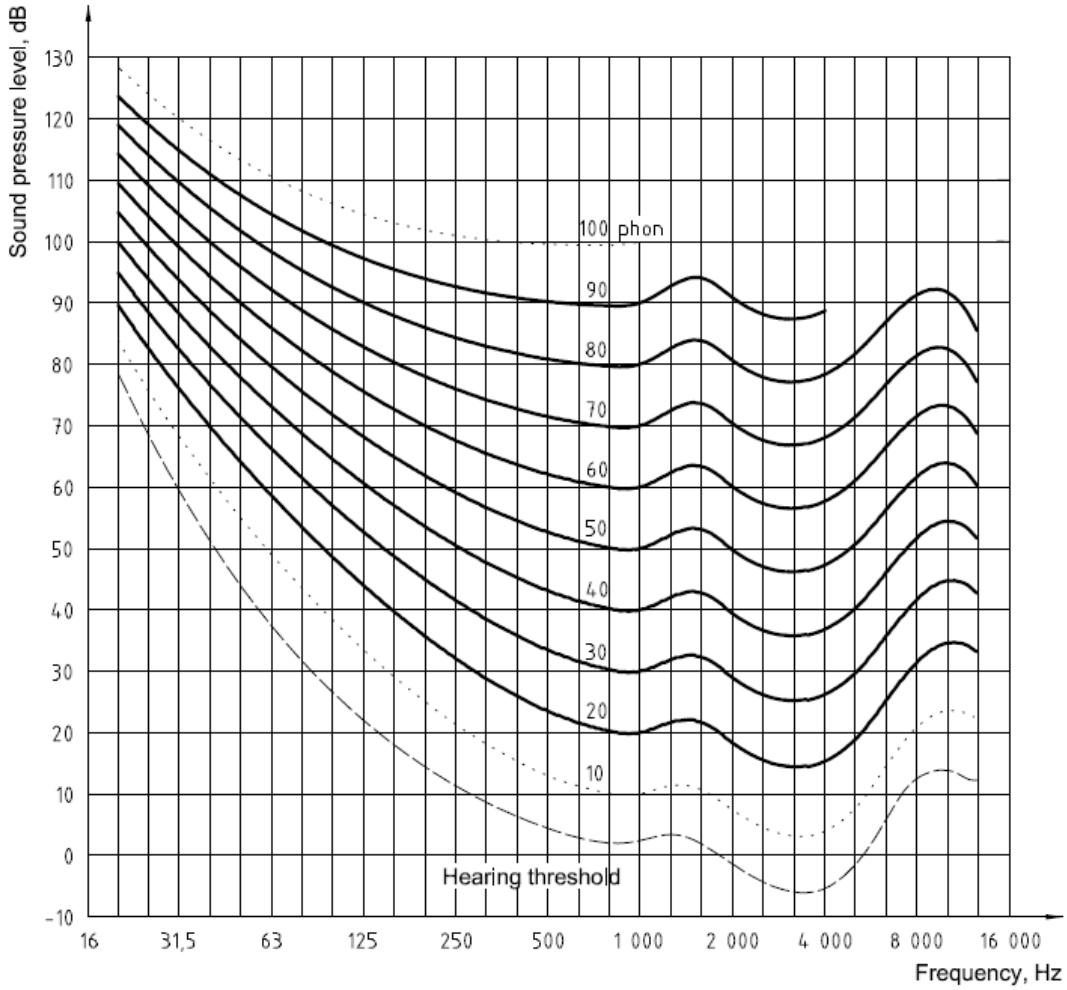

Figure 2.11: Equal-loudness contours from ISO 226:2003

The overall sound pressure level from 0 Hz to 5000 Hz at different direction for the hairdryer with smooth surface and with rough surface at the inlet of the casing is demonstrated in Figure 2.12. Roughly speaking, the overall sound pressure level is

reduced by about 0.5 dB when the roughness is used at the inlet. This result has been validated by using the sound level meter (RION NA27).

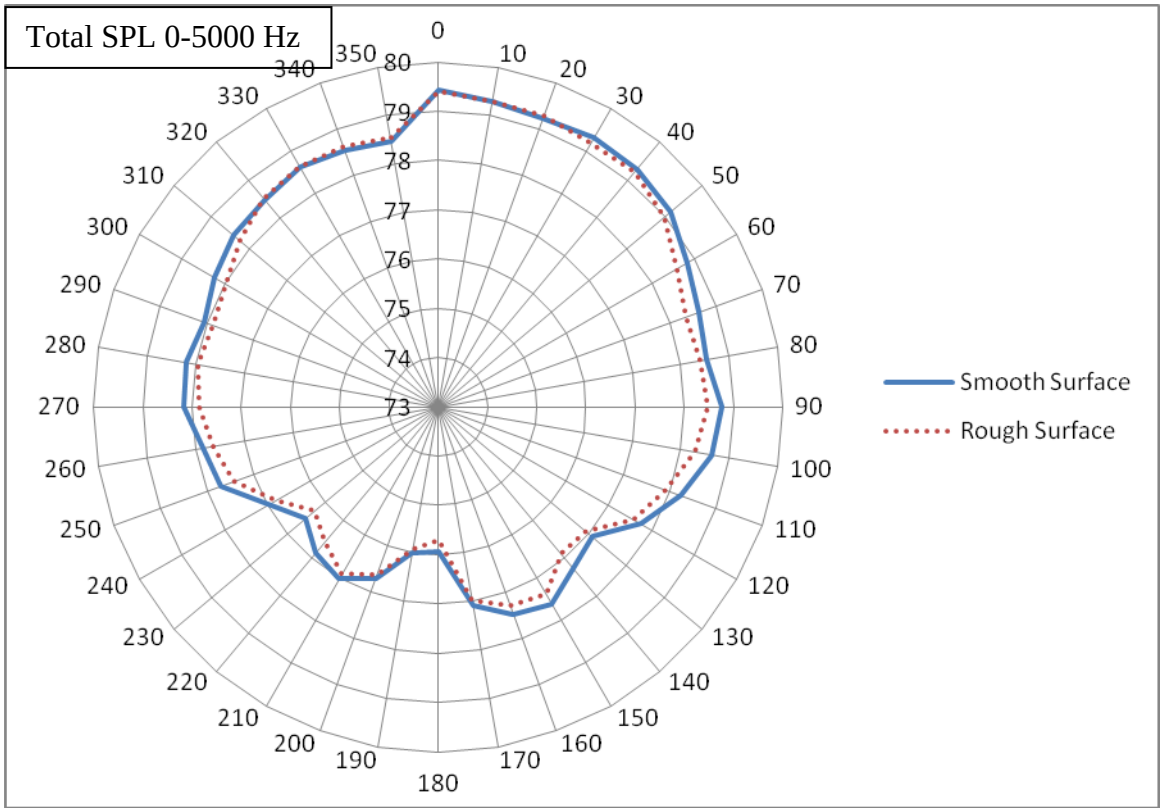

Figure 2.12: Comparison of total SPL contour between smooth surface and rough surface at the inlet

2.4.2 Vibration test

In order to have more understanding of the relationship between the sound pressure level and vibration induced by the motor operation, the vibration performance of three different locations are to be investigated with the attachment of accelerometer. One is the position on the outer surface of casing near the inlet of the hairdryer and another position is the point closed to the motor as shown in Figure 2.13 (a). And the third position is on the ground in order to examine whether the vibration will

transfer to the ground which will demonstrate whether the mounting quality of hairdryer is good or not.

(a)

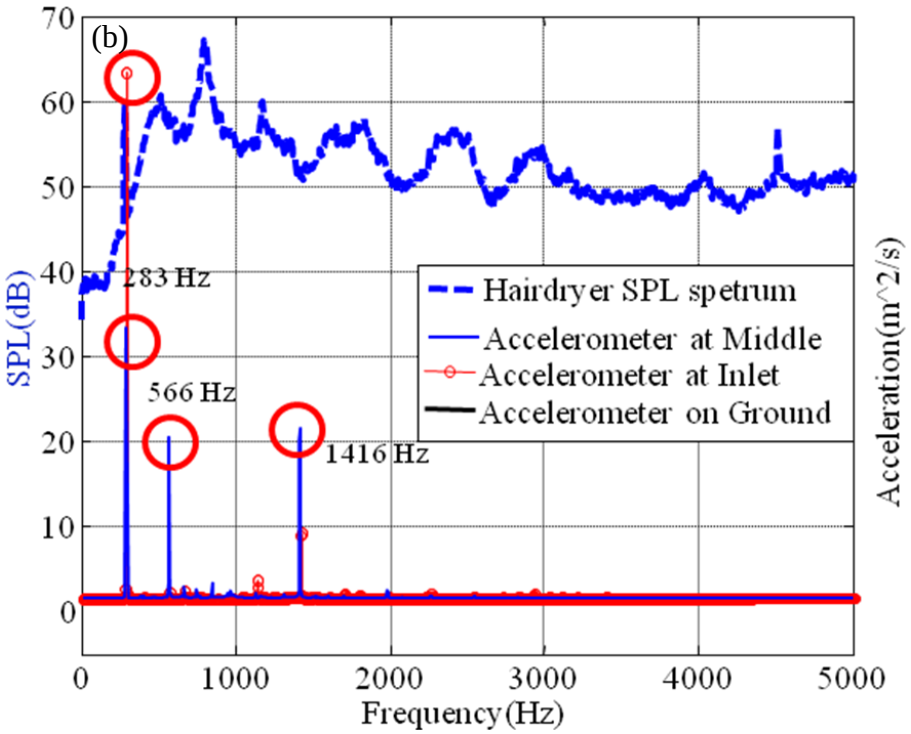

Figure 2.13: Vibration measurement (a) attachment of accelerator on the casing of hairdryer (b) Comparison between vibration signal and SPL spectrum of the hairdryer

Figure 2.13(b) shows the sound pressure level spectrum (blue dashed line) as well as the vibration response measured by the accelerometers attached on three different locations. Three obvious peaks are observed in the vibration response attributed to the point near the motor (blue thin solid line). They are 283 Hz, 566 Hz and 1415 Hz. For the accelerometer on the ground (black solid line), the vibration signal is rather weak which means that the mounting of hairdryer is rather good to isolate the vibration. The magnitude of the vibration response at 283 Hz is extremely high for the point near inlet and middle, the position of fan-motor-assembly, and this peak is also corresponding to the first peak of the noise

spectrum. It indicates that the first noise source around 280 Hz is probably attributed to the operation of the motor.

2.4.3 Flow measurement

In order to obtain the volume flow rate and flow pattern of the hairdryer, the liquid manometer (see Figure 2.14(a)) and digital manometer (see Figure 2.14(b)) with the pitot-tube are used to measure the flow speed at each discharge point of the hairdryer. The measured air flow velocity variation along vertical direction at the outlet of the hairdryer with smooth backing enclosure and rough backing enclosure is indicated in Figure 2.14(c). The x-axis stands for the velocity of flow and y-axis represents the position of the measurement starting from the bottom of outlet to the top in the vertical center line. At the region near the wall surface y=2 mm or y=44 mm, the velocity is about 10 m/s due to no-slip boundary condition at the wall surface. In the region of y=3 mm to y=42 mm, the velocity can be maintained between 15 m/s to 25 m/s with some fluctuations so that non-uniform air velocity profile is obtained. Within this region, the minimum velocity is found to be roughly at the center of the outlet. It may be probably due to the blockage of the motor at the centre. And the maximum velocity appears near the wall which matches well with the CFD prediction shown as Figure 2.2. From the comparison of flow profile, it can be found that with the utilization of rough surface at the inlet, the flow speed of the product is maintained which is rather important as the flow rate and flow speed are key issues for product of hairdryer.

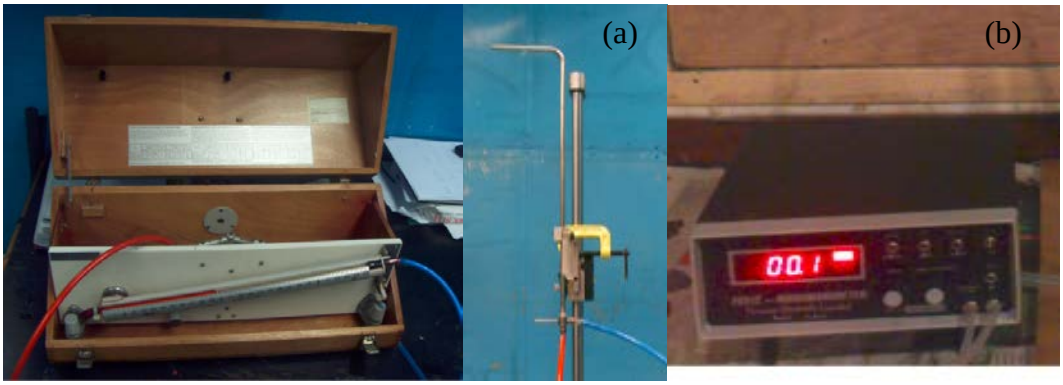

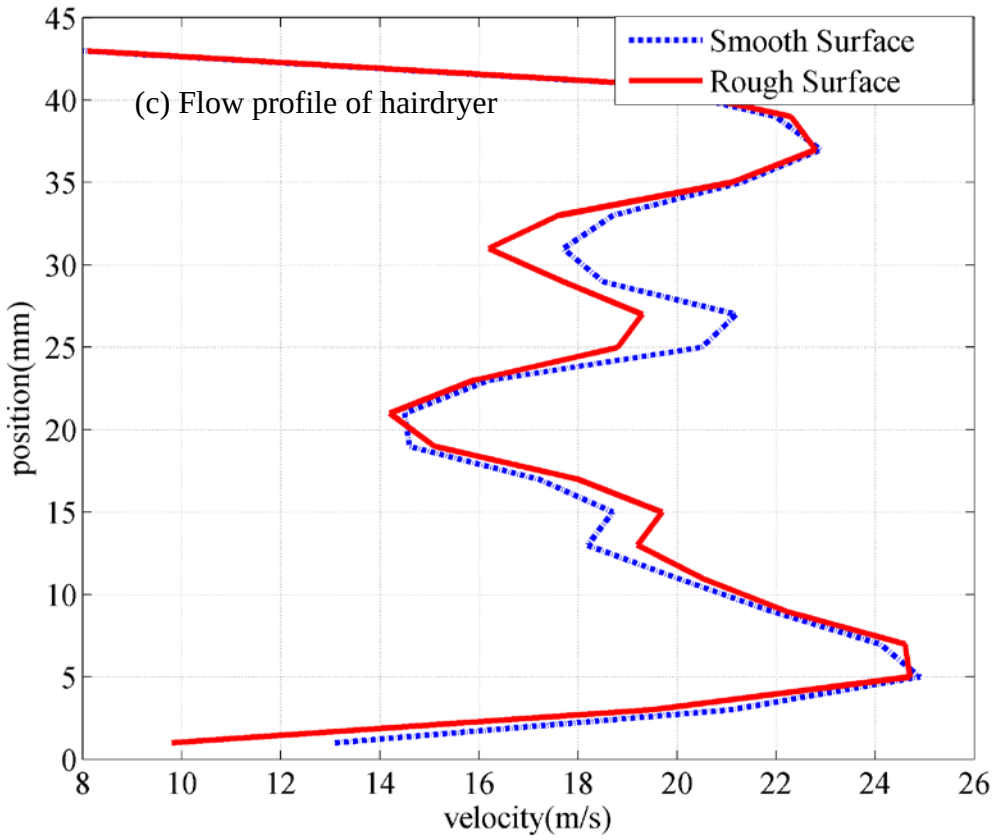

Figure 2.14: Air flow speed test (a) Liquid Manometer and (b) Digital Manometer; (c) Air flow velocity profile at the outlet of the hairdryer

Particle image velocimetry (PIV) is a well-developed technique in the field of fluid velocity measurement nowadays. In this study, a simple PIV test has been carried out to investigate the change of fluid field when the rough surface at the inlet of hairdryer is used. The experimental setup of a PIV system consists of several

subsystems, including the laser, the high-speed camera and the processing algorithm. The small tracer particles generated by the olive oil have been added to the flow in the experiment. The local displacement vector for the tracer particles in the pre-determined image plane between the first and second illumination is determined by means of statistical methods (auto- and cross-correlation). It is assumed that all particles within one interrogation area have moved homogeneously between the two illuminations.

The experimental results are demonstrated in Figure 2.15 (1a), (2a), (1b) and 2(b), Figure 2.16(1c) and (2c), with the comparison between the original smooth enclosure provide by Kenford Company and modified rough inlet hair dryer. The image plane shown in the results is a rectangular plane $290\ mm\ X\ 220\ mm$. The first pair results represent the PIV measurement results of V_{rms} at the middle plane, with Figure 2.15 (1a) smooth enclosure and (2a) rough backing enclosure. It can be clearly found that the turbulence fluctuation V_{rms} of modified rough enclosure hairdryer at the fan blade region is smaller than the original smooth one. The second pair results are for the inlet plane, with Figure 2.15 (1b) smooth enclosure and (2b) rough backing enclosure. Comparing the turbulence fluctuation V_{rms} in the red circle region, which indicates the inlet of hairdryer, the turbulence fluctuation of modified case will be smaller. It indicates that through the rough surface modification, the flow will be more steady or smoother than the smooth one. Figure 2.16 (1c) and (2c) show the particle trace lines of hair dryer before and after the modification with same resolution processed by Tecplot from PIV measurement data. It is further confirmed that the flow field of hair dryer will be

more uniform by the introducing of rough surface thus the broadband noise around 800 Hz is eliminated.

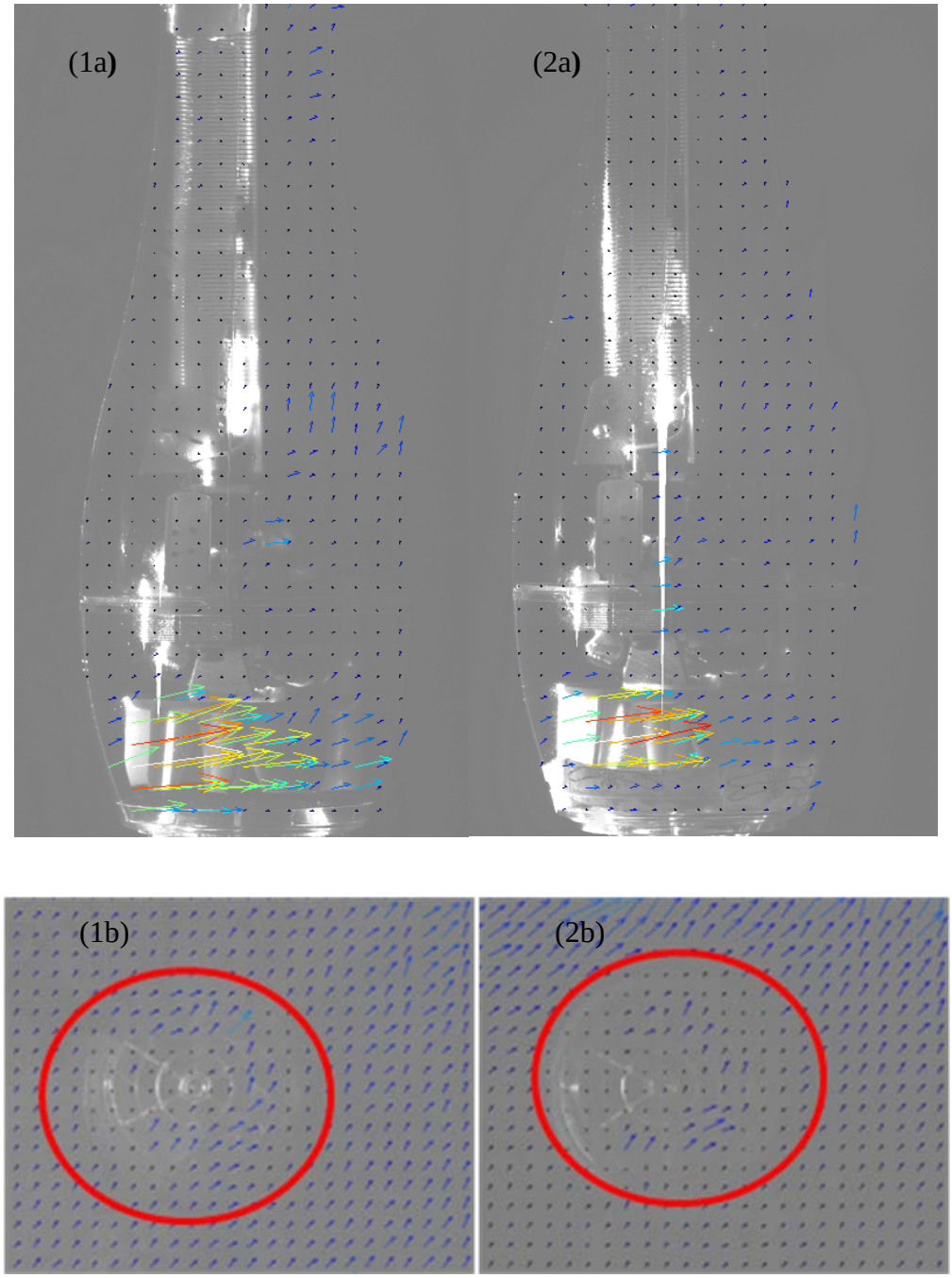

Figure 2.15: PIV measurement results of V_{rms} at the middle plane (1a) Smooth backing enclosure and (2a) Rough backing enclosure; at the inlet (1b) Smooth backing enclosure and (2b) Rough backing enclosure

(1c)

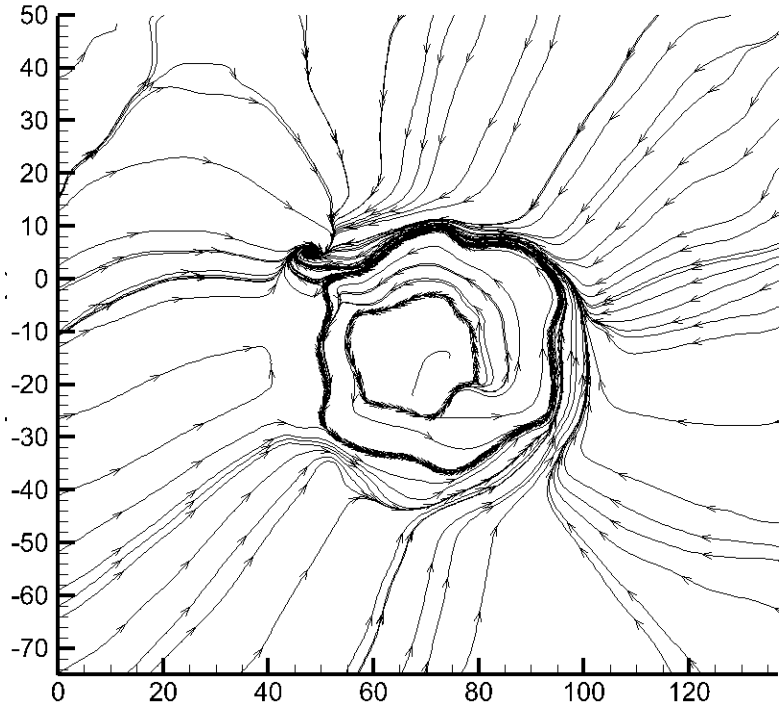

(2c)

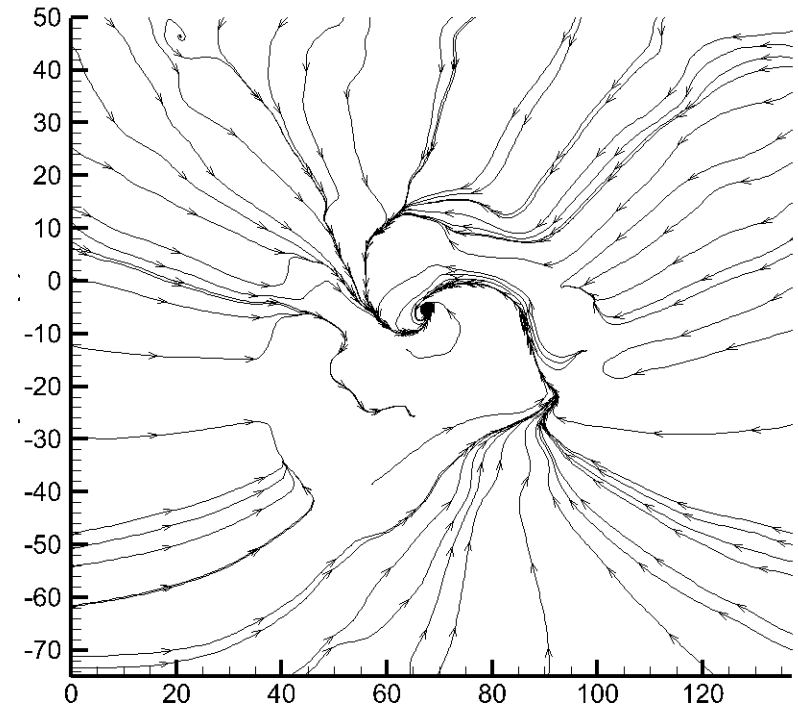

Figure 2.16: Trace line of hairdryer at the inlet surface from post-processing of PIV measurement (1c) Smooth enclosure and (2c) Rough backing enclosure

2.5 Summary of noise identification

With the aid of different aspects of test, the dominant noise sources can be classified. Having done the vibration test on the enclosure, peak A around 280 Hz in the sound spectrum is attributed to the motor operation. For the experiments regarding the utilization of the roughness at the inlet and rubber ring in the vacancy volume at the inlet of the casing and the PIV measurement, broadband noise C at 800 Hz is attributed to the unsteady inlet flow and can be eliminated through the modification of inlet configuration. Peak D at 4480 Hz noise is the 2^{nd} BPF and with the application of rough surface or rubber ring the first BPF noise of 2241 Hz will be increased. Summaries of the noise sources are shown as follows:

(1) Peak A: motor noise is 280 Hz

(2) Broadband noise C: unsteady inlet flow 800 Hz

(3) Peak D: 2241 Hz BPF noise and second harmonic at 4482 Hz.

Chapter 3 Theoretical and numerical study of MPP housing device controlling a dipole source

3.1 Introduction

Having accomplished the noise source identification of the hairdryer, the key work is to develop a proper noise control method that can be adopted to the duct-fan systems like hairdryer to providing quieter products. When the fan operates at low rotational speed such as in domestic product, the low frequency noise component is normally dominant with a broadband and it is very annoying. Aiming to design a broadband passive noise control device which can work effectively from low to medium frequency range without pressure drop, Huang (2002) introduced the concept of a drum-like silencer which is formed by an expansion chamber with light membranes covering on the side-branch cavities under a fairly high tension. To ease the installing process without any machine for exerting force, the membranes have been replaced by plate (Huang, 2006) and non-uniform plate (Wang *et al*., 2007) and even plate with perforations (Wang *et al*., 2012). Considering that the duct length is usually limited in the real application, thus the silencer would be installed close to the sound source. Liu *et al*. (2012) developed a tensioned membrane housing to control the ducted-fan noise which is a dipole nature at the source position undergoing sound cancellation mechanism. But the requirement of the extra mechanism for the entering tension on the membrane

restricts its real application. Although the tension needed is relatively small, the whole system is still complex for construction and difficult for maintenance. Therefore, a MPP housing device sharing the feature of drum-like silencer with clamped MPP covering on the two side-branch cavities to control dipole sound source is developed. This chapter focuses on the establishment of theoretical model, numerical validation and investigation of the sound attenuation mechanism of such vibro-acoustic coupling device.

3.2 Theoretical model of MPP housing device

A two-dimensional model of cavity-backed MPP housing a dipole sound source is shown in Figure 3.1. It consists of a rectangular duct with height h^* and two rigid side-branch cavities with length L_c^* and depth h_c^*. The cavities are covered by two pieces of MPP equal to the cavity length. For the convenience of installing in the application or the experiment validation, the clamped boundary is preferred. Therefore, the two ends of the plate are set as fixed boundary forming part of the otherwise rigid duct. A dipole source which is applied to simulate fan noise is located at the mid-point of the MPP: $x^*=0.5\,L^*$, $y^*=0.5\,h^*$.

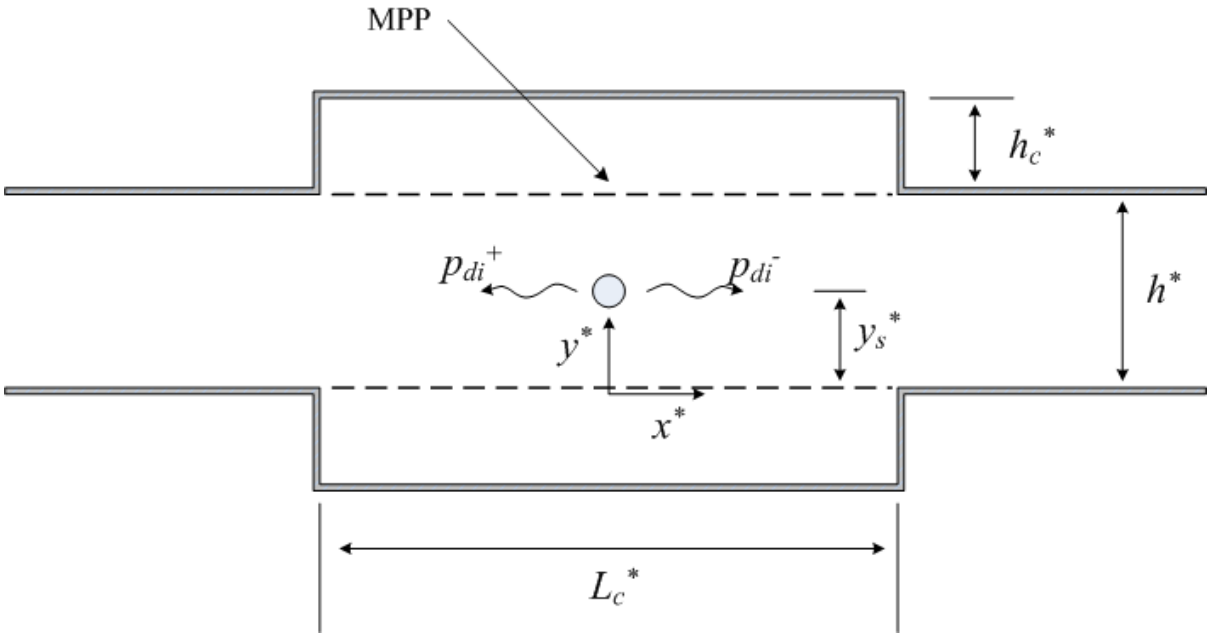

Figure 3.1: Theoretical model of the dipole noise control by MPP with back cavities

For convenience, all variables are non-dimensionalized by three basic quantities, air density ρ_0^* , duct height h^* , and speed of sound in free space c_0^* as follows:

$$x=\frac{x^*}{h^*},\ y=\frac{y^*}{h^*},\ h_c=\frac{h_c^*}{h^*},\ L=\frac{L^*}{h^*},\ L_c=\frac{L_c^*}{h^*}$$
$$f=\frac{f^*h^*}{c_0^*},\ \omega=\frac{\omega^*h^*}{c_0^*},\ k_0=2\pi f,\ m=\frac{m^*}{\rho_0^*h^*}$$
$$B=\frac{B^*}{\rho_0^*c_0^{*2}h^{*3}},\ F=\frac{F^*}{h^*\rho_0^*(c_0^*)^2},\ p=\frac{p^*}{\rho_0^*(c_0^*)^2} \qquad (3.1)$$

where *m* stands for the mass ratio of plate, *B* is the non-dimensionalized bending stiffness of the panel, *F* is the concentrated force exerted on the fluid by the dipole source, and *p* is the sound pressure. Based on such a normalization scheme, the first cut-on frequency of the duct with rigid walls is *f*=0.5. Whenever a dimensional variable is used, there would be a star symbol together a physical unit.

Otherwise, all variables in current study are considered as dimensionless based on the above normalization scheme.

The dipole sound waves p_d radiated from the mid-point to upstream for $x< 0.5L$ and downstream side for $x>0.5L$ inside a duct is expressed as Rodarte and Miller (2001):

$$p_d = \sum_{n=0}^{\infty} \frac{(2-\delta_{0n})F\cos(n\pi/2)\cos(\mathrm{n}\,\pi y)}{(1-M^2)(k_n^+ - k_n^-)}\left[k_n^+ e^{ik_n^+(x-0.5L)}H(x-0.5L)+k_n^- e^{ik_n^-(x-0.5L)}H(0.5L-x)\right]$$

$$k_n^{\pm} = \mp\frac{-k_0 M - i\sqrt{(1-M^2)(n\pi/h)^2 - k_0^2}}{1-M^2} \tag{3.2}$$

Here $H(x)$ is the Heaviside function, δ_{0n} is Kronecker delta function (δ_{0n} = 1 when n=0, otherwise 0), M is the Mach number, $k_0=\omega/c_0$ is the wave number, ω is the angular frequency, c_0 is the speed of sound and n is any integer.

The radiated sound waves from the dipole source excite the panel into vibration with a transverse displacement of complex amplitude η in the y direction with velocity $v_p=\partial\eta/\partial t$. In the real case, the panel should be 3D plate. In the simplified 2D model, the panel will be treated as a 2D beam. The vibrating panel will radiate sound into the duct and cavity which are denoted by p_{rad} and p_{cav} respectively. The vibration of the panel at y=0 with the pressure difference between the duct and the cavity is governed by

$$\frac{B}{i\omega}\frac{\partial^4 v_p}{\partial x^4} + mi\omega v_p + p_d + p_{rad} - p_{cav} = 0 \tag{3.3}$$

Considering the micro-perforation in the MPP, it can be regarded as a lattice of sub-millimeter holes distributed uniformly over the plate surface. For the existing

of sound pressure difference between the two sides of the plate, there will be air particles vibration produced in the holes. For the wavelength of the impinging acoustic waves will be much larger than the orifice diameter, the distribution of air particle velocity of each hole is considered as uniform within the area. The interaction between the air and rigid structure is governed by the following equation given by Takahashi and Tanaka (2002):

$$Z_{i,resist}(v_0 - v_p) + Z_{i,react}v_0 + (p_d + p_{duct} - p_{cav}) = 0 \tag{3.4}$$

$$\text{with} \quad Z_{i,resist} = \frac{32\mu t}{\rho_0 c_0 d^2}\left[\left(1+\frac{K^2}{32}\right)^{1/2} + \frac{\sqrt{2}}{32}K\frac{d}{t}\right] \quad \text{and} \tag{3.5}$$

$$Z_{i,react} = i\cdot\frac{\omega t}{\sigma c_0}\left[1+\left(1+\frac{K^2}{32}\right)^{-1/2} + 0.85\frac{d}{t}\right] \tag{3.6}$$

where v_0 is the particle velocity of fluid in the holes, $K = d\sqrt{\omega\rho_0 / 4\mu}$, d is the hole diameter, t is the panel thickness, σ is the perforated ratio, μ is the coefficient of viscosity, ρ_0 is the air density, and c_0 is the air speed. The real part $Z_{i,resist}$ is the acoustic resistance which relates to the energy radiation and viscous losses. The imaginary part $Z_{i,react}$ is called the acoustic reactance which in nature is the inertial.

The average velocity of whole plate with micro-perforations associated with the plate vibration and the particle velocity in the holes, $\overline{V}(x)$, is defined as $\overline{V}(x) = (1-\sigma)v_p(x) + \sigma v_0(x)$. Eqs. (3.3) and (3.4) can be solved by standard Galerkin procedure and v_p is expanded as a series of *in-vacuo* modes φ_j by clamped-clamped MPP with modal amplitude $V_{p,j}$,

$$v_p(x) = \sum_{j=1}^{\infty} V_{p,j}\varphi_j(\xi), \quad \xi = x/L + 1/2;$$

$$\text{where} \quad \phi_j(\xi) = \frac{1}{2}(1-\varepsilon_j)e^{\lambda_j \xi} + \frac{1}{2}(1+\varepsilon_j)e^{-\lambda_j \xi} + \varepsilon_j \sin(\lambda_j \xi) - \cos(\lambda_j \xi); \tag{3.7}$$

$$with \quad \varepsilon_j = \frac{\cosh(\lambda_j) - \cos(\lambda_j)}{\sinh(\lambda_j) - \sin(\lambda_j)}, \cos(\lambda_j)\cosh(\lambda_j) = 1.$$

Similarly, the mean velocity of surrounding air $\overline{v}_0 = \sigma v_0$, can also be expanded over the same series $\varphi_j(\xi)$ as

$$\bar{v}_0(x) = \sum_{j=1}^{\infty} \overline{V}_{0,j}\varphi_j(\xi), v_0 = \sum_{j=1}^{\infty} V_{0,j}\varphi_j(\xi), \text{ with } V_{0,j} = \frac{\overline{V}_{0,j}}{\sigma} \tag{3.8}$$

Hence, Eq. (3.3) and Eq. (3.4) become

$$\left\{ \frac{B}{i\omega}\left(\frac{\lambda_j}{L}\right)^4 + mi\omega \right\} V_{p,j} + \int_0^1 (p_d + p_{rad} - p_{cav})\varphi_j(\xi) d\xi = 0 \tag{3.9}$$

$$Z_{i,resist}(V_{0,j} - V_{p,j}) + Z_{i,react}V_{0,j} + \int_0^1 (p_d + p_{rad} - p_{cav})\varphi_j(\xi) d\xi = 0 \tag{3.10}$$

The radiated pressure in the duct P_{rad} from the plate at y=0 can be calculated as Doak (1973):

$$p_{rad}(x,y) = \frac{L}{2}\sum_{n=0}^{\infty} c_n \psi_n(y) \times \int_0^1 V(x')\psi_n(0)[H(x-x')e^{-ik_n(x-x')} + H(x'-x)e^{+ik_n(x-x')}]d\xi' \tag{3.11}$$

$$\text{with} \quad c_n = \frac{i}{\sqrt{(n\pi/\omega)^2 - 1}}, \quad k_n = \frac{\omega}{c_n}, \quad \psi_n = \sqrt{2 - \delta_{0n}}\cos(n\pi y) \tag{3.12}$$

and c_n is the modal phase speed, k_n is the modal wave number, and ψ_n is the modal velocity potential. The value of x' varies within the range of [-L/2, L/2].

The sound pressure inside the cavity with rigid walls can be delivered in terms of acoustic modes *r* and *s* with light damping (Cheng *et al*., 2005)

$$P_{cav}(x,y)=\sum_{r,s}^{\infty}\frac{-i\omega\phi_{rs}(x,y)}{L_C h_C(\kappa_{r,s}^2-k^2+2i\zeta_{r,s}\kappa_{r,s}k)}\int_0^1 V(x',0)\phi_{rs}(x',0)dx' \tag{3.13}$$

$$\text{with } \phi_{rs}(x,y)=\sqrt{(2-\delta_{0r})(2-\delta_{0s})}\cos(\frac{r\pi x}{L_C})\cos(\frac{s\pi y}{h_C}),\ \kappa_{rs}=\sqrt{(\frac{r\pi}{L_C})^2+(\frac{s\pi}{h_C})^2} \tag{3.14}$$

where $\zeta_{r,s}$ is the damping ratio of the (*r*,*s*) acoustics mode, and $\kappa_{r,s}$ is the corresponding acoustic wave number. In current study, the damping effect is ignored first and the damping ratio is a rather small value near zero.

The modal coefficient of dipole sound waves I_{dj} , the duct modal impedance $Z_{rad,j}$ and the cavity modal impedance $Z_{cav,j}$ are defined as

$$\begin{aligned} I_{dj} &= \int_0^1 p_d\varphi_j(\xi)d\xi \\ Z_{rad\,j} &= \int_0^1 p_{rad}\varphi_j(\xi)d\xi \\ Z_{cav\,j} &= \int_0^1 p_{cav}\varphi_j(\xi)d\xi \end{aligned} \tag{3.15}$$

As a result, Eqs. (3.9) and (3.10) become

$$[(B/i\omega)(\lambda_j/L)^4+mi\omega]V_{p,j}+(Z_{rad}-Z_{cav})[(1-\sigma)V_{p,j}+V_{0,j}]=-I_{dj} \tag{3.16}$$

$$Z_{i,resist}(V_{0,j}-V_{p,j})+Z_{i,react}V_{0,j}+(Z_{rad}-Z_{cav})((1-\sigma)V_{p,j}+V_{0,j})=-I_{dj} \tag{3.17}$$

respectively.

Eq. (3.16) and Eq. (3.17) are expressed into the matrix format,

$$\begin{bmatrix} (B/i\omega)(\lambda_j/L)^4+mi\omega+(Z_{rad}-Z_{cav})(1-\sigma) & (Z_{rad}-Z_{cav}) \\ -Z_{i,resist}+(Z_{rad}-Z_{cav})(1-\sigma) & Z_{i,resist}+Z_{i,react}+(Z_{rad}-Z_{cav}) \end{bmatrix}\begin{bmatrix} V_{p,j} \\ V_{0,j} \end{bmatrix}=-\begin{bmatrix} I_{dj} \\ I_{dj} \end{bmatrix} \tag{3.18}$$

Having done the transformation, the mode amplitudes $V_{p,j}$ and $V_{0,j}$ can be obtained. Then the sound pressure transmitted to the upstream and downstream side of the duct can be expressed as

$$P_{radup}(x,y)\big|_{n=0,x\to-\infty}=\frac{L}{2}\sum_{j=1}^{\infty}V_j\int_0^1\varphi_j(\xi)e^{ik_0(x-x')}d\xi' \tag{3.19}$$

$$\text{and } P_{raddn}(x,y)\big|_{n=0,x\to+\infty}=\frac{L}{2}\sum_{j=1}^{\infty}V_j\int_0^1\varphi_j(\xi)e^{-ik_0(x-x')}d\xi' \tag{3.20}$$

Equations (3.2)-(3.20) are solved in a coupled manner. The sound insertion loss (*IL*) defined as the acoustical power loss resulting from insertion of silencing device is computed out in the following strategy: integrate the sound energy at the exits of straight duct with uniform cross section area with identical length of silencing device to obtain the reference value; then subtract the sound energy at the silenced duct outlets with same sound source. So the insertion loss actually depends on the sound power difference at the omelets of the reference duct and the silencing device.

$$IL=10\log10\left(\frac{\int_{str}|p|^2ds}{\int_{mpp}|p|^2ds}\right) \tag{3.21}$$

where p is the pressure at the duct outlets, the "*str*" refers to the straight duct without MPP housing device as reference, and "*mpp*" refers to the duct with MPP and backing covered cavity.

3.3 Numerical results and discussion

The analytical model is mainly used to provide the fundamental understanding of the vibro-acoustic coupling among the acoustic field in duct, cavity and the panel vibration in a mathematical way. In order to give instructions to the design of such a MPP housing device with different geometries and configurations, there is a need to adopt the finite element tool for numerical simulation to ease the parametric study as well as design and modification process. The commercial software Comsol Multiphysics® for numerical simulation is employed because of its strong multi-physics capability. In the numerical simulation, two domains are considered. One is two-dimensional domain for fluid to describe the sound wave propagation in the duct and cavity. Another is the two-dimensional domain for the structural vibration of the panel with micro-perforation properties. With the length L_c =3 and height h_c=0.5 for the cavity, the mesh size of 0.1 for both duct and cavity, a total of 5,400 triangular elements are used for the fluid domain and 150 nodes are used for the perforated panel. In the analytical calculation, the duct mode number is truncated as 40 and the panel's vibration mode is 25. In the current study, the damping ratio is set as 0 at first as the main target is to examine the effect of geometry configuration, panel mass and bending, perforation properties to the sound attenuation performance of the proposed device. Besides, the panels used in the experiment are balsa wood and stainless steel, and the damping ratios of the materials are rather small.

The comparison between analytical solution for M=0 (without flow) and finite element simulation is shown in Figure 3.2. The normalized mass of the panel is m=0.2 and the bending stiffness is B=0.0014 with perforation ratio of 2.7% and hole size d^*=0.1 mm. The analytical solution is shown as a solid line, and the

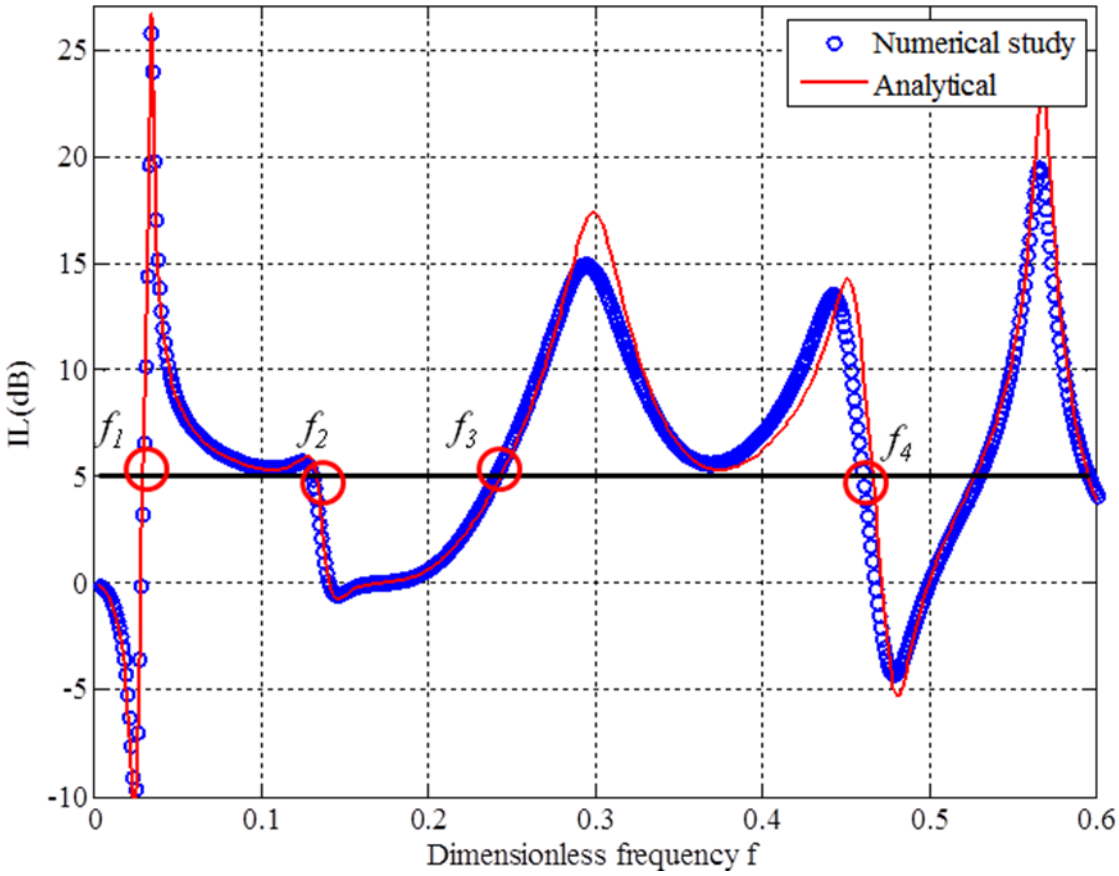

Figure 3.2: Comparison between the numerical calculation (open circles) and the analytical solution (solid line) for the dimensionless parameters of length Lc=3, mass m=0.2, and bending stiffness B=0.0014 with perforation 2.7% of hole size d^*=0.1 mm. The circles indicate the location of starting point and ending point in IL spectrum that the IL is greater than the criterion level $ILcr$ =5 dB

numerical prediction is given as open circles. There is no visible difference between the two IL spectrum curves at the frequencies below f < 0.25. The accuracy of the analytical calculation depends on the duct mode number and the panel's vibration mode number. For the numerical simulation, the accuracy depends on the mesh size and total number of mesh elements. For a better match between the analytical and numerical results, the duct mode number and the panel's vibration mode number should be larger in the analytical calculation, and the mesh size in the numerical simulation should be smaller. In that case, more

computer resources will be required and the calculation time will be much longer. Although some deviations at the peaks and minor frequency shifts around the spectral peaks, the main concern in the current study is to widen the stopband of the proposed design and therefore this finite element simulation is considered as a proper way for design purpose in this study. The circles located in the spectrum marked as f_1 and f_2 indicate the lower limit and upper limit of the stopband in the low frequency region, and the f_3 and f_4 represent the lower and upper limit of stopband in the medium frequency.

3.3.1 Parametric study of panel properties

The performance of such device is characterized by the widest stopband that can be achieved. In order to achieve the effective abatement of noise at the first and second blade passage frequency at the same time, one or two stopbands covering these two frequencies are the design target. Here, two stopbands refer to the frequency range, $f \in [f_1\ f_2]$ in low frequency range and $f \in [f_3\ f_4]$ in medium frequency respectively in which the *IL* is above a criterion level IL_{cr} (see Figure 3.2). The criteria value IL_{cr} is defined as the maximum noise reduction achieved by the simple expansion chamber with the same geometry size of current MPP housing device. Huang *et al*. (2010) pointed out that the maximum *IL* can be observed at the frequency approaching zero when the device is used to control the dipole noise at the source position.

Moreover, the cost function for the optimization of the performance is set as the ratio of the band limits $f_r = f_2/f_1$ and f_4/f_3. The performance of such MPP housing

device used for controlling fan noise radiation depends on many parameters such as geometric configurations of cavity, length of panel, structural properties and perforation parameters. In order to begin with the investigation of parametric effect, majority of the variables are fixed first. Aiming to develop a MPP housing device with a compactable geometry to control the ducted-fan noise, the cavity is fixed at length L_c=3 and height h_c=0.5. In this configuration, the IL_{cr} is 5 dB. Results of the performance optimization of the structural properties of the panel without perforations are shown in Figure 3.3.

Figure 3.3(a) to Figure 3.3(d) show the optimal bending stiffness, the maximum bandwidth, lower and higher band limit as functions of m for the clamped panel. As shown in Figure 3.3(b), when the panel mass keeps increasing, the maximum bandwidth will decrease roughly. In the range of m<0.8, the maximum bandwidth can be achieved at least 3.95. The performance of the proposed device deteriorates as m increases. It is because *IL* drops below the criterion level for heavy panel that result in narrow stopband. Figure 3.3(a) suggests that the optimal bending stiffness remains at around B_{opt}=0.0014 when $m \le 0.4$ and then gradually falls to a low bending stiffness of B_{opt}=0.0007. Roughly speaking, the optimal performance can be obtained under two conditions: $0.0013 \le B_{opt} \le 0.0015$ and $m \le 0.4$. As shown in Figure 3.3(d), when the panel mass increases, the upper band limit f_2 decreases too. On the other hand, the lower band limit remains almost the same value f_1=0.0308 when m<0.3 and then it decreases as m increases for m>0.3. As the bandwidth is the ratio between the upper band limit and lower band limit, together with the fact that the decrease speed of two band limits are different, the decrease trend of bandwidth will be different from the others. With 7 fan blades and rotational speed of 4000 *rpm*, the dimensionless first and second blade passage

frequency are about 0.14 and 0.28 respectively with respect to the duct height of 0.1 m. In order to control the dominant noise at the first and second blade passage frequency effectively, the upper band limit cannot be lower than 0.14 and hence the optimal mass ratio m=0.2 and bending stiffness B_{opt}=0.0014 are chosen.

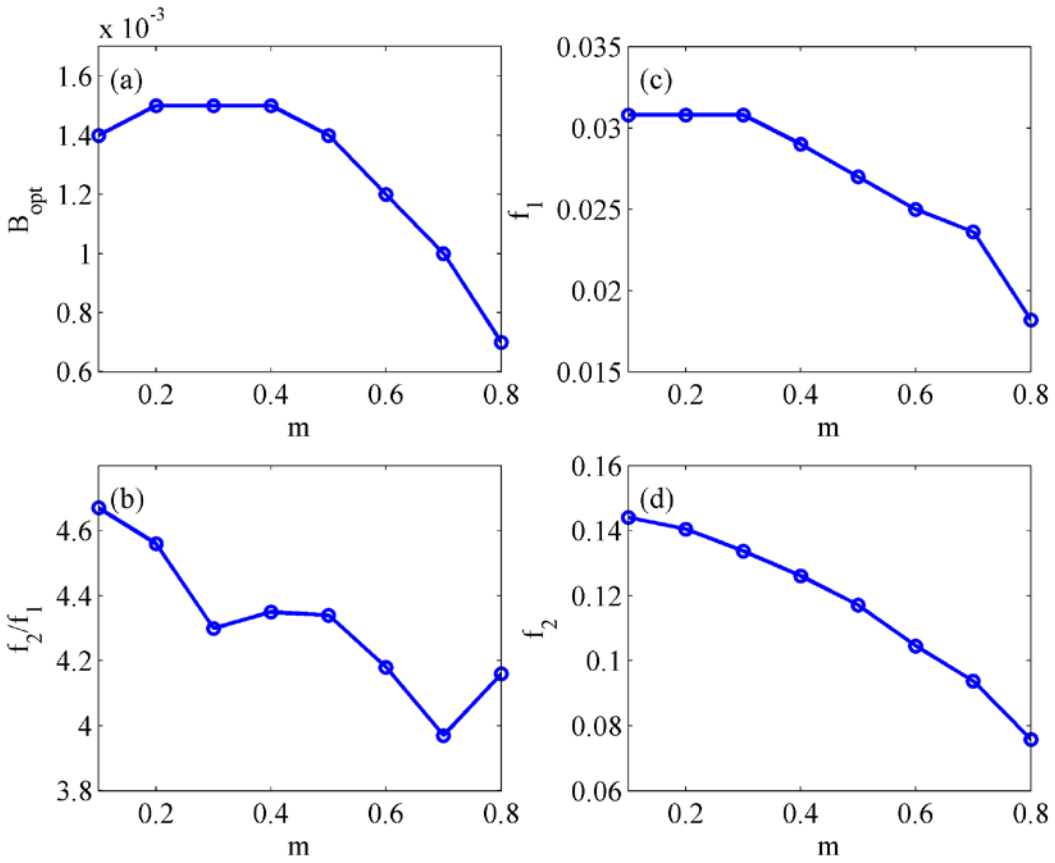

Figure 3.3: Mass ratio and bending stiffness effect study. (a) the variation of the optimal bending stiffness B_{opt} with mass m; (b) the variation of frequency ratio f_r (f_2/f_1); (c) the dimensionless lower band limit f_1; (d) the dimensionless upper band limit f_2 varies with mass m

By fixing the mass ratio of m=0.2 and bending stiffness of B=0.0014, other influential parameters such as perforated ratio and hole size of MPP have to be varied in order to optimize the performance. Figure 3.4(a) shows the comparisons

of *IL* of the proposed device with various hole sizes of MPP when perforation ratio is kept to be 1%. When the dimensional diameter of the hole d^*=0.1 mm, two peaks around the frequency range of f=0.04 to f=0.14 are observed. When the dimensional diameter is increased to 0.3 mm or 0.5 mm, the second peak drops drastically such that the trough point between f_1 and f_2 gradually falls below the criterion level IL_{cr}. So it results in very narrow stopband of 5 dB.

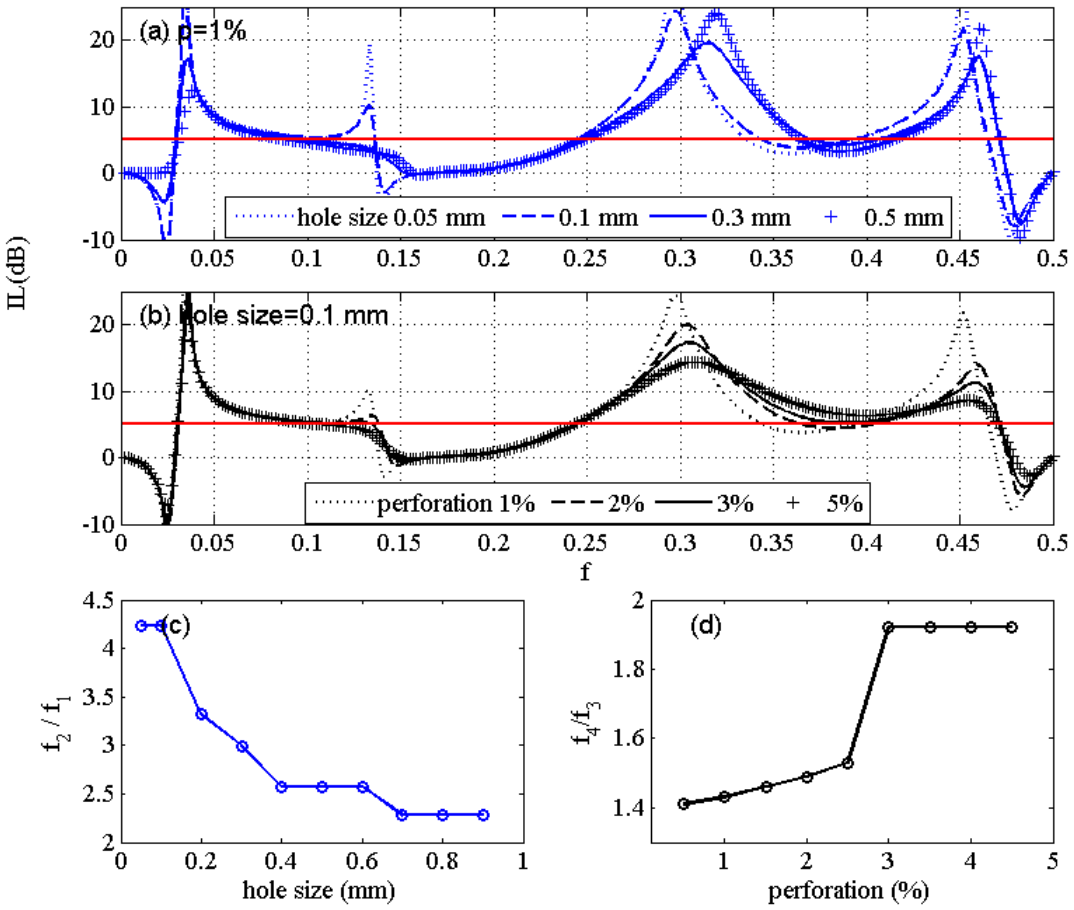

Figure 3.4: Perforation and hole size effect investigation of panel under optimal mass and bending stiffness: (a) the *IL* performance with variation of hole size, perforation fixed; (b) the *IL* performance with change of perforation as hole size d^*=0.1 mm; (c) variation of frequency ratio f_2/f_1 when hole size is varied (fixed perforation 1%); (d) variation of frequency ratio f_4/f_3 when perforation is changed (fixed d^*=0.1 mm)

Figure 3.4(b) shows the variation on the *IL* spectrum for different perforation ratios when the diameter of hole is fixed to be 0.1 mm. When the perforation ratio varies from 1% to 3%, the second peak slightly drops but it has no noticeable influence on the stopband in the frequency range of f=0.04 to f=0.14. On the other hand, the trough point at frequency around f=0.4 raised up with the increase of perforation ratio such that the stopband is widened in the frequency range of f=0.24 to f=0.48. This means that the effect of perforation may be beneficial for widening stopband at medium frequency range. Figure 3.4(c) shows the stopband ratio of f_2/f_1 as a function of hole size perforation while Figure 3.4(d) depicts the stopband ratio of f_4/f_3 as a function of perforation ratio. Roughly speaking, the stopband ratio f_2/f_1 decrease monotonically with the diameter of the holes when diameter increasing from 0.1 mm as shown in Figure 3.4(c). The Figure 3.4(d) shows that the stopband ratio f_4/f_3 grows from about 1.4 to 1.92 and then remains constant when perforation reaches 3%. In summary, the widest frequency band [f_1 f_2] can be obtained with perforation around 3% with the diameter of the hole of about 0.1 mm. This perforation property can be helpful for obtaining quite desirable performance in the range of [f_3 f_4] simultaneously.

3.3.2 Performance and sound suppression factor among

Figure 3.5 compares the *IL* performance of the proposed device with and without plate and plate with micro-perforations as well as the membrane housing introduced by Liu *et al*. (2012). The *IL* curve of the proposed plate housing the dipole source without perforation with B=0.0014, previously determined as the

optimal bending stiffness is shown as the dashed line. The performance MPP housing device is indicated in solid line with symbol '+' and membrane housing device with same configuration for controlling dipole source is shown as the solid line.

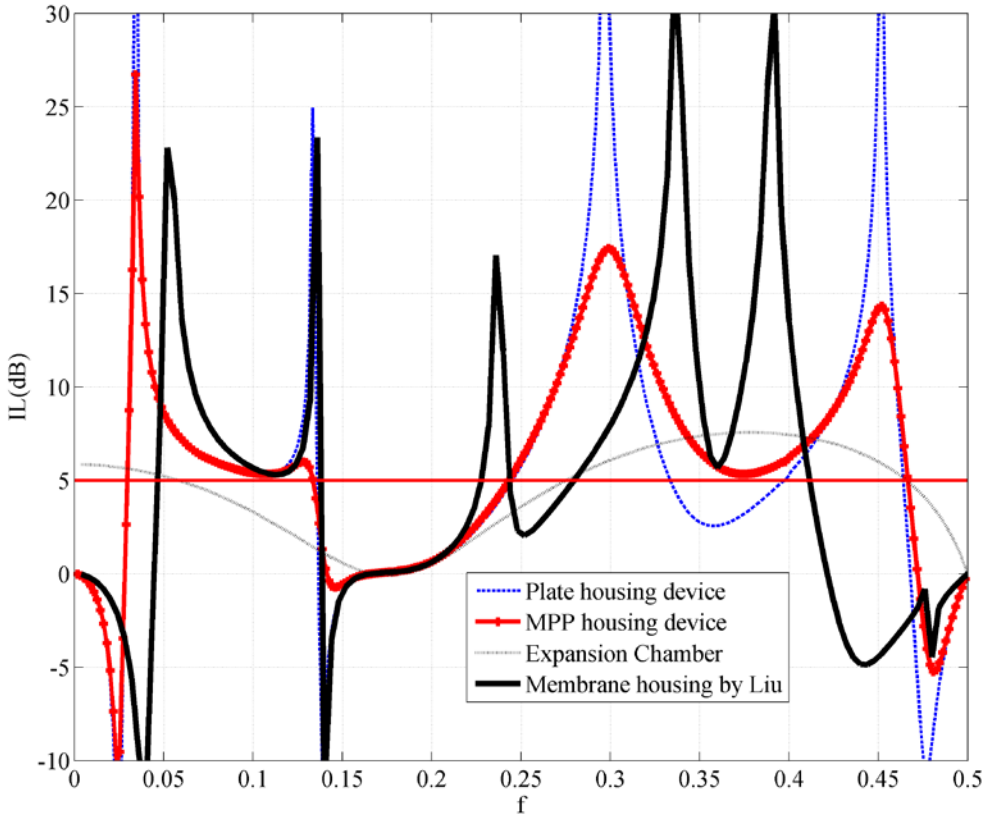

Figure 3.5: Comparison of the *IL* spectra among the plate housing device (dashed line), MPP housing device (solid line with symbol '+') with optimal panel parameters and the expansion chamber (dotted line) as well as membrane housing device (solid line) with same configuration for controlling dipole source

For the plate housing device, two peaks are observed at the low frequencies, which are caused by the sound cancellation between the radiated sound from the dipole source with anti-phase relationship and radiated sound from the panels. The

stopband begins from f_1=0.03 and stops at f_2=0.14, corresponding to f_2/f_1=4.7. Besides, the third peak is observed in the middle frequency range and the stopband ranges from f_3=0.246 to f_4=0.33, corresponding to f_4/f_3=1.34. With these two stopbands at low and middle frequency range, the proposed device with panel is effective for controlling the ducted-fan noise with the first and second blade passage frequency range of f=0.12 to f=0.14 and f=0.24 to f=0.28 respectively. When perforations with σ=3% and dimensional diameter d^*=0.1 mm is introduced into the panel, the second peak slightly drops but the width of stopband has no noticeable change. The trough point between the third and fourth peak lift up so that a wide stopband $f\in$[0.24 0.485] of 5 dB is obtained. It is beneficial for controlling the fan noise at wider working band of first and second blade passage frequency. Comparing with the tensioned membrane housing the dipole source with same cavity height, the MPP housing device achieve a lower frequency limit at f_1=0.03 such that the stopband at the low frequency regime has an encouraging improvement. In addition, the stopband at middle frequency range is also widened.

3.3.3 Sound radiation efficiency investigation

In order to understand the physics behind of the formation of *IL* trough and peak in the *IL* spectrum, the sound radiation efficiency is employed to investigate the source radiation ability in various kinds of configurations and the sound suppression factor is introduced to examine the noise restrain effect of the housing device. The sound radiation efficiency ξ_r (Squicciarini *et al*., 2014) and sound suppression factor (F_s) are defined as

$$\xi_r = \frac{W_s}{W_{str}} \text{ and } F_s = 1 - \frac{W_{outlets}}{W_{str}} \tag{3.22}$$

where W_s is the total sound power radiated by the source obtained by integrating all the sound power including the part radiated to the outlets and the part absorbed by the MPP. $W_{outlets}$ is the sound power at the outlets of housing device and W_{str} is the sound power of source in the straight duct. Regarding this, the sound radiation efficiency in a straight duct without any silencing should be 1 for there is no change of sound power. Figure 3.6(a) is the *IL* spectrum comparison among expansion chamber (solid line), plate housing a dipole without perforation (line with "x" symbol) and MPP housing device (dashed line). Figure 3.6(b) and 3.6(c) show total sound power radiated out and corresponding sound radiation efficiency respectively. The given dipole source is 10Pa, and the sound power radiation in straight duct is 25 watts with the duct height h=1. The conclusion can be clearly given that the ability of sound power radiation will be varied when the source is put into different geometries as demonstrated in the sound radiation and radiation efficiency figures. For plate and MPP housing device, the sound power radiated out is very high in the frequency range of f=0.024 to f=0.14 in which negative *IL* is obtained. This is due to the too strong radiation from the plate or MPP to the outlets. On the other hand, there is 70% deduction of sound power radiation in the frequency range of [0.03 0.13] and [0.24 0.48] with positive *IL*. This also results in high value of sound suppression factor as shown in Figure 3.6(d). Generally, the sound power radiation of MPP housing device is lower than that of plate housing device without perforation in the middle frequency range f=0.33 to f=0.4 and the corresponding suppression factor is increased. This probably implies that the sound cancellation capability between the MPP and dipole sources is reduced but it is compensated with the enhancement of sound absorption by MPP. Therefore *IL* is

increased at this frequency range obtaining a widened effective band in the medium frequencies from f=0.24 to f=0.485.

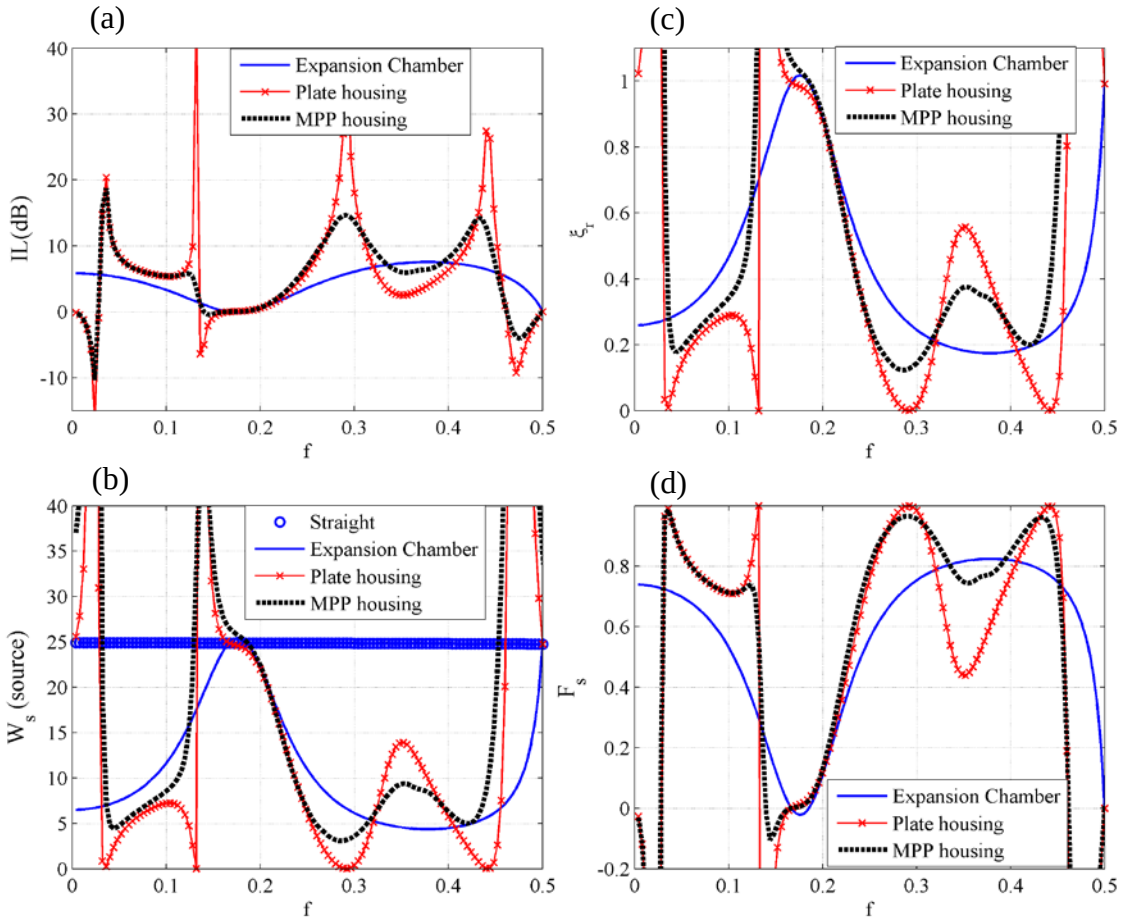

Figure 3.6: Sound radiation of source and sound suppression factor study. (a) *IL* spectrum comparison; (b) Sound radiation of dipole source in different configurations; (c) sound radiation efficiency and (d) sound suppression factor for corresponding housing

3.3.4 Modal Analysis

In order to further investigate the sound radiation of the MPP, the modal response of the default plate at the optimal performance (m=0.2, B_{opt}=0.0014) is studied in this section. In Figure 3.7 the *IL* spectrum is demonstrated on the top row to facilitate the study of the peak. The square symbols with numbers from 1 to 4 denote the first four peaks in the *IL* spectrum. The four columns below illustrate

the responses of first four peaks respectively from different aspects. The vibration of each individual mode $|V_j|$, is shown in the second row. The third row shows the amplitude of the modal radiation coefficient $|R_j|$ of the *jth* mode induced vibration, defined as $R_j = \int_{-L/2}^{L/2} \varphi_j(\xi^{'}) e^{ik_0 x^{'}} dx^{'}$. The last row is the amplitude of the single modal radiation $|V_j R_j|$, which is related to the sound radiation ability from the plate to the outlet of the duct.

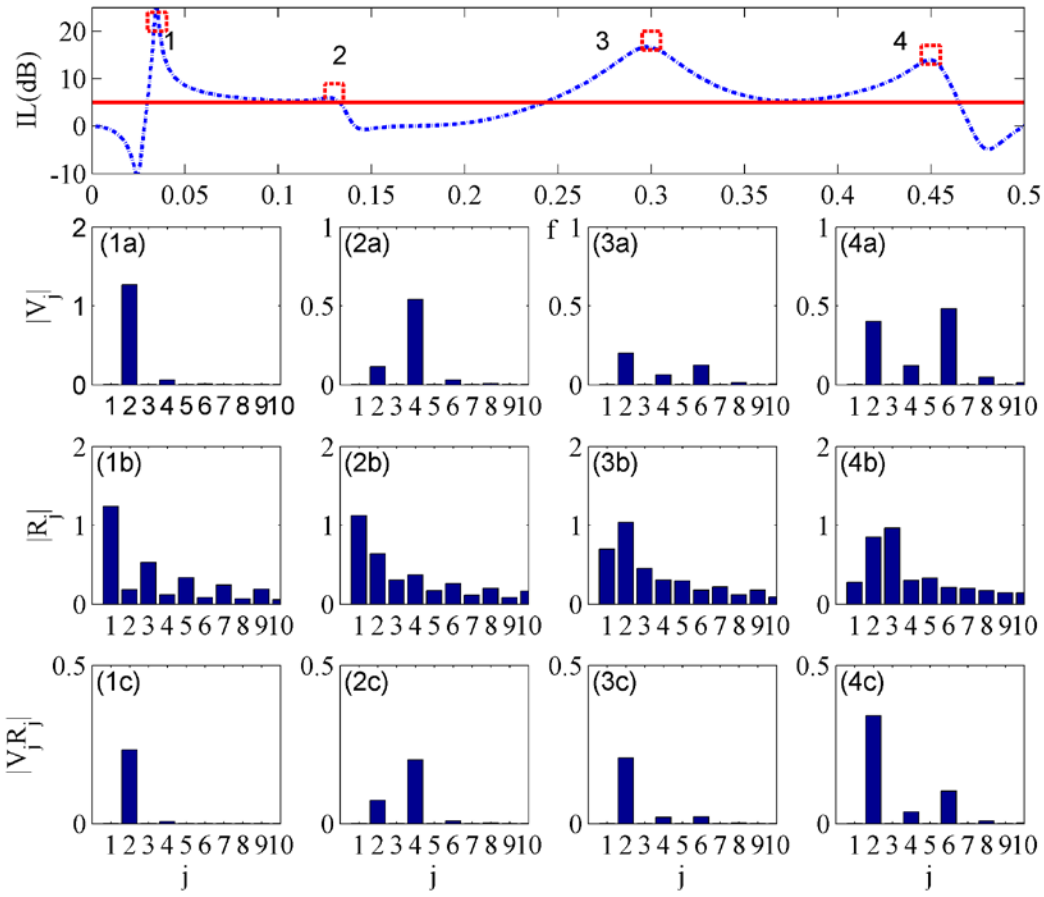

Figure 3.7: Modal radiation analysis with bar chart. The top figure is the *IL* spectrum at the optimal configuration. The second row is the modal amplitude $|V_j|$, the third row is the modal radiation coefficient $|R_j|$, and the last row is the single modal radiation $|V_j R_j|$

At the first peak point (*f*=0.036), there is only one sharp peak in the second mode $|V_2|$ and $|V_2R_2|$; for the second peak (*f*=0.128), (2a) shows that the fourth mode $|V_4|$

dominates although $|R_2|$ is more weighted than $|R_4|$, still resulting in only one peak in the fourth mode of radiation in Figure (2c); the third column demonstrates that the plate vibration is dominated in the second mode at the peak frequency of 0.292 and the last column shows the first three even modes of plate response are critical. As the findings stated above, the plate response in the selected peaks is dominated by the even modes rather than the odd modes in the amplitude of the vibration.

The bar chart shows the modal response of several peak point frequencies but it is still not clear about what happens at other frequencies especially for the troughs. In Figure 3.8, the *IL* spectrum is demonstrated on the top row and the vertical dash lines present the position of trough points in the *IL* spectrum for reference. The four rows below illustrate the responses of first four modes of velocity amplitudes respectively, including all frequencies. The higher order modal responses are rather weak, so only first four modes are analyzed here. The second and forth modal responses are much higher than the odd modal at f=0.024 according to Figure 3.8(a) to Figure 3.8(d). And the magnitude of the second mode response is the highest among them. This means that the second mode is dominant at this frequency and it leads to a very strong sound radiation to the outlet of the duct and thus insertion loss is negative. At trough points of *IL* at f=0.14 and at f=0.48, there are peaks in the second mode $|V_2|$ and fourth mode $|V_4|$ respectively. Moreover, the fourth modal response is dominant for second trough f=0.14 while the first two even modes contributes to the third trough of *IL* at f=0.48 with an equal weighting of influence. Generally speaking, the plate response is dominated by the even modes

of the vibration due to the dipole source nature and the trough points are attributed to the too strong radiation of the sound from the plate to the outlets of duct.

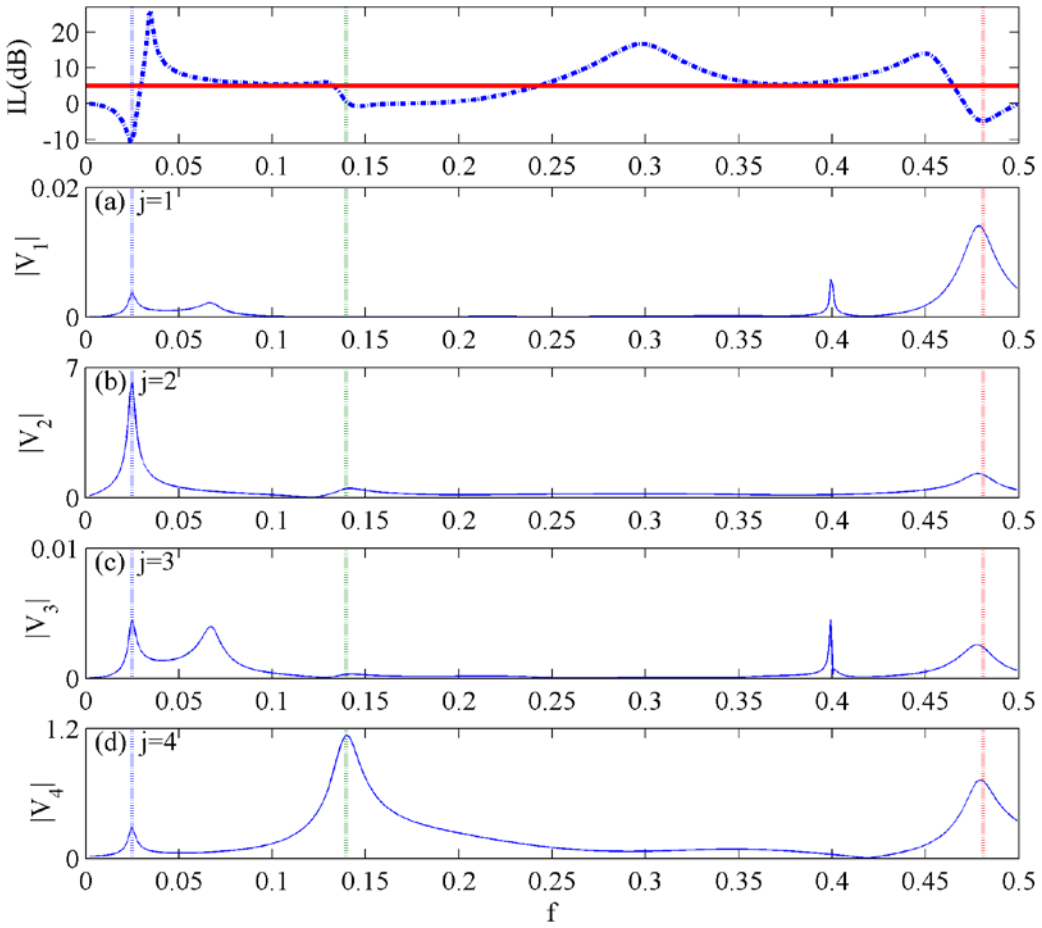

Figure 3.8: Modal radiation analysis. The top figure is the *IL* spectrum at the optimal mass ratio and bending stiffness with 2.7% perforation and hole size 0.1 mm. The following four rows are the corresponding first four modes of modal amplitude $|V_j|$

3.3.5 Sound intensity visualization

In order to understand the sound field distribution at the frequency of trough and peak points, visualization of sound intensity vectors ($\vec{I} = \frac{1}{2}\mathrm{Re}(p\vec{v}^{*})$) as shown in Figure 3.9(a) to Figure 3.9(c) is performed. The first column of each pair shows the real intensity field in the MPP housing device and the second column is the "normalized" vector fields which mean that the lengths of the intensity vectors have all been drawn the same in order to emphasize the directional nature of the intensity field (Russell *et al*., 2013).

(1a) *f*=0.024 (2a) *f*=0.024

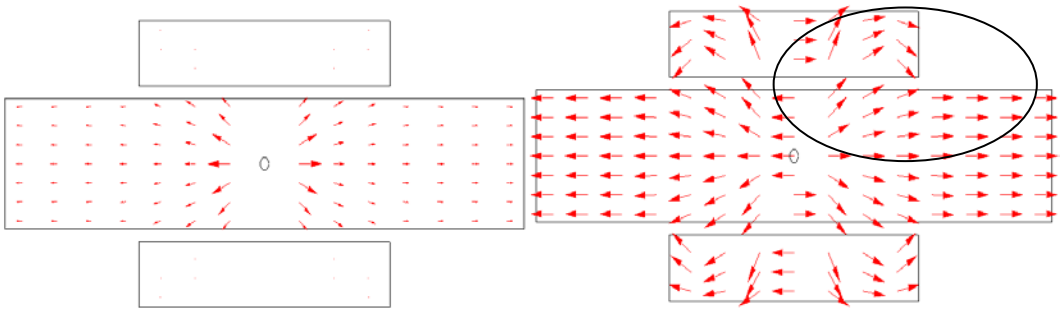

(1b) *f*=0.036 (2b) *f*=0.036

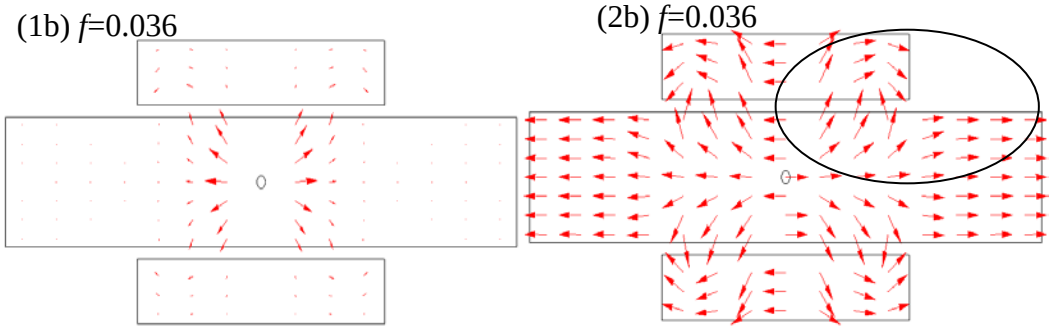

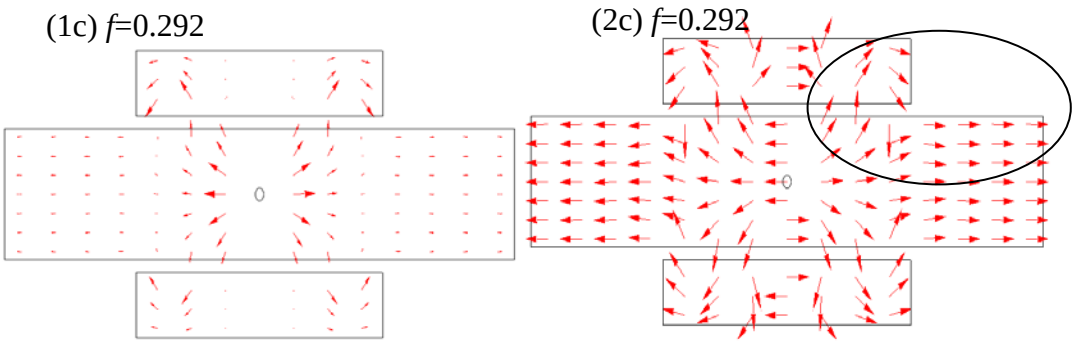

(d) Angle difference

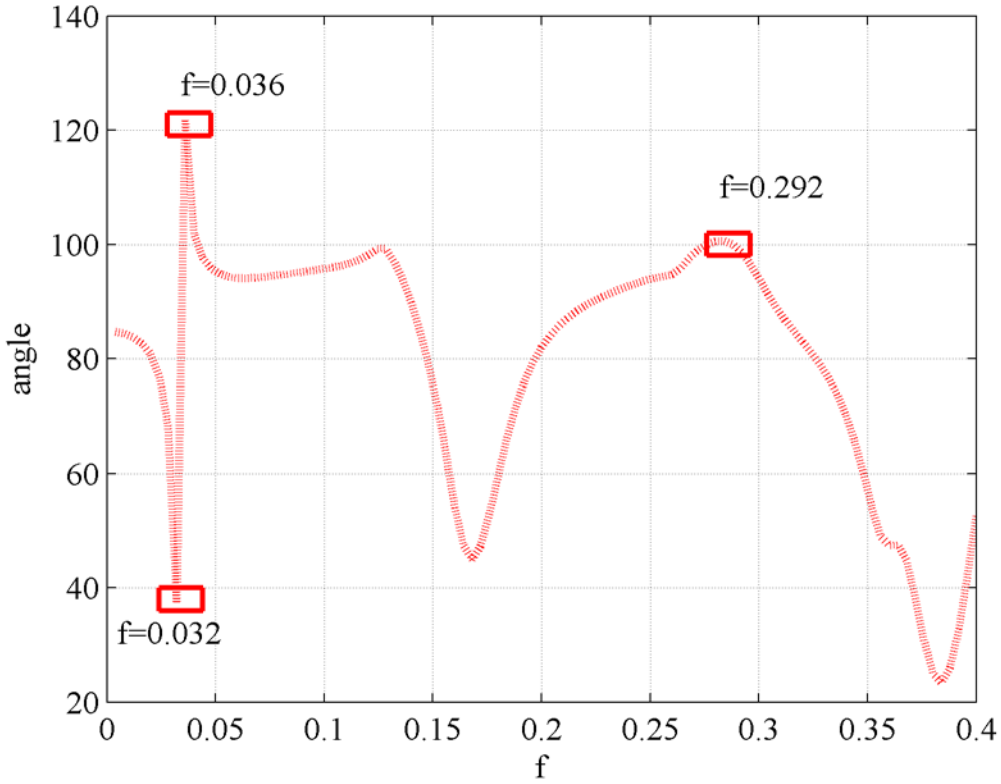

Figure 3.9: Sound intensity field plot (1a) real intensity field and (2a)"normalized" vector field at *f*=0.024; (1b) real intensity field and (2b)"normalized" vector field at *f*=0.036; (1c) real intensity field and (2c)"normalized" vector field at *f*=0.292; and (d) Angle difference of the intensity flow between the cavity and duct

At the trough point of *IL* at *f*=0.024, Figure 3.9(1a) and Figure 3.9(2a) indicate that the energy flow in the cavity starts from the centre, one part moving clockwise to MPP trailing edge (right hand side and downstream) and the other part traveling anti-clockwise to the leading edge (left hand side and upstream), and then

converges with the sound radiated by the source transmitting to two outlets of the duct. For the energy flows in the cavity and in the duct are with little angle difference, the sound pressure is increased. Thus, the plate vibration is fully induced and the sound radiation is rather strong towards the two ends of the duct at the trough point, and the noise abatement is extremely weak. Figure 3.9(1b) and 3.9(2b) shows the situation at the first peak point (f=0.036), the energy flow in the cavity also converges with that from duct, but the two energy flows offset each other and it is expected that sound cancellation happens, resulting in good performance in noise reduction. From the real intensity field (1b), it can be clearly found that there is more sound energy transmitted in to the cavity while less energy to the two outlets compared with the Figure 3.9(1a). For Figure 3.9(1c) and Figure 3.9(2c) representing the third peak (f=0.292), the two streams of energy flow start from the centre of the cavity forming two circles; and there is sound cancellation expected inside the cavity since there is opposite direction intensity existing. Figure 3.9(d) indicates the angle difference of the intensity flow between the cavity and duct in the black circle region of intensity field and give a clearer image of in-phase and anti-phase of intensity flow. Briefly speaking, the plate vibrates strongly at the low frequency range, while sound radiated by the plate converges with that in the duct with an in-phase at the *IL* troughs and anti-phase at *IL* peaks; in higher frequency range, there is sound cancellation happening inside the cavity at the peak points.

3.3.6 Monopole and dipole source comparison

The operation of real fan may have dipole and monopole nature, so the performance of MPP housing device to reduce monopole and dipole source is investigated in this section. Figure 3.10(a) compares the *IL* of MPP housing device with perforation ratio of 2.7% and diameter 0.1 mm as the previous determined optimal configuration to control monopole and dipole source with the same source strength.

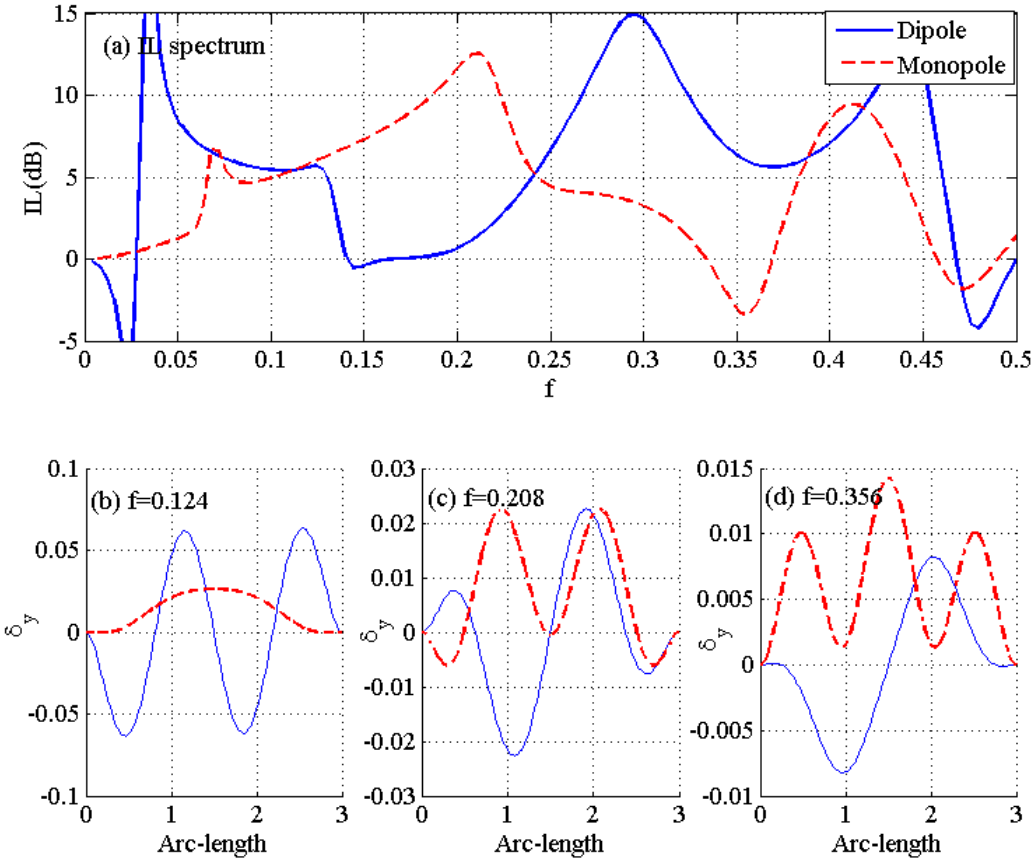

Figure 3.10: MPP housing *IL* and panel vibration comparison between dipole (solid line) and monopole (dashed line) source. (a) the *IL* performance variation; (b) the *y*-displacement of panel at *f*=0.124; (c) *f*=0.208 and (d) *f*=0.356

With the same property of MPP, the *IL* for controlling monopole is higher than that for controlling dipole at the frequency of *f*=0.12 to *f*=0.23. On the other hand, MPP housing device for controlling dipole outperforms controlling monopole source at the low frequency range at *f*=0.03 to 0.14 and the relative high frequency range of *f*=0.24 to 0.485. Although the MPP housing device with monopole source cannot report good *IL* performance in the low and medium frequency range simultaneously, the noise reduction effect is rather appreciate in the low to medium frequency range and can be used to control some sources with monopole characteristics like the motor. Figure 3.10(b) to Figure 3.10(d) show the panel vibration response at different frequencies: *f*=0.124, *f*=0.208 and *f*=0.356 respectively. For the dipole source, the *IL* is at the peak when *f*=0.124 and the panel vibration is more intense compared to the other two frequencies. For the monopole source, odd modes are dominant and the vibration of panel at frequency *f*=0.124 and *f*=0.208 are stronger than the *f*=0.356 which is at the trough. In summary, the source characteristics should be taken into account in the silencer design stage as the performance will be dramatically influenced due to different sound source.

3.4 Conclusion

A two dimensional theoretical model for in-depth understanding of vibro-acoustic coupling between the vibrating MPP and the sound fields of a duct and backed cavities with a non-uniform dipole sound source excitation has been established. The theoretical results have been validated by finite element simulation. The optimization process has been conducted on several parameters such as the panel

mass, bending stiffness and the perforation properties. The noise reduction mechanism has been investigated through the modal analysis, sound source radiation ability and sound intensity field study. The excitation source has been varied from dipole to a monopole to look into the sound attenuation performance change. The following conclusions can be drawn:

i) With optimal configuration (L_c=3, H_c=0.5, B=0.0014, m=0.1, σ=2.7 and d^*=0.1 mm) and dipole source excitation, the sound suppression can achieve 70% in the desired low frequency ($f \in$ [0.03 0.14])and medium frequency ($f \in$ [0.24 0.485]) range. The housing device reports effectiveness in merely one frequency range from low to medium frequency ($f \in$ [0.06 0.2]) when the source is changed to a monopole.

ii) The panel vibration induced by the dipole source radiates sound waves to the duct interacting with the direct source radiation and such interference determines the performance of the device. With the dipole source nature, the second and fourth modes dominate the vibration and play the most important role in the noise reduction. In majority frequencies, the panel radiations in return eliminate the source radiation with anti-phase relationship and undergo the sound cancellation. However, at certain frequencies, the sound waves radiated by the panel vibration converge with source radiation in-phase resulting in negative *IL* and sound suppression. Sound radiation efficiency and sound suppression factor are introduced to give reasonable explanation to the *IL* performance in the noise source control cases.

iii) The proposed 2D theoretical model with limited duct length has been validated by the prediction. The MPP housing device with a compact geometry

of expansion ration 2 can achieve more than 5 dB insertion loss with wide frequency range at the low and medium frequency range to cover the first BPF noise of ducted-fans with corresponding rotation speed, and simultaneously, can eliminate the second harmonic effectively. Compared with tensioned membrane housing, the MPP housing device is easier for application without any mechanism for exerting force. In addition, the MPP housing device achieves a lower frequency limit at f_1=0.03 and the stopband at middle frequency range is also widened, exceeding the performance of tensioned membrane housing.

Chapter 4 Experimental validation and application of MPP housing device

4.1 Introduction

A two dimensional theoretical model utilizing MPP control the dipole sound at the source has been established in Chapter 3. A numerical model has also been built up to validate the theoretical model. The working mechanism has been deeply investigated through the modal analysis, intensity field and sound radiation efficiency study. With optimal configuration, the MPP housing device can report wide effective band in both low and medium frequency in order to suppress the first two BPF noises with corresponding operation speed. In this chapter, it mainly focuses on an experiment conducted to validate the proposed 2D theoretical model and followed by a successful application of the proposed MPP housing device to the product of hairdryer. In the validation process, balsa wood with perforations is employed. Although it is not the optimal one, the results are valuable for the theory validation. The MPP housing device is then applied on the hairdryer to control the newly induced BPF noise at 2200 Hz after the elimination of low frequency broadband unsteady inlet flow noise by rough surface at the inlet. Due to the limit space and length of hairdryer, a very compact geometry of the housing device is demanded and the MPP housing device is very close to the motor-fan assembly. It has been certified by the successful application that the MPP housing device has the potential to control ducted-fan noise without volume flow rate deduction.

4.2 Experimental procedures

The experiments were carried out in the anechoic chamber, with a cutoff frequency 80 Hz. The background noise level of the anechoic chamber is about 20 dB. Thus, it can maximally eliminate noise from outside components that may affect the accuracy of the measurement, making the validation process favorable.

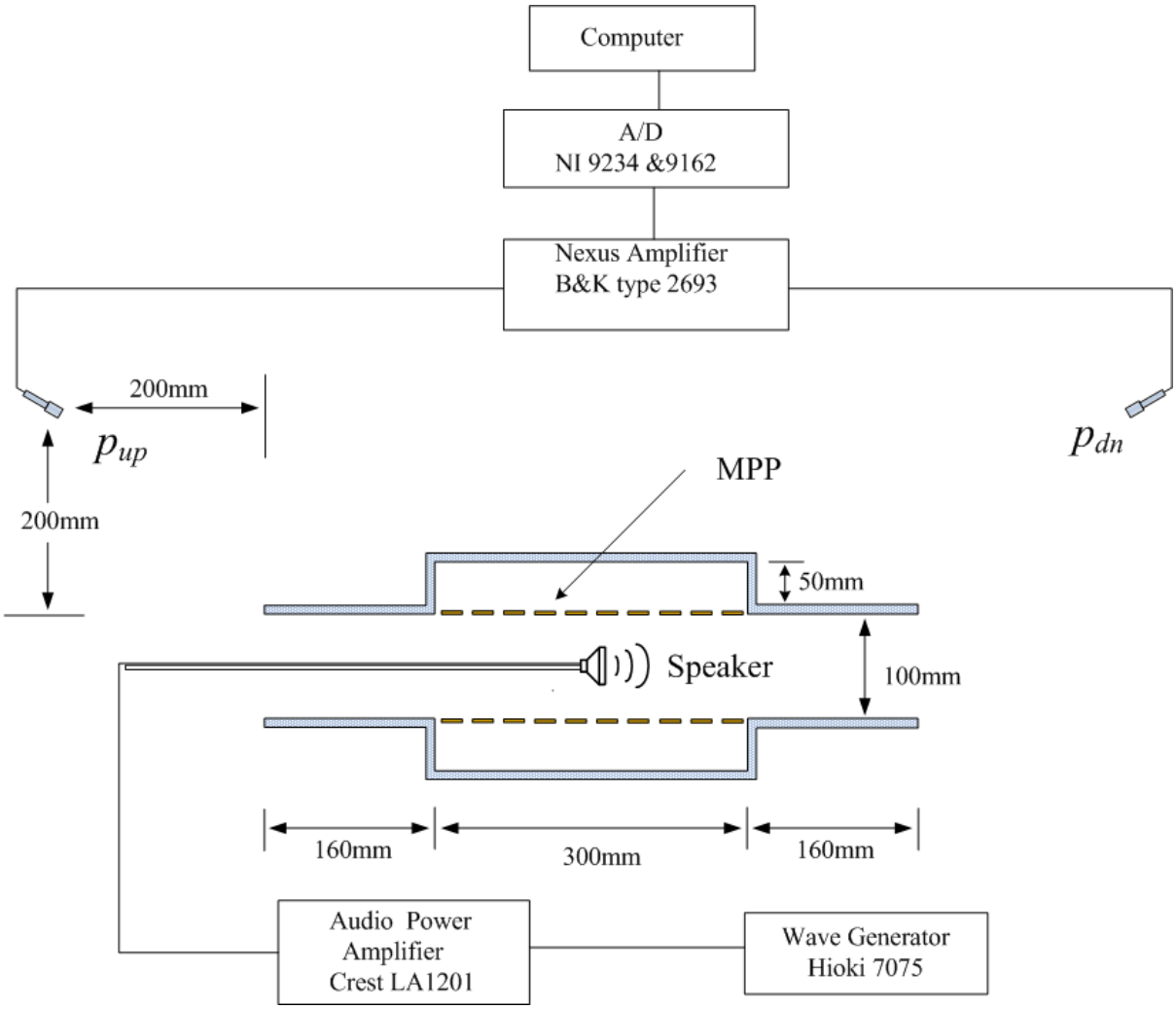

Figure 4.1: Experimental setup for measuring the actual sound pressure radiated at the outlet by using two microphones at two exits of the duct

The experimental setup (Liu *et al.*, 2012) is illustrated in Figure 4.1. The duct used had a dimension of h^*=100 mm by w^*=100 mm cross section, the MPP had a

length of $L^*=3h^*=300$ mm, and cavity depth of $h_c{}^*=50$ mm. The first cut-on frequency in the duct is about 1700 Hz. As shown in Figure 4.1, a small loudspeaker of 40 mm in diameter was utilized to simulate the dipole sound source. The loudspeaker was held as a cantilever by a very rigid rod and located at the centre of the duct in the vertical direction. The radiated noise was measured at the outlet of the duct with an angle of 45 degrees from the centre line. One pair of 1/2-in. microphones type B&K 4189 were used and supported by Nexus Conditioning Amplifier type B&K 2693. The loudspeaker was driven by a function generator Hioki 7075 via an Audio power amplifier Crest LA 1201 with white noise. The signals from the microphones were acquired through an analog-to-digital converter NI 9234 & 9162 with MATLAB program. Finally, the sound pressures were directly measured at the exits at the upstream and downstream duct, denoted by p_{up} and p_{dn}, respectively.

In real case, the radiation from the loudspeaker is not a pure dipole. It is regarded as two components: one dipole with anti-phase relation and another monopole with in-phase relation. Meanwhile, the measurement at one point at the left hand side outlet will be contaminated by the sound pressure at the right hand side outlet. Therefore, the extraction of the dipole component from the real noise source is needed during the signal processing. The sound wave decomposition procedure developed by Huang at al. (2010) is followed.

The radiations of the equivalent source are decomposed into two parts: one with antiphase relation in the upstream and downstream regions, and another with in-phase relation,

$$p = (p_m + p_d)e^{ikx} + C_1 e^{ikx} + C_2 e^{-ikx},\ x < -L_c / 2;$$
$$p = (p_m - p_d)e^{-ikx} + C_1 e^{ikx} + C_2 e^{-ikx},\ x > L_c / 2 \quad (4.1)$$

where p_d and p_m represent the amplitudes of the dipole and monopole components, respectively. x=-L_c/2 is the leading edge of the chamber which is in the upstream side and x=L_c/2 indicates the trailing edge in the downstream side. In this experiment, the source is located at x=0. C_1 and C_2 are the reflections of the equivalent source radiation by the duct ends.

At the two ends of the duct, the pressure p_L and p_R at the left and right end are:

$$p_L = (p_m + p_d + C_1)e^{-0.5ikL_{total}} + C_2 e^{0.5ikL_{total}} \quad (4.2)$$

$$p_R = (p_m - p_d + C_2)e^{-0.5ikL_{total}} + C_1 e^{0.5ikL_{total}} \quad (4.3)$$

L_{total} is the total length of the whole test rig from the opening at left hand side to another opening at the right hand side.

The reflection coefficient of the open ends β is related to the open-end impedance Z_{open}

$$\beta = \frac{Z_{open} - 1}{Z_{open} + 1} \quad (4.4)$$

$$\text{and } Z_{open} = \begin{cases} 0.25(ka)^2 + ik(0.6133a) & unflanged\ \ pipe \\ 0.25(ka)^2 + ik(0.8216a) & infinitely\ \ flanged\ \ pipe \end{cases} \quad (4.5)$$

with a the radius of the duct. Thus, we can obtain that,

$$\beta = \frac{C_2 e^{0.5ikL_{total}}}{(p_m + p_d + C_1)e^{-0.5ikL_{total}}} \quad (4.6)$$

$$\beta = \frac{C_1 e^{0.5ikL_{total}}}{(p_m - p_d + C_2)e^{-0.5ikL_{total}}} \quad (4.7)$$

For the two ends of the duct radiate sound to each microphone acting as air pistons, the contribution of the two open ends should be added up. Sound pressure radiated by each air piston is proportional to

$$\frac{e^{-ikr}}{r^2}(x_{observer} - x_{source})\vec{n} \tag{4.8}$$

where subscript "observer" denotes observer position and "source" for the duct end position, and $\vec{n}$ denotes the outward normal direction of the piston The ratio of radiation from the far-side of the duct of length L_{total} to that from the near side is defined as the

$$\gamma = -\left(r_{near}/r_{far}\right)^2 \frac{L_{total} + r_{near}\cos(\theta)}{r_{near}\cos(\theta)} e^{-ik_0(r_{far} - r_{near})} \tag{4.9}$$

here r_{near} and θ are the distance and angle between the microphone and the near-side duct opening (left hand side) respectively. r_{far} is the distance between the microphone and the far-side duct opening (right hand side).

The total sound measured at the two microphone positions at the upstream (p_{up}, left side) and downstream (p_R, right side) are

$$p_{up} = p_L + \gamma p_R \tag{4.10}$$

$$p_{dn} = p_R + \gamma p_L \tag{4.11}$$

Define the measured transfer function between the two microphones as r_{up}^{dn},

$$r_{up}^{dn} = \frac{p_{dn}}{p_{up}} \tag{4.12}$$

Then the Eq. (4.6), Eq. (4.7), Eq.(4.10) and Eq.(4.11) can be solved to obtain the pressure amplitudes p_m, p_d, and the coefficients C_1 and C_2. The upstream dipole component can be gained:

$$p_{ud} = \frac{p_{up}(e^{ikL}+\beta)\left[1-\left(r_{up}^{dn}-\gamma\right)/\left(1-\gamma r_{up}^{dn}\right)\right]}{2e^{0.5ikL}(1+\beta)\left[1+\gamma\left(r_{up}^{dn}-\gamma\right)/\left(1-\gamma r_{up}^{dn}\right)\right]} \tag{4.13}$$

4.3 Experimental validation of theoretical model

The predicted results are compared with the experimental results from the plate housing device and the MPP housing device respectively as shown in Figure 4.2. Despite the plate and the MPP not being the optimal one, the results satisfy the objective of model validation. Note that during the measurement, the lower limit frequency is 150 Hz due to the capability limitation of the small loudspeaker acting as a dipole source, and the upper limit is 1700 Hz which is the cut-on frequency of the duct.

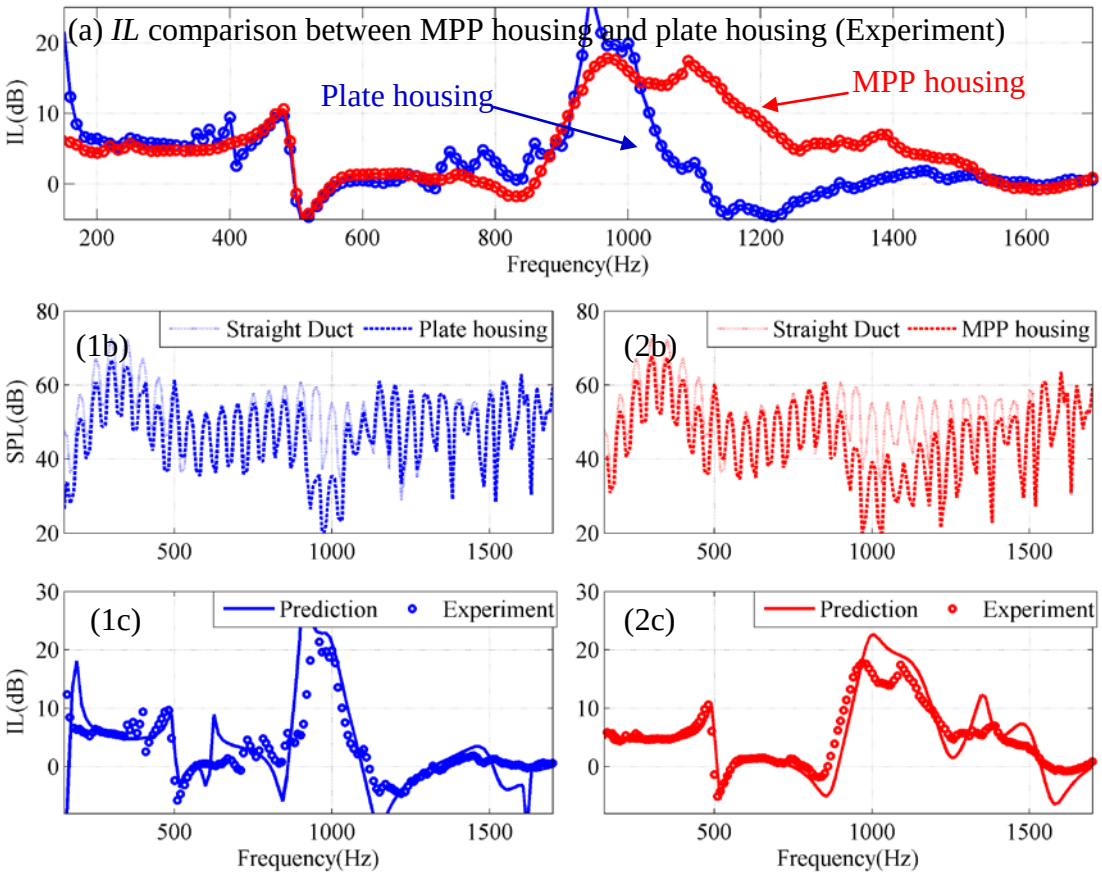

Figure 4.2: Experimental validation results. The top figure is the *IL* performance comparison between plate housing device (B=0.0056, m=0.98) and MPP housing device (B=0.0032, m=0.98, σ=2.7 and d^*=0.5 mm), the second row is sound pressure level comparison between straight duct and housing device, and the third row shows the comparison between prediction (solid line) and experiment measurement (circles)

The first row indicates the *IL* performance comparison between the plate housing device and the MPP housing device. By introducing perforation with small holes, the *IL* performance will be enhanced in the middle frequency around 1000 Hz to 1500 Hz, which matches the trend prediction in Section 3.3.2. The second row shows the sound pressure level of straight duct (dotted line) and housing device (dashed line) with extraction of the dipole component from the source. Figure 4.2 (1b) shows the sound pressure level of straight duct (dotted line) and plate housing

device (dashed line), and the sound pressure level radiated from the straight duct is generally higher than that from the plate housing device: about 5 dB from 150 Hz to 500 Hz and the difference is most visible in the range from 850 Hz to 1100 Hz. For the MPP housing device demonstrated in Figure 4.2 (2b), the performance in the low frequency stays roughly the same while it is enhanced in the middle frequency range, for the sound pressure level difference is visible in a broader frequency range of 850 Hz to 1500 Hz. The *IL* performance of the housing devices is displayed in the third row in comparison to the predicted results. The experimental data with dipole extraction is depicted in open circles, and the numerical prediction of *IL* for the pure dipole source is indicated by solid lines. Roughly speaking, the experimental data agrees well with the numerical prediction in terms of the overall *IL* level and the spectral pattern, although the experimental result is smoothed at the peak and trough points. On average, for the plate housing device, the *IL* is about 5 dB in the frequency range of 150 Hz to 500 Hz and 850 Hz to 1100 Hz, and the performance will be promoted in the middle frequency range with wider effective band by introducing the perforation .The two ranges are expected to cover the first two BPFs of fan noise in the ventilation system with rotation speed around 4000 *rpm* (7 blade fans).

The loudness is a key parameter of Psychoacoustic annoyance (Fastl and Zwicker, 2007) which will strongly determine the sound quality of the product. The unit of loudness is the *sone.* A loudness of 1 *sone* is equivalent to a signal of 40 dB pure tone at 1000 Hz with a loudness level 40 phons. The Figure 4.3 shows the loudness comparison among speaker in straight duct (solid line), speaker in plate housing

device (dashed line) and speaker in MPP housing device (line with circles) from low frequency 150 Hz to 2500 Hz. The loudness is calculated according to the ISO 532 (1975). During the experiment, the white noise is generated by a small speaker which simulates a dipole sound source inside the duct. The dominant loudness region is 250 Hz to 600 Hz about 1.7 *sone*. Both the plate housing device and the MPP housing divice can decrease the loudness from 150 Hz to 500 Hz region sinificantly, about 0.3 *sone*. There will be also loudness decrease in the medium frequency from 700 Hz to 1400 Hz, although it is not the dominant laoudness rigion for the white noise generated by the speaker.

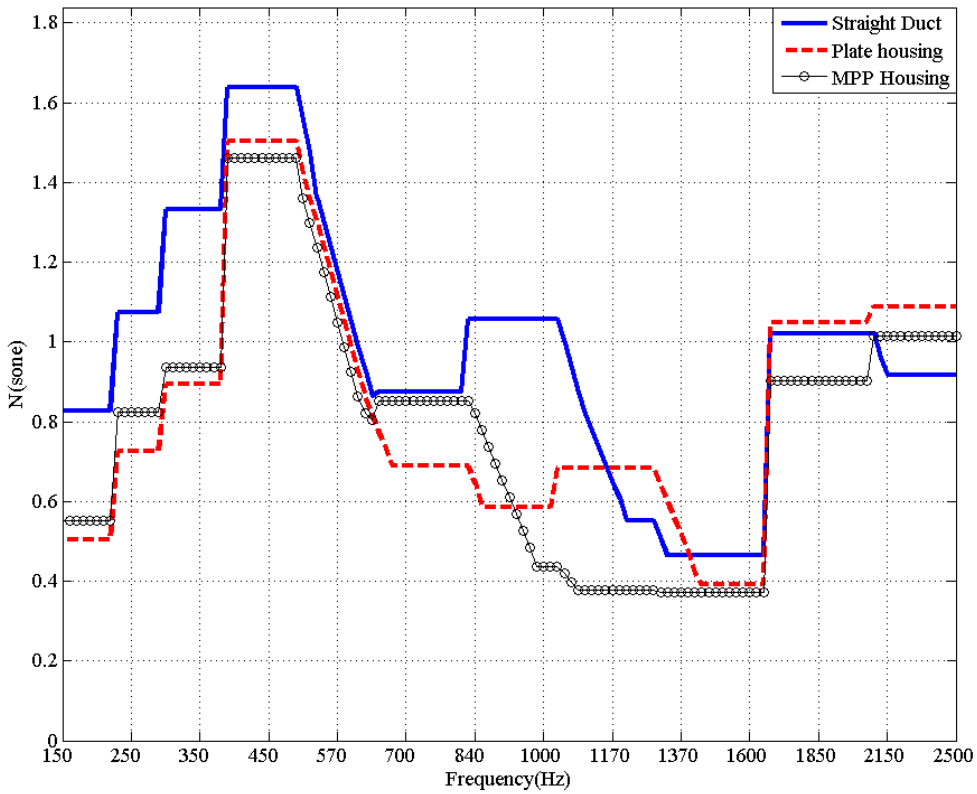

Figure 4.3: Loudness comparison among speaker in straight duct (solid line), speaker in plate housing device (dashed line) and speaker in MPP housing device (line with circles)

4.4 Application of MPP housing device on hairdryer

From Chapter 2, by the application of rough surface at the inlet of hairdyer, the 800 Hz broadband noise would be eliminated but there is another problem of the pure tone noise at first and second BPF. In order to deal with such narrow band high frequency noise, MPP housing device is to be adopted. The detailed noise reduction mechanisms have been studied theoretically in Chapter 3.

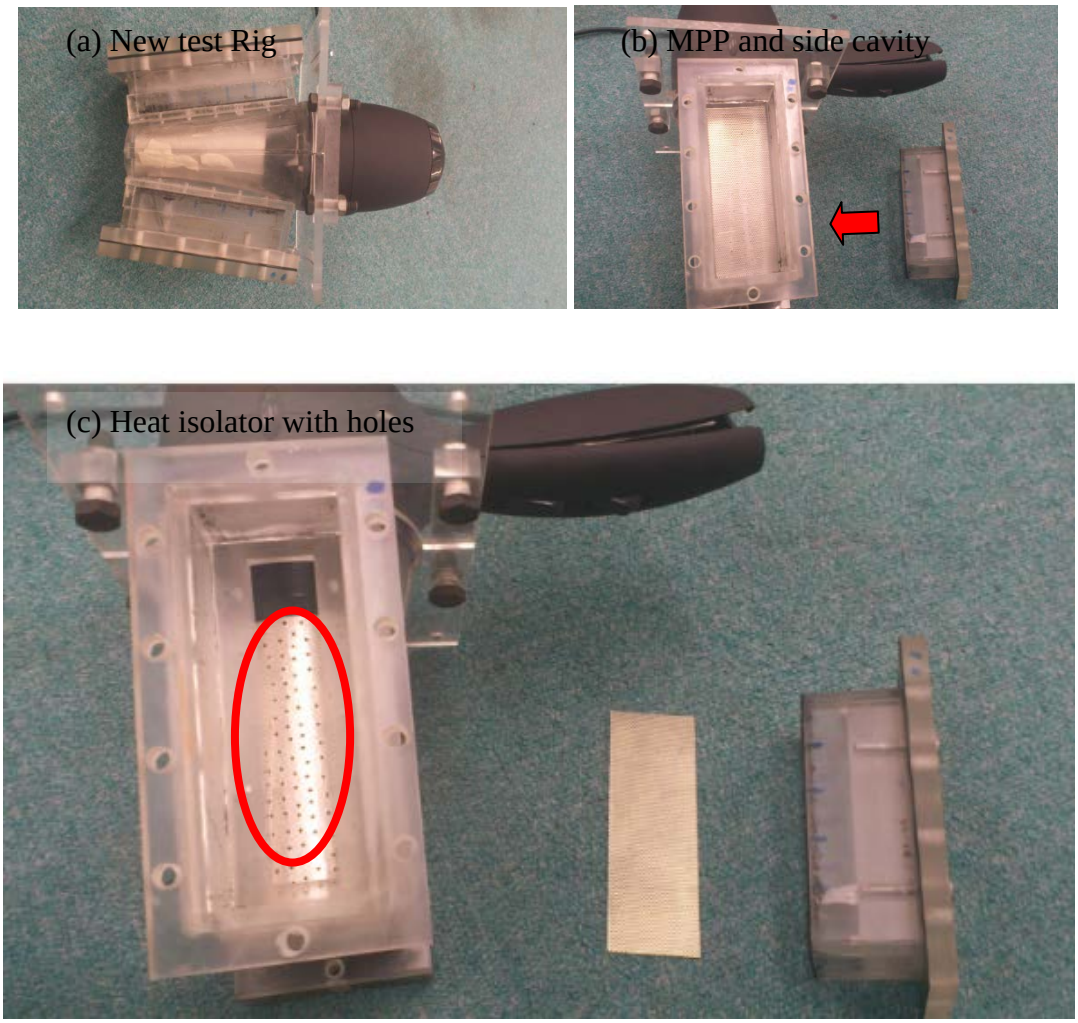

Figure 4.4: Design of side-mounting cavity with MPP attached on the current hairdryer. (a) the whole view of new test rig (b) the MPP installed on the hairdryer and the cavity (c) the holes on the heat isolator

Figure 4.4 shows the design of MPP housing device which composed of a thin MPP (hole size 0.5 mm and perforation ratio 6%, 0.5 mm thickness stainless steel) covered with a rigid cavity and the housing device is flush mounted on the duct wall of the hairdyer. Therefore the whole device is so called hairdryer with side mounting cavity with MPP. And in order to ensure the sound penetration into the MPP, the isolator paper inside the hairdyer is required to drill numerous holes with diameter of 1 mm. Figure 4.4 (a) shows the whole view of new test rig, Figure 4.4 (b) demonstrates the closed side cavity used to cover the MPP and Figure 4.4 (c) represents the holes on the heating isolator.

The theoretical model of MPP housing device has been built in Chapter 3 for the understanding of vibro-acoustic coupling among the acoustic field in the duct, cavity and the vibration of panel in a mathematic way. After the basic understanding of sound attenuation mechanism, the theoretical model has been validated by both the numerical simulation and the experiment. Then the numerical simulation is mainly employed to give the instructions of design and optimization of the MPP housing device. Before the application of the proposed MPP housing device on to a converging duct with limited length, that is, the hairdryer, a simplified numerical model for the converging duct section case has been built for the design of the device configuration as shown in the Figure 4.5. There is a dipole source located at the position of the fan blade to simulate the BPF fan noise with a dipole nature. Although the model shape of the enclosure of is not exactly the same as the original hairdryer, it still can give instructions to the design of cavity configuration and chosen of the panel properties, the diameter of hole size and the perforation of the MPP. By the numerical simulation, the optimal configuration of

the MPP housing device geometry and the perforation properties can be determined to obtain a wide stopband covering the BPF noise at about 2200 Hz. The simplified numerical model will also be validated by the speaker functioned as the dipole source first.

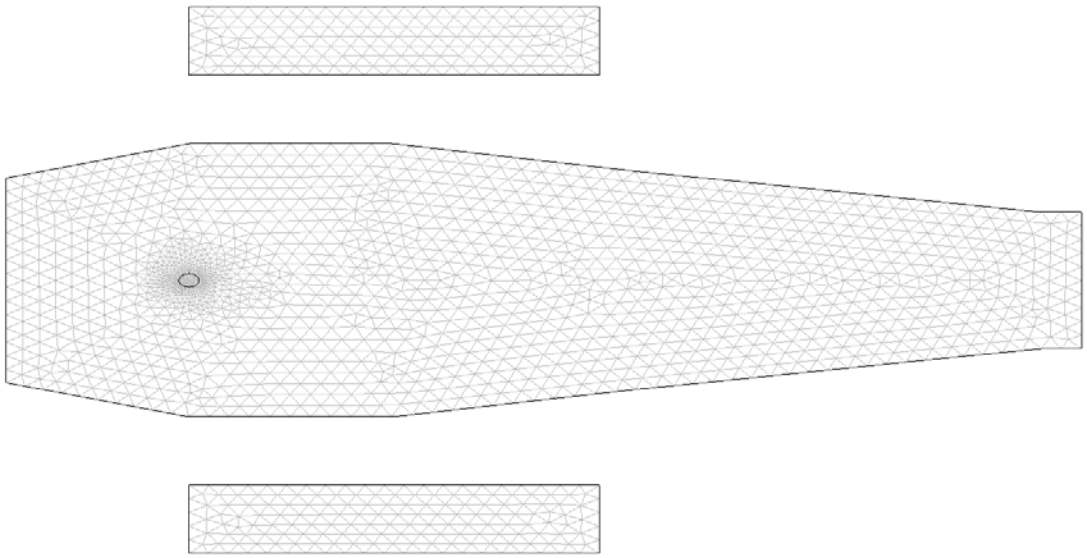

Figure 4.5: Simplified numerical model of the converging duct section case of hairdryer

The comparison between the numerical prediction in two-dimensional configuration by FEM and measurement of the hairdryer enclosure with the replacement of the fan by a loudspeaker for the MPP housing device (MPP with hole size of 0.6 mm and 5% perforation) is shown in Figure 4.6. The cavity depth used in the experiment is only 20 mm, with 20 mm width and 90 mm length, which is a rather compact geometry satisfying the requirement of the company. Roughly speaking, the variation of *IL* of the measurement and numerical prediction by FEM are similar but there are deviations at the frequency range of 200 Hz to 1000 Hz.

This is because the numerical FEM is based on a simplified two-dimensional geometry without accurate curvature. It is found that the main effective stopband is about 1000 Hz to 2500 Hz with a *IL* of 5 dB. It could be helpful for the BPF noise attenuation for the BPF is about 2200 Hz.

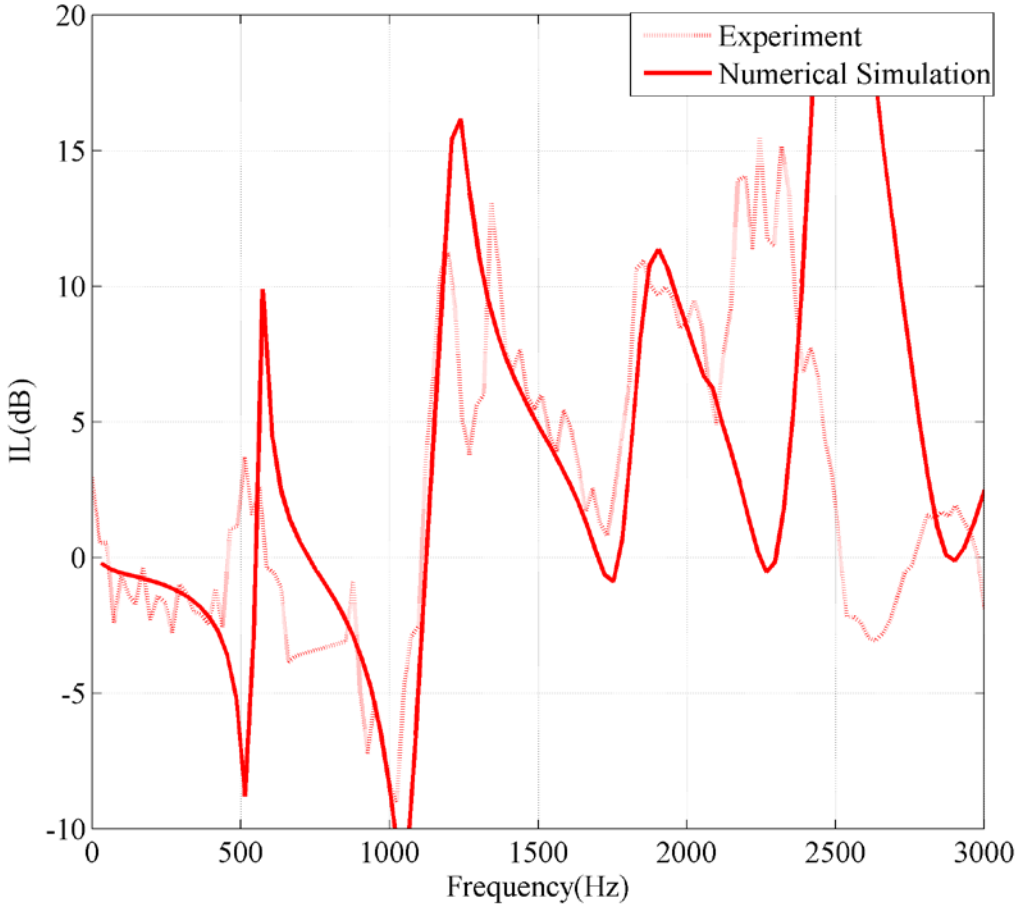

Figure 4.6: SPL comparison of prediction (solid line) and experiment validation (dashed line) of siplified numerical model for hairdryer

Figure 4.7 expresses the comparison of the sound pressure level between hairdryer with MPP housing device and with side mounting cavity but rigid plate on the duct wall. The hair dryer with rigid plate on the duct wall is utilized to function as the

original smooth enclosure hairdryer as reference to examine the performance of fresh introduced MPP housing device. The solid line represents the sound pressure level of hairdryer with side-mounting cavities with rigid plate while the dashed line represents the results of changing the rigid plate to a piece of MPP. Figure 4.6 (b) indicates that there is noise reduction of 3 dB on average in the frequency range of 1100 Hz to 2400 Hz and the total sound pressure level is decreased from 80.7 dB to 79.4 dB.

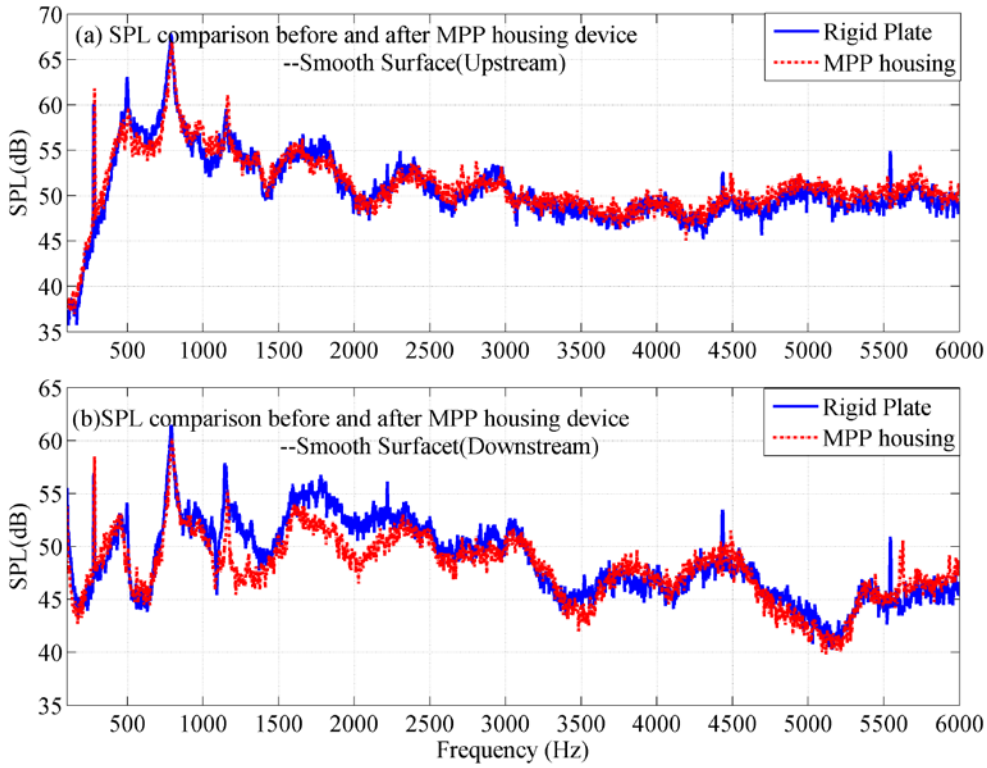

Figure 4.7: SPL spectrum of side-mounting cavities with MPP housing at (a) upstream and (b) downstream

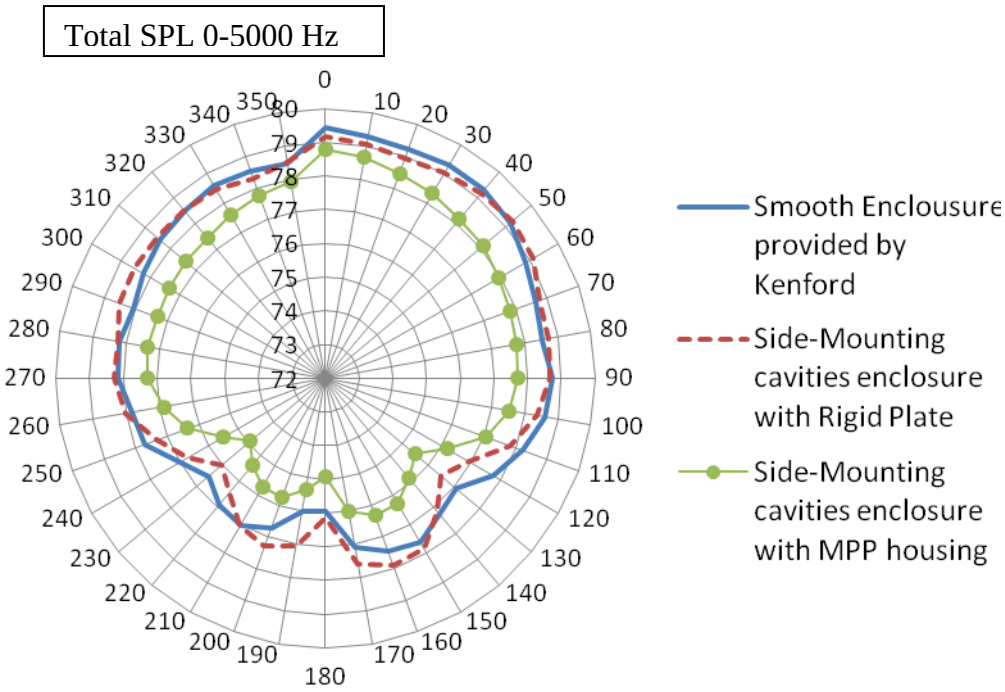

Figure 4.8: Total SPL contour comparison between casing provided by Kenford Company, modified side-mounting cavities with rigid plate and with MPP housing

In order to ensure the noise being reduced in different direction, the directivity measurement is conducted. Figure 4.8 shows the total sound pressure level contour for three different condition: smooth casing provided by Kenford Industrial Co., Ltd. (solid line), modified casing with side-mounting cavities with rigid plate (dashed line) and that with MPP housing device(line with dots). Roughly speaking, the sound pressure level distribution given by the smooth enclosure (Kenford) is similar to that given by the modified casing with rigid plate and cavity. Because of about 1 mm discontinuity of the cross sectional area due to the replacement of the original wall by a flat rigid plate, there is sound reflection and sound scattering and thus slightly change sound pressure level radiated out. With the use of MPP housing device, the overall sound pressure level in different direction is obviously reduced by about 2 dB even though the inlet region of the hairdryer is smooth.

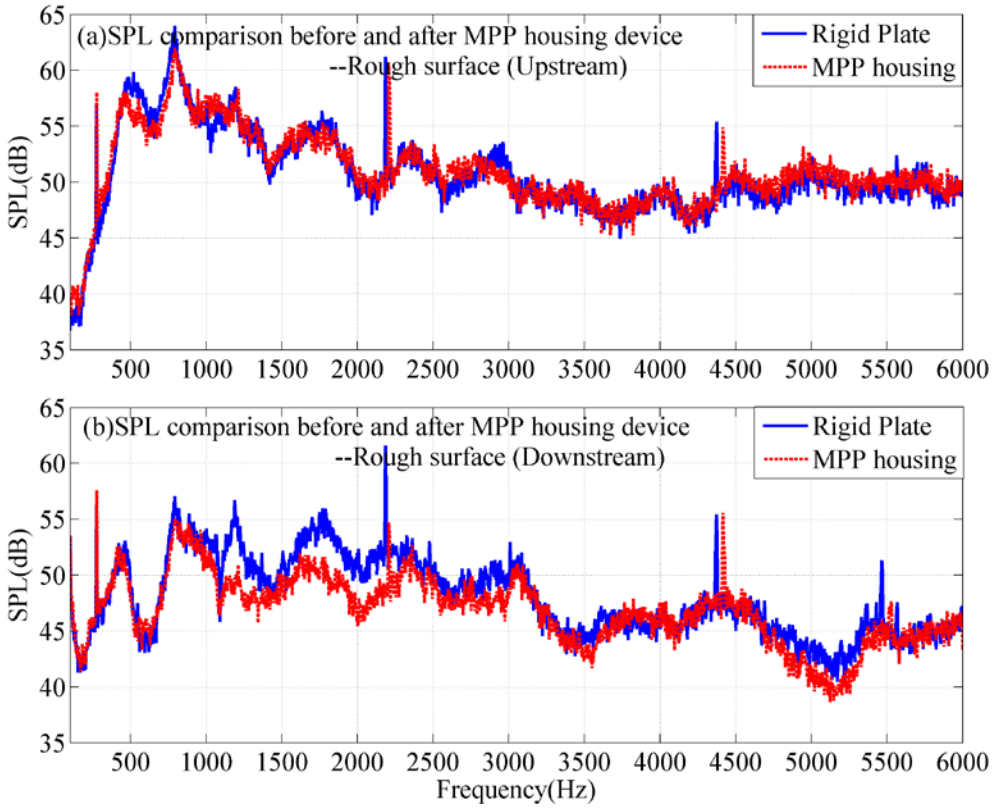

Figure 4.9: SPL spectrum of modified side-mounting cavities with MPP housing with rough surface at the inlet

Figure 4.9 depicts sound pressure level spectrum with the use of MPP housing device and with rough surface at the inlet of hairdyer. The sound pressure level spectrum for the hairdryer with side-mounting cavities with rigid plate in case of the rough surface at the inlet wall is respresented by solid line. Due to placing the roughness at the inlet, the sound pressure level at the downstream at the frequency range around 800 Hz drops down. In addition, when the rigid plate is replaced by MPP (dashed line), the sound pressure level in the frequency range from 1000 Hz to 2200 Hz is decreased by about 4 dB on average. The most important thing is that the first blade passage frequency is highly reduced by 10 dB. Such MPP housing device in case of flow could effectivley work for reducing the dominant noise of first blade passage frequency with certain bandwidth. As a result, the total sound

pressure level calculated by integration or using sound level meter directly is reduced by about 3 dB roughly. It is believed the annoyance to user is reduced accordingly.

Table 4.1: Total sound pressure level table

	Smooth surface (dB)	Rough surface (dB)
Original casing provided by Kenford Indusrial Co., Ltd.	80.7	80.2
Rigid plate with side mounting cavity	80.9	80.3
MPP with side mounting cavity	79.4	78.8

Table 4.1 summarizes the total sound pressure level change measured by sound level meter or by integration of the sound pressure level at different frequency. With the installation of MPP housing device, the total sound pressure level of the current hairdyer provided by Kenford Industrial Co., Ltd. is decreased from 80.7 dB to 79.4 dB and from 80.2 dB to 78.8 dB in case of smooth inlet surface and rough inlet surface respectively.

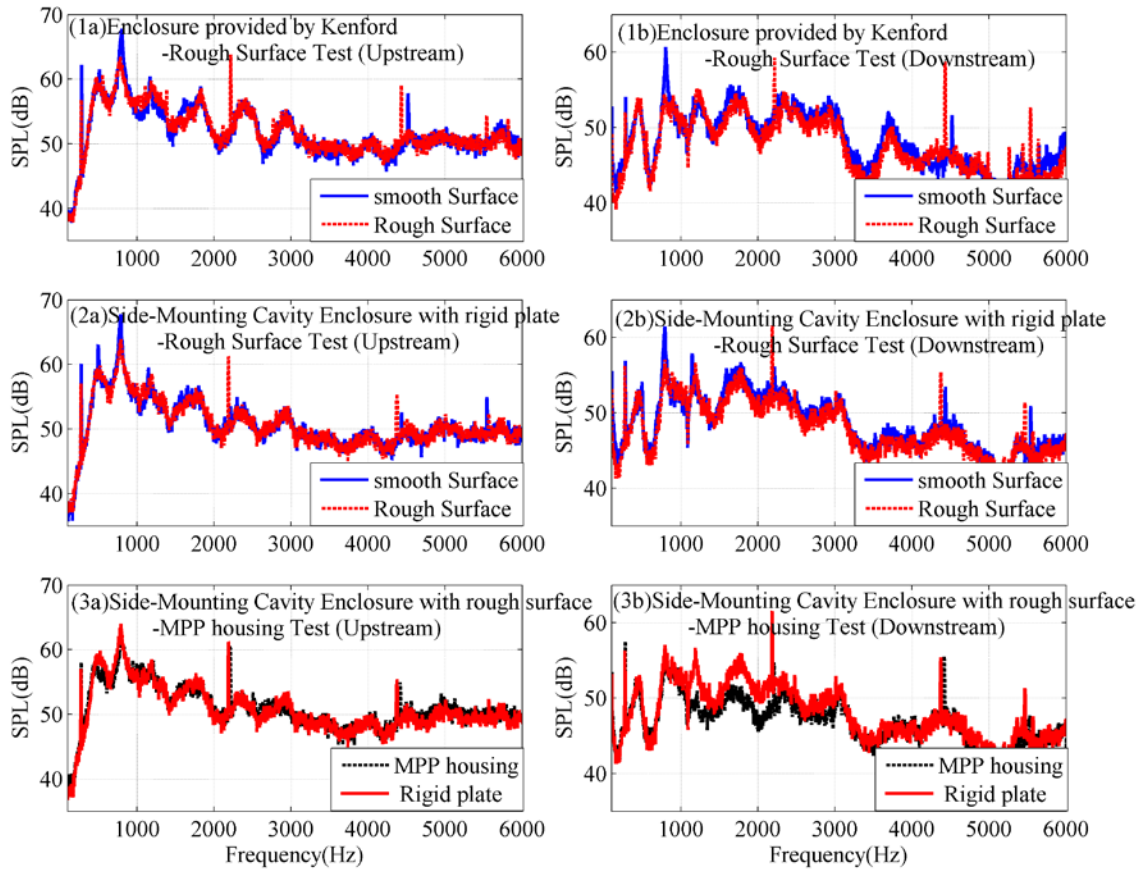

Figure 4.10: Comparison of SPL spectrum for different operation conditions. The first row: original casing provided by Kenford Company. The second row: rigid plate with side mounting cavity and the third row: comparison between MPP housing device and rigid plate covered by cavity and with roughness surface at the inlet wall

Figure 4.10 shows the comparison of sound pressure level spectrum for different operation conditions. Figure 4.10 (1a) and Figure 4.10 (1b) are the sound pressure level spctrum for the original casing provided by Kenford Company in case of smooth or rough surface at the inlet wall at upstream and downstream respectively. The noise level is obviously reduced at the downstream when the rough surface is added. However, it increases drastically BPF tonal noise at a frequency of 2200 Hz. Figure 4.10 (2a) and Figure 4.10 (2b) demonstrate the performance of the modificed casing with a flat rigid plate which is covered by side-mounting cavity

at upstream and downstream respectively. By comparing the results given by the orginal casing by Kenford Company and the modificed casing with a flat rigid plate, the sound pressure level spectrum for smooth and roughness surface are similar. Figure 4.10 (3a) and Figure 4.10 (3b) show performance of the MPP housing deivce with the rough surface at the inlet wall. The sound pressure level in the frequency range from 1000 Hz to 2200 Hz is decreased by about 4 dB on average. The tonal noise first blade passage frequency is also reduced by 10 dB. Such MPP housing device in case of flow could effectivley work for reducing the dominant noise of first blade passage frequency with certain bandwidth.

Figure 4.11 gives a clearer image of the noise attenuation effect at the outlet side: blue dashed line is the SPL spectrum of smooth surface enclosure hairdryer , red solid line is for rough surface enclosure and black thin dashed line is for the hairdryer with MPP housing device with a rough inlet. By introducing the rough surface, the 800 Hz noise will be reduced a lot and the first BPF will be induced becoming the dominant noise component. Then by the utilization of MPP housing deivce with a rough inlet surface, the sound pressure level in the frequency range from 1000 Hz to 3000 Hz is decreased by about 4 dB on average, compared to the original smooth one. Therefore, the noise level of the product will be decreased, and the product will be more comfortable for the consumers.

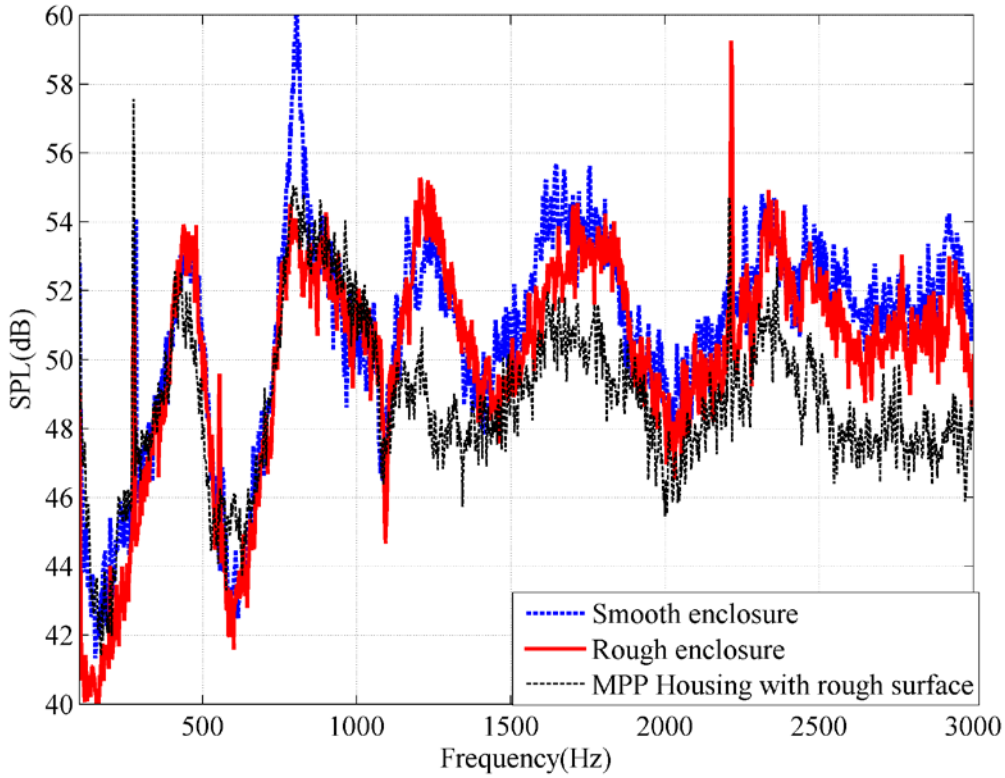

Figure 4.11: Comparison of SPL spectrum at outlet side among smooth enclosure (dashed line), rough enclosure (solid line) and hairdryer with MPP housing device as well as roughness surface at inlet (thin dashed line)

For product measurement, A-weighted SPL is the most common way to examine the loudness of the product perceived by consumers. The reason is that, the human ear will be less sensitive to low frequency noise. It is utilized by introducing a table of correction values to the octave or one-third octave bands of the measured SPL spectrum. In this study, the one-third octave band is chosen to study the loudness of the hairdryer. Figure 4.12 shows the one-third octave A-weighted SPL comparison among the smooth enclosure (blue), rough enclosure (green) and hairdryer with MPP housing device with rough inlet surface (red).

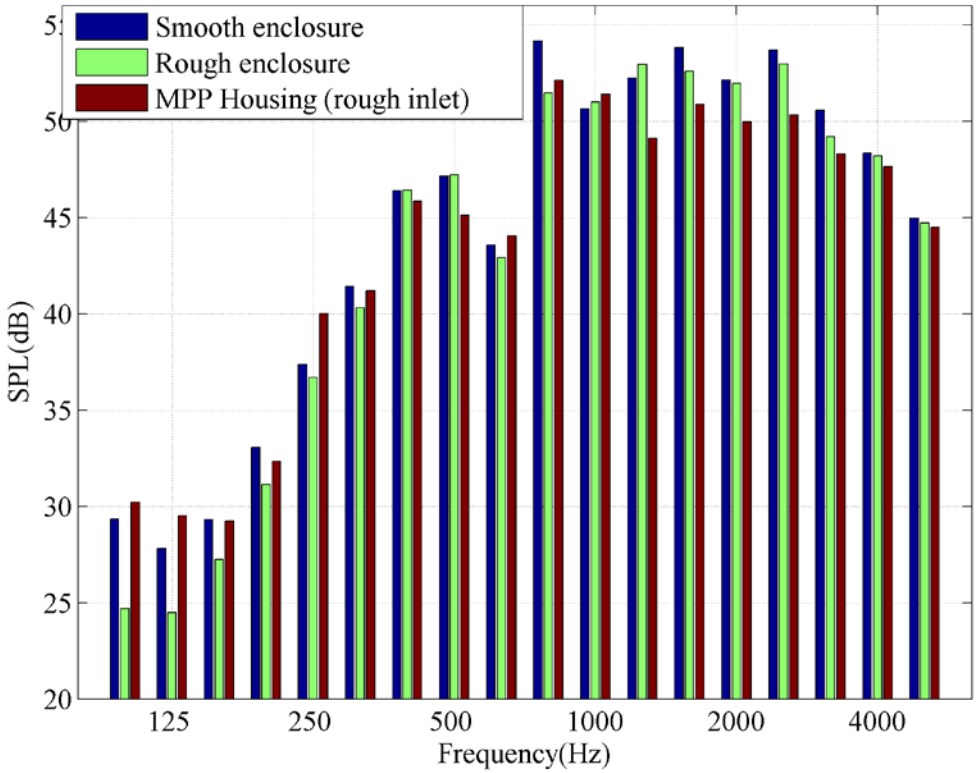

Figure 4.12: A-weighted 1/3 octave SPL spectrum comparison at outlet side among smooth enclosure (blue), rough enclosure (green) and hairdryer with MPP housing device with rough inlet (red)

From the Figure 4.12, it can be easily concluded that the low frequency noise is not that sensitive to human ears, as the previous 280 Hz noise component almost disappear in the A-weighted SPL curve. The 800 Hz noise is still the dominant noise component. By introducing the rough surface, the dominant noise component will be decreased a lot. In the previous SPL spectrum, the BPF aroung 2200 Hz will be induced and become the dominant noise component. However, in the A-weighted SPL spectrum, the contribution of BPF noise is not that high. By the application of MPP housing device on the hairdryer with rough surface at the inlet, the sound pressure level will be reduced 4 dB on average from 800 Hz to 3000 Hz.

The Figure 4.13 shows the loudness comparison among hairdryer with smooth enclosure (solid line), rough enclosure (dashed line) and hairdryer with MPP housing device with rough surface at inlet (line with circles) from very low frequency 25 Hz to 12500 Hz. The loudness of the product under different work conditions is calculated according to the ISO 532 (1975). The loudness of the original product with smooth surface is rather high in the frequency 100 Hz to 3000 Hz, around 0.8 *sone*. For the existing of 800 Hz dominannt noise component, the loudness around 800 Hz is extremely high, up to 0.9 *sone*. By introducing the rough surface, the noise level will be greatly reduced around 800 Hz, so the loudness value will be much smaller than the original smooth enclosure shown as the red dashed line. However, there is no significant improvement in the frequency range around 2000 Hz, the position of another loudness peak region. By introducing the proposed MPP housing device with the rough surface at the inlet, the SPL will be greatly decreased from 800 Hz to 3000 Hz as demeonstrated in the previous SPL spectrums, as shown in Figure 4.11. Regarding the loudness, the loudness will be much lower than the original smooth enclosure hairdryer from 700 Hz to 3000 Hz, covering the two dominant peak regions existing in the loudness curve of hairdryer with smooth enclosure. Thus, the sound quality of the product will be improved a lot by introducing the rough surface and the utilization of MPP housing device.

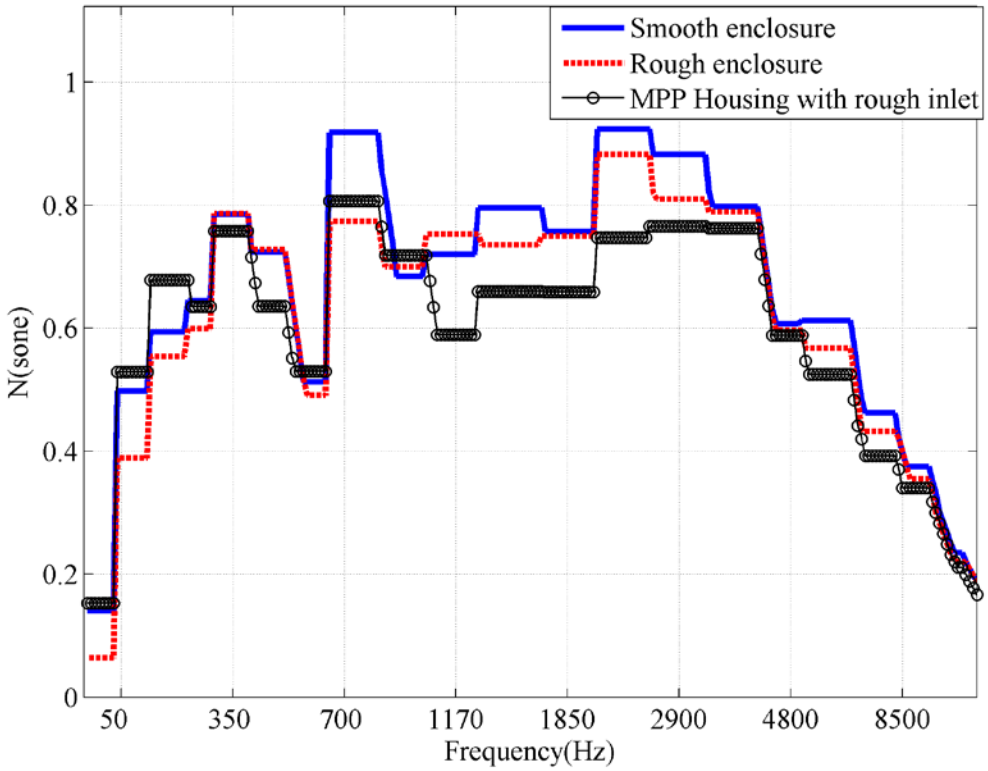

Figure 4.13: Loudness comparison among smooth enclosure hairdryer provided by Kenford company (solid line), rough enclosure hairdryer (dashed line) and hairdryer with MPP housing device (line with circles)

Sharpness (von Bismarck, 1974) is another quantity of psycho-acoustic playing a prominent role in sound quality. Its unit is "*acum*" and the definition of 1 *acum* is that, a equivalent sound source at 1000 Hz with a narrow bandwidth less than 150 Hz with a sound pressure level of 60 dB. It is frequently used to quantify the sound quality of product such as engines, domestic appliances such as vacuum cleaners or hiradryers. Using Fastl and Zwicker's approach (2007), the sharpness can be calculated as:

$$Sn = 0.11\frac{\int_0^{24} N'g(z)zdz}{\int_0^{24} N'dz}\,acum$$

$$z \leq 14, \rightarrow g(z)=1 \qquad (4.14)$$

$$z > 14, \rightarrow g(z) = 0.00012z^4 - 0.0056z^3 + 0.1z^2 - 0.81z + 3.51$$

Where S_n is the sharpness, N' is the weighted first moment of specific loudness.

For the product of hairdryer in this study, the sharpness of the hairdryer with smooth enclosure provided by Kenford Company is 1.7756 *acum*. By introducing the rough surface, the first BPF at 2200 Hz will be induced and become the dominant noise compomnent, so there will be a slight increase in the sharpness, becoming 1.7878 *acum*. By the utilization of proposed MPP housing device with the rough surface at the inlet, the sound pressure level will be decreased about 4 dB on average from 800 Hz to 3000 Hz. The sharpness of the hairdryer becomes 1.7396 *acum*. For the sharpness of the product has also been decreased, the product will be less annoying and will make the consumers more confortable.

The directivity measurement is conducted to give a clear image of noise control strategy. Figure 4.14 shows the total sound pressure level distribution at different angle for different casing. The results tell that: SPL of modified casing with side-mounting cavities with rigid plate (dashed line) is similar with that of original enclosure provided by Kenford Company (solid line); then by the application of rough surface at the inlet (solid line with triangles), the SPL will be reduced by about 2 dB at the downstream while is reduced by about 1 dB at upstream; finally, by using the combination of rough surface and MPP housing (dashed line with cross), the sound pressure level can be reduced significanly (about 2 dB) compared with the original casing given by Kenford Company at the discharge.

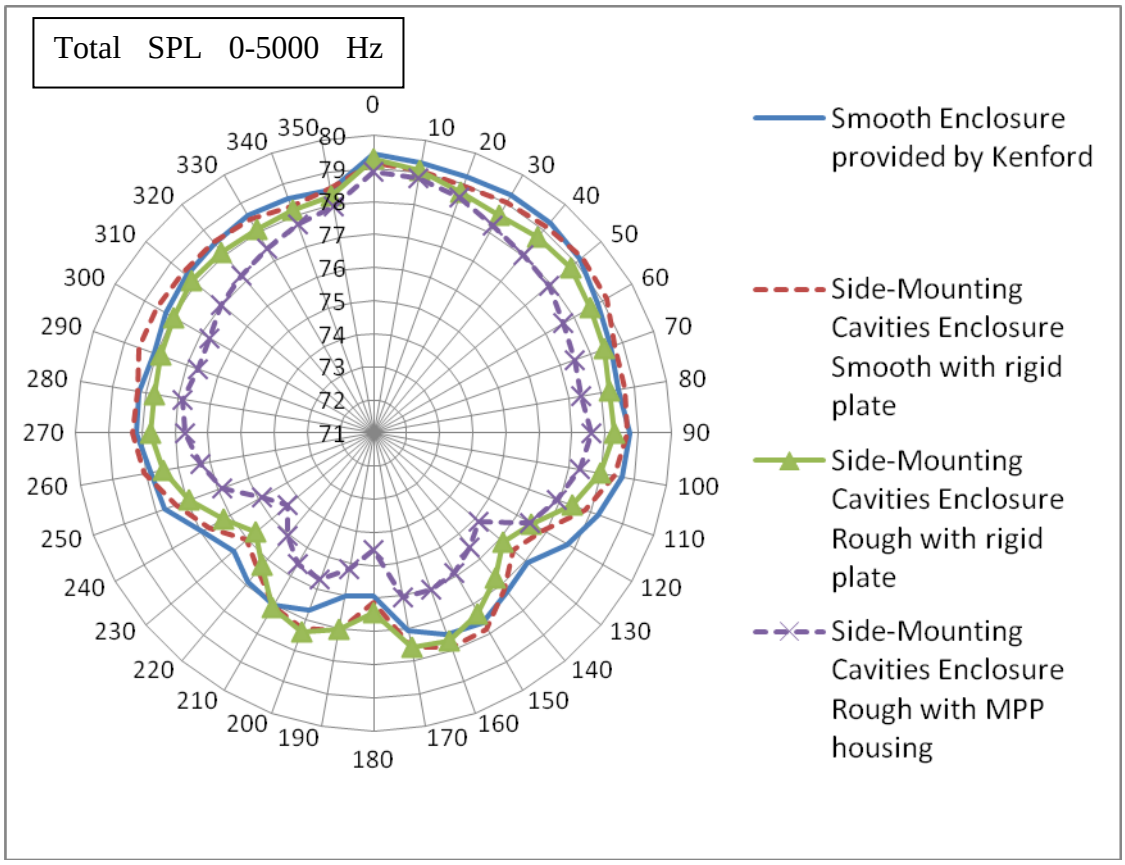

Figure 4.14: Total SPL contour for different casing with smooth or rough surface and with rigid plate or MPP housing device

Table 4.2: Flow Rate for different casing

	Smooth surface(L/s)	Rough Surface(L/s)
Enclosure provided by Kenford Company	23.08	23.08
Side-mounting Enclosure with Rigid Plate	24.17	24.18
Side-mounting Enclosure with MPP housing device	24.18	24.18

Table 4.2 summaries the measured net flow rate for different casing. The original casing provided by Kenford Company gives the net flow rate of 23.08 L/s while the modified casing with MPP housing or rigid plate with cavity can give the flow rate of about 24.18 L/s. The diffence between them is about 4.7%.

4.5 Conclusions

The proposed 2D theoretical model of MPP housing device has been validated by experiment and good agreement between the measured and predicted results has been achieved. The MPP housing device with a compact geometry of expansion ration 2 can achieve larger than 5 dB insertion loss with wide frequency range at the low and medium frequency range to cover the first two BPF noises of ducted-fans with corresponding rotation speed. Besides, by using the combination of rough surface and MPP housing device, the sound pressure level of hairdryer is reduced by about 8 to 10 dB at the low frequencies around 800 Hz contribued by the unsteady inlet flow, the tonal noise at first blade passage frequency can be greatly reduced by about 10 dB and the noise at the frequency range of 800 Hz to 2400 Hz by about 4 dB on average. By comparing the original smooth casing provided by Kenford Company and the modified casing with MPP housing, the noise level can be reudced by about 2 to 3 dB in all directions.

From loudness analysis,by introducing the rough surface, the loudness value will be much smaller than the hairdryer with original smooth enclosure at around 800

Hz, which is the frequency range of the dominant noise component. However, there is no significant improvement in the frequency range around 2000 Hz, the position of another loudness peak region. By introducing the proposed MPP housing device with the rough surface at the inlet, the loudness will be much lower from 800 Hz to 3000 Hz, covering the two dominant peak regions existing in the loudness curve of hairdryer with smooth enclosure. At the same time, the sharpness of the product will be lower down, making the product sound not that annoying. Thus, the sound quality of the product will be improved, making the consumers more comfortable.

For the flow rate measurement, the ultimate flow rate for the modified side mounting device is inceased to 24.18 L/s with 4.7% increment by comparing the orginal casing provided by Kenford Company.

Chapter 5 Hybrid MPPHQ device for controlling the dipole source

5.1 Introduction

The current study mainly aims to exhume a compact device to inhibit the ducted-fan noise at the source with broadband noise suppression. The performance of MPP housing device is examined theoretically in Chapter 3 and experimentally in Chapter 4. It has been confirmed that the device owns effective performance of noise mitigation in both low and medium frequency range. The noise reduction mechanism of such device integrates with sound cancellation and absorption. Sound cancellation dominates in most of the working range, while the absorption introduced by MPP can compensate for the insufficiency of cancellation in certain frequencies. As a result, the rather wide stopbands in both low and medium frequency range can be expected to cover the first two BPFs of fan noise in the ventilation system with corresponding rotation speed.

However, there is passband existing due to the cavity length as there is no insertion loss when the chamber length is any odd multiples of half wavelength (Huang, 2010). In the preferred MPP housing device absorber L_c=3 case, the passband appears in the low frequency f=0.167 as the chamber length is exactly the half wavelength. No matter what variations to the panel properties, there is no *IL* improvement around this frequency. Aiming to develop a broadband passive noise control device that can work effectively in the low frequency range, a hollow tube with the nature of Herschel-Quincke tube is introduced to integrate with the MPP

housing (MPPHQ, hereinafter). With proper configuration, the hybrid device can maintain the performance of MPP housing device and can simultaneously report enhancement in the previous passband with a still compact geometry.

A single HQ tube for the plane wave control is illustrated in Figure 5.1. The incident sound in the main duct with cross section area A_1 is divided into two parts: one part travels along the straight main duct with section area A_2 and duct length l_2, the other part enters into the side branch called " HQ-tube" with section area A_3 and center-to-center interface length l_3. The two sound waves will encounter again in the downstream main duct with section area A_4 forming the transmitted sound wave. Briefly speaking, the working mechanism of HQ tube is that, part of the acoustic energy goes through the HQ tube and then converges with the remaining acoustic energy in the main duct. For path difference exists between the two sound waves, at certain frequencies the sound wave from the HQ tube is out of phase with the sound in the main duct and the sound cancellation undergoes.

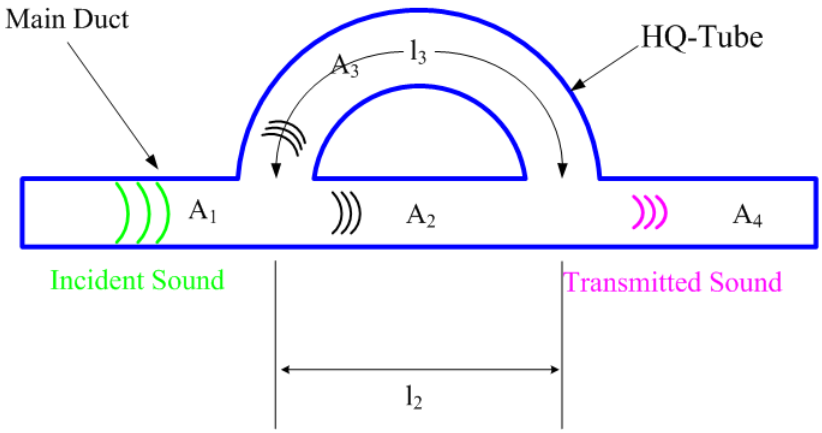

Figure 5.1: Schematic of traditional Herschel-Quincke tube for the control of plane wave

The concept of HQ-tube was first introduced by Herschel (1833) who theorized that, "No motion is, strictly speaking, annihilated; but it may be divided, and the divided parts made to oppose and, in effect, destroy each other." He predicted that the sound cancellation will appear if the given sound in a duct is divided into two branches with equal area, with the path length difference between the recombined signals $(2n+1)(\lambda/2)$ and forming out-of-phase acoustic interference, where λ is the wavelength of the acoustic wave and n is any integer.

This theory was experimentally validated by Quincke (1866). In the 20th century, Stewart (1928) improved Herschel's theoretical explanation by observing that sound cancellation also appears when $l_2+l_3=n_1\lambda$ provided that $l_3-l_2 \neq n_2\lambda$ where n_1 and n_2 are independent integers. Stewart also showed that almost no sound attenuation at other frequencies. More recently, Selamet *et al*. (1994) extended the study to derive an analytical model without any geometry restrictions on duct cross-section area and found that broadband sound attenuation can be achieved by removing the geometry restrictions.

In this chapter, a non-uniform section area Herschel-Quincke tube is applied to integrate with the MPP housing device aiming a broadband sound attenuation in the low frequency range. Following this brief introduction, the modeling of the hybrid noise control system will be described in Sec. 5.2. The simulation model is established to predict the insertion loss of MPPHQ device with a finite duct length controlling the dipole sound at the source. Optimization process of the device's performance is executed through the variation of hollow tube geometry and the numerical results are presented in Sec.5.3 with the comparison between optimal

MPPHQ and MPP housing device with equivalent chamber length. Sec. 5.4 describes the experimental validation with a loudspeaker functioned as a dipole source and the conclusions will be drawn in Sec. 5.5.

5.2 Numerical modeling of hybrid MPPHQ device

The two-dimensional finite element model of the MPPHQ is shown in Figure 5.2. It consists of four parts: the main duct, two backed cavities, the MPP and the newly introduced hollow tube. For the duct, there are middle segment for the MPP housing device with length L_c^*, two small segments for the hollow tube, and upstream and downstream sides with length of L_{up} and L_{dn} respectively, with the same duct height of h^*. For the cavity, it is in the rectangular shape with height h_c^* and length L_c^* parallel to the duct, and the inner surfaces are covered by the perforated panel with two ends fixed. Just outside the cavity wall, a shallow non-uniform cross-section area hollow tube is employed with side width W^* and upper width H^*. Thus, based on the previous optimal MPP housing device, together with the newly introduced hollow tube, the so-called MPPHQ device is formed. A dipole source is located at the mid-point of the MPPHQ: $x^*=0.5L_c^*$, $y^*=0.5h^*$. Note that there is certain difficulty to install both the compact MPP housing device and the hollow tube in one surface of the duct. For the model is a 2D prediction, in the experiment validation process which is a real 3D case, the hollow tube component can be moved to the side surface of square duct. By this approach, the complicated 3D model can be maximally simplified as a 2D model to save the computer resource and simulation time. At the same time, the predicted results can be conveniently validated by the experiment with rather high accuracy.

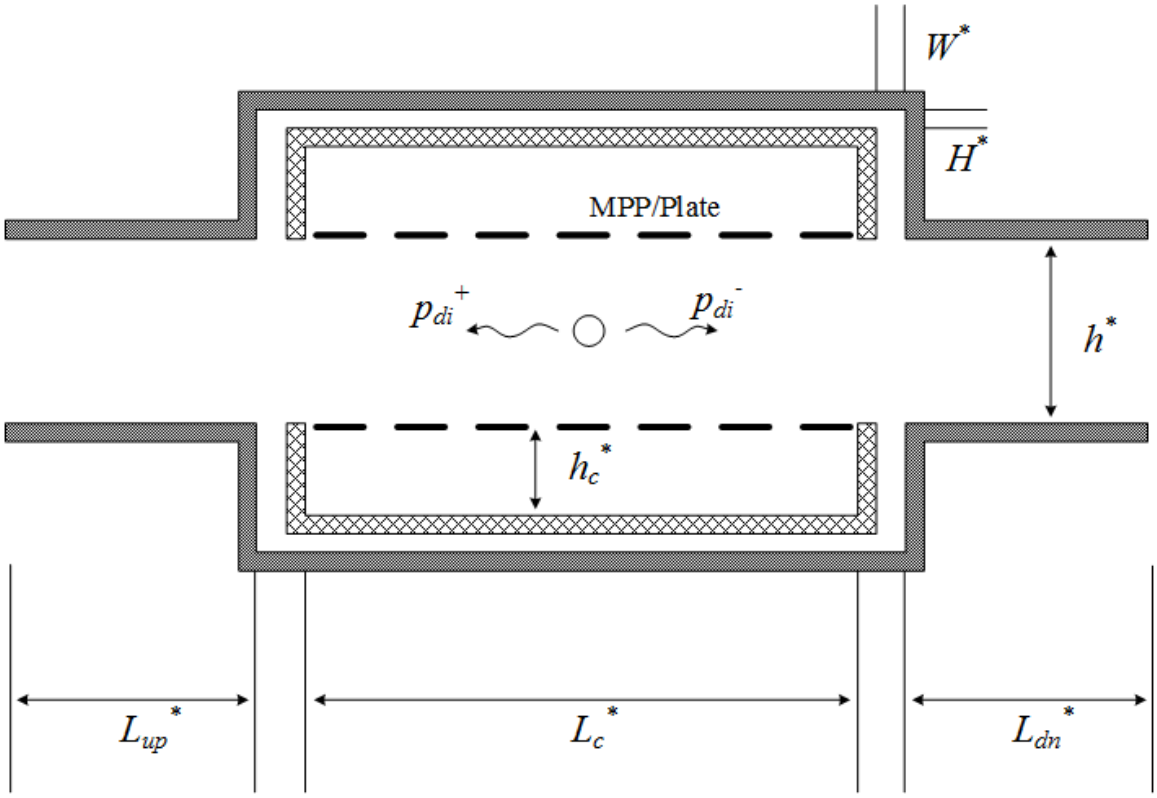

Figure 5.2: Configuration of 2D numerical model of MPPHQ device

To simplify the model, the flow is not considered at first. In the numerical modeling process, the software package of COMSOL MultiPhysics is utilized, with detailed calculation, plotting and optimization process realized by MatLab. COMSOL Multi-Physics can solve partial differential equations for coupled physics conditions, which is our major concern in model analysis. To simulate the practical configuration, the duct, cavities as well as the hollow tube component are set to be two-dimensional in the model of in Acoustics Module via Pressure Acoustics and the plates are set to be two-dimensional in the model of in Structural Mechanical Module via In-plane Euler Beam.

In the simulation, all the variables used are dimensionless values. The following shows the process of converting dimensional value to dimensionless and all

dimensional variables are normalized based on three basic quantities, the air density ρ_0^*, the speed of sound c_0^* and the duct height h^*:

$$
\begin{gathered}
H = \frac{H^*}{h^*},\ W = \frac{W^*}{h^*},\ h_c = \frac{h_c^*}{h^*},\ L = \frac{L^*}{h^*},\ L_c = \frac{L_c^*}{h^*} \\
f = \frac{f^* h^*}{c_0^*},\ \omega = \frac{\omega^* h^*}{c_0^*},\ k_0 = 2\pi f,\ m = \frac{m^*}{\rho_0^* h^*} \\
B = \frac{B^*}{\rho_0^* c_0^{*2} h^{*3}},\ F = \frac{F^*}{h^* \rho_0^* (c_0^*)^2},\ p = \frac{p^*}{\rho_0^* (c_0^*)^2}
\end{gathered}
\tag{5.1}
$$

where *m* is the plate-to-air mass ratio, *B* is the dimensionless bending stiffness of the plate, *F* is the concentrated force exerted on the fluid by the dipole source, and *p* is the sound pressure.

The acoustic field in the duct is governed by the following equation

$$\nabla^2 p + k^2 p = q \tag{5.2}$$

where *q* is the source strength of dipole source.

For the two ends of the duct, the impedance boundary condition is used as the following:

$$\frac{\partial p}{\partial n} + \frac{ikp}{Z_{rad}} = 0 \tag{5.3}$$

Here $\vec{n}$ is the local outward normal direction and Z_{open} is the so-called radiation impedance of the tube termination. The terminating impedance is usually complex number with the real part representing radiation loss of sound energy and the imaginary part representing the inertia. The empirical formulas of the radiation impedance of the circular pipe (Atig, 2004) for unflanged and flanged pipe ends are

$$
Z_{open} = \begin{cases} 0.25(ka)^2 + ik(0.6133a) & unflanged\ \ pipe \\ 0.25(ka)^2 + ik(0.8216a) & infinitely\ \ flanged\ \ pipe \end{cases}
\tag{5.4}
$$

with a the radius of the duct. For special case that the pipe is infinitely long or with absorption termination, Z_{open} =1.

Other boundaries (the wall) of the duct are modeled as acoustically rigid, and the boundary condition on the hard walls is well known as

$$\frac{\partial p}{\partial n} = 0 \tag{5.5}$$

The radiated sound waves from the dipole source (p_d) excite the panel into vibration with a transverse displacement of complex amplitude η in the y direction with velocity $v_p=\partial\eta/\partial t$. The vibrating panel will radiate sound into the duct and cavity which are denoted by p_{rad} and p_{cav} respectively. The vibration of the panel at y=0 with the pressure difference between the duct and the cavity is governed by

$$\frac{B}{i\omega}\frac{\partial^4 v_p}{\partial x^4} + mi\omega v_p + p_d + p_{rad} - p_{cav} = 0 \tag{5.6}$$

$$v_p = \frac{\partial \eta}{\partial t} = ik\eta \tag{5.7}$$

where v_p is vibration velocity of plate, η is the displacement of plate.

For the micro-perforated panel, it can be considered as a lattice of short narrow tubes, separated by distances which are much larger than their diameters, but small compare to the wavelength of the impinging wave. The acoustic impedance of the short narrow tubes has been studied by many scholars. The air and rigid structure interaction governing equation as well as the approximate formulation for the acoustic impedance of the micro-perforated panel are

$$Z_{i,resist}(v_0 - v_p) + Z_{i,react}v_0 + (p_d + p_{duct} - p_{cav}) = 0 \tag{5.8}$$

$$Z_{i,resist} = \frac{32\mu t}{\rho_0 c_0 d^2}\left[\left(1+\frac{K^2}{32}\right)^{1/2}+\frac{\sqrt{2}}{32}K\frac{d}{t}\right]$$
$$Z_{i,react} = i\cdot\frac{\omega t}{\sigma c_0}\left[1+\left(1+\frac{K^2}{32}\right)^{-1/2}+0.85\frac{d}{t}\right] \quad (5.9)$$

where v_0 is the particle velocity of fluid in the holes, $K = d\sqrt{\omega\rho_0/4\mu}$, d is the hole diameter, t is the panel thickness, σ is the perforated ratio, μ is the coefficient of viscosity, ρ_0 is the air density, and c_0 is the air speed. The real part $Z_{i,resist}$ is called the acoustic resistance and is associated with the energy radiation and viscous losses in case of mean flow. The imaginary part $Z_{i,react}$ is called the acoustic reactance which is inertial in nature.

Equations (5.1)-(5.9) are solved in a coupled manner and the sound insertion loss (*IL*) can be expressed as:

$$IL = 10\log 10\left(\frac{\int_{str} |\, p_{out}\,|^2\, ds}{\int_{mppHQ} |\, p_{out}\,|^2\, ds}\right) \quad (5.10)$$

where p_{out} is the sound pressure at the duct outlet, the "*str*" refers to the straight duct as reference and the "*mppHQ*" refers to the device consisting of the MPP housing device and the shallow hollow tube segment.

5.3 Device performance and optimization

After proper modeling of our proposed design using COMSOL Multi-physics, the MatLab package was utilized for post-stage analysis. Codes generated

automatically from COMSOL were further programmed in MatLab for looping of various geometries in our model and also for better results comparison. Note that for this MPPHQ device, the MPP housing device part is maintained as the optimal configuration in the Chapter 3 which means that the length of the cavity, the height of chamber and the properties of the panel are kept as the same. The aim of fresh employed hollow tube segment is to enhance the *IL* performance in the previous passband. Thus, there are only two parameters for variation in this section, i.e., the side width *W* and upper width *H* of the hollow tube. For each parameter, rough step size was adopted at preliminary stage for general trend prediction. For example, when looping for side width W, the setting of W varying from 0.05 to 1 (with the step size to be 0.05) would be implemented, with other parameters remaining as default. Further calculation will target those parameter values until a favorable *IL* performance is obtained with minor step size for more accurate analysis.

5.3.1 Variation of tube upper width *H*

Side width H is varied from 0.1 to 0.25 to examine its influence on the IL capacity of the proposed model. The numerical results are presented in Figure 5.3. The figures from (a) to (d) show the insertion loss spectrum change as the width varies from 0.1 to 0.25 while the side width of tube is fixed as *W*=0.1. The horizontal solid line is the criteria IL_{cr} 5 dB, curve solid line shows the *IL* spectrum of optimal MPP housing device and the dashed line stands for the result for corresponding MPPHQ. The closed circles in the dashed line denoted with f_1 and f_2 represent the lower limit and upper limit of the effective frequency band (within which range $IL>IL_{cr}$) of the MPPHQ device respectively.

With introducing the tube segment, the *IL* performance is better in the previous passband regime which is around *f*=0.167, although there is a little drop existing in the medium frequency range in $f \in [0.37\ 0.43]$ while the *IL* is still larger than the IL_{cr}. It should be pointed out that, with introducing the new tube component, there is another trough around *f*=0.15 due to the tube length as shown in the *IL* spectrums. The overall trend of *H* influence on device performance is clearly illustrated by the blocks that as H increases, the upper limit of effective frequency band f_2 is shifted towards low *f* region, from about 0.23 to 0.18. For convenient application for the varies kinds of industry products with fans or for the products operating with various rotational speed which will result in different frequency BPF noise, the widest stopband (the effective frequency band) is our option. Therefore, the upper width of the hollow tube should be rather small, which also matches the requirement of a compact geometry of the device.

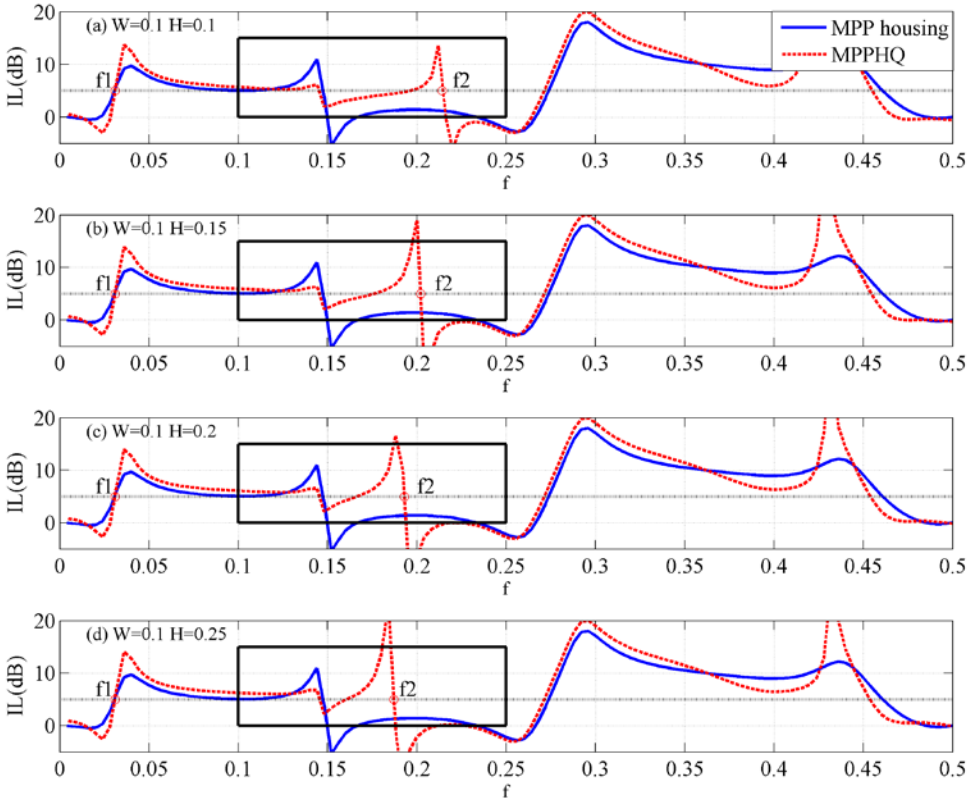

Figure 5.3: Device performance comparison when the upper width *H* is varied from 0.1 to 0.25 with fixed side width *W*=0.1

5.3.2 Variation of tube side width *W*

After preliminary prediction of a small upper width *H* for the hollow tube (shown in Figure 5.3), it is then necessary to identify influences from the side width *W*. The simulation results are illustrated in Figure 5.4, with comparing the device performance when *W* varies from 0.1 to 0.25 with constant *H*=0.1. From the sub-figures 5.4 (a) to 5.4 (d), we can find that the performance in the previous passband existing in the MPP housing device in low frequency regime is improved. The general tendency of side width is that as the width grows, the effective frequency range [f_1 f_2] in the target passband regime gradually becomes wider. However,

when the W exceeds 0.2 there is a drop appearing just before the upper limit of effect band f_2 even lower than the criteria IL_{cr} 5 dB. At the same time, the trough region around f=0.15 due to the tube length marked as circle in the dashed MPPHQ line will keep deteriorating, and there is no noise abatement when the side width reaches 0.2. Thus, the side width should be around 0.15 that it can obtain a wider stopband and can maintain a good IL output between the two peaks simultaneously.

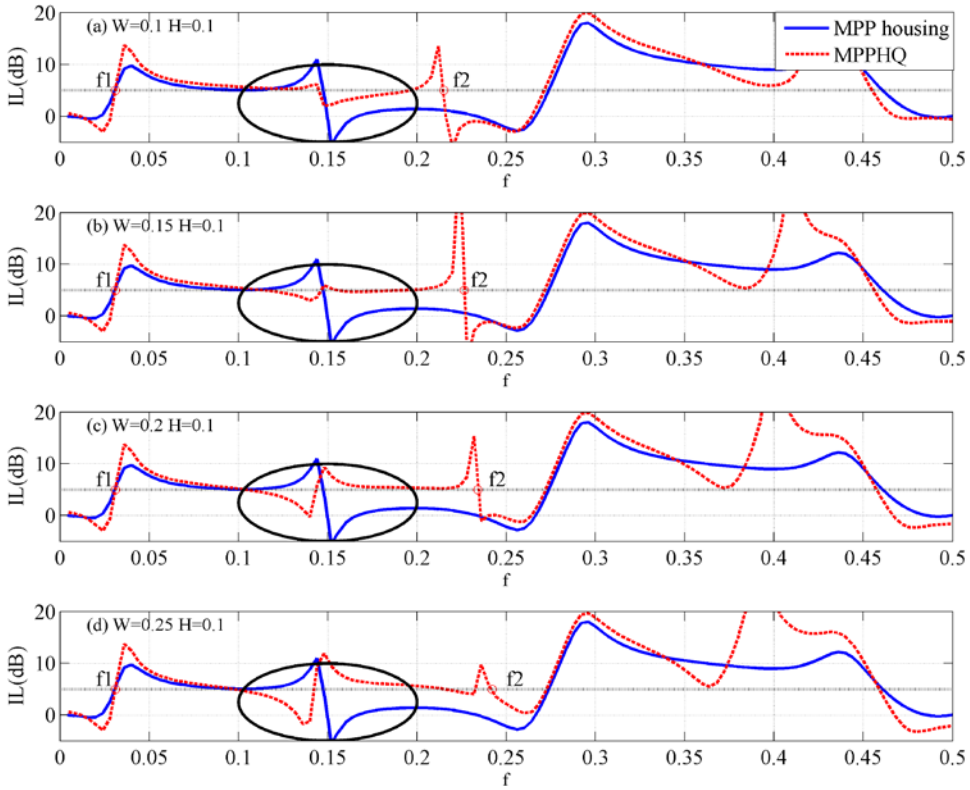

Figure 5.4: Device performance comparison when the side width H is varied from 0.1 to 0.25 with fixed upper width H=0.1

5.3.3 Optimization of hollow tube configuration

Note that due to the effect of tube length, there is always trough region between the two peaks around f=0.15, so it is difficult to achieve the previous criteria IL_{cr} 5 dB.

However, aiming to maintain the MPP housing device effect and improve the device performance in the passband region, the criteria of *IL* level can be relaxed to 3 dB in the trough region as 3 dB means half energy dissipation. Therefore, during the optimization process, the cross functions are as following: 1) the *IL* output in the trough region around f=0.15 larger than 3 dB and; 2) selecting the widest frequency ratio of effective band $f_r=f_2/f_1$.

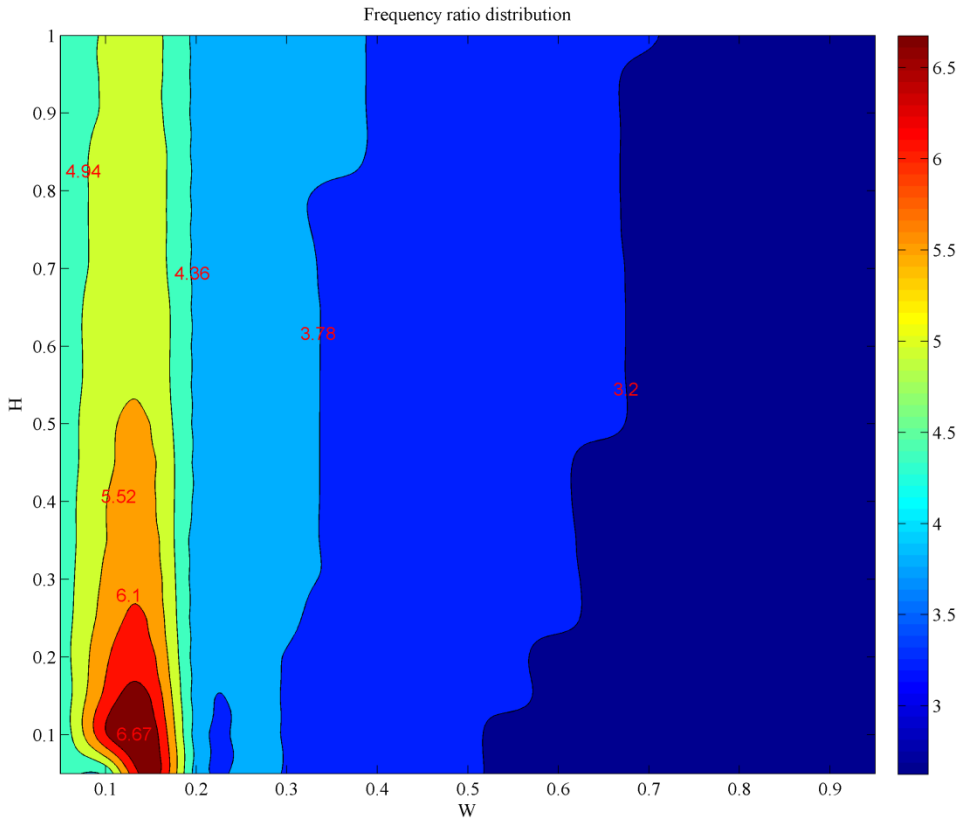

Figure 5.5: Frequency ratio varies with tube width

The Figure 5.5 expresses the distribution of frequency ratio as a function of tube geometry with side width and upper width varying from 0.1 to 1. Through the contour plot, the frequency ration varies in the range 2.5 to 7. The red region which denotes the widest stopband appears in the position of side width around 0.15 and

upper height 0.1. With this geometry, the MPP housing device capacity can be maintained and the performance in the previous passband can be greatly improved with a still geometry: the total length of side branch 3.5 and height 0.7, including the MPP cavity part L=3, H_c=0.5 as well as wall thickness 0.1.

5.3.4 Comparison between optimal MPPHQ and equivalent length MPP housing device performance

With introducing the shallow tube, the *IL* outcome of the housing device has been improved. As the geometry of the newly formed has enlarged a little, there is a need to compare the *IL* performance of MPPHQ with the MPP housing device with equivalent geometry, that is, L=3.5 and H_c=0.7. The Figure 5.6 shows the *IL* comparison between the previous optimal MPP housing device (solid line), newly designed MPPHQ (solid line with circles) and the equivalent geometry MPP housing device (the dashed line). In summary, both the MPPHQ and the equivalent MPP housing device report good *IL* performance in the previous passband [0.15 0.25]. However, the *IL* drop due to the side branch length of the equivalent geometry MPP housing device is worse compared with the MPPHQ around f=0.14. This phenomenon is more obvious in the medium frequency f=0.42, thus the equivalent geometry MPP housing device results in a very shallow effective frequency band [0.26 0.37] and the MPPHQ reports a wider stopband [0.27 0.46]. That is the motivation to design the MPPHQ, as there is no chance to improve the passband situation while keeping the optimal MPP housing device performance through altering the geometry size of cavity.

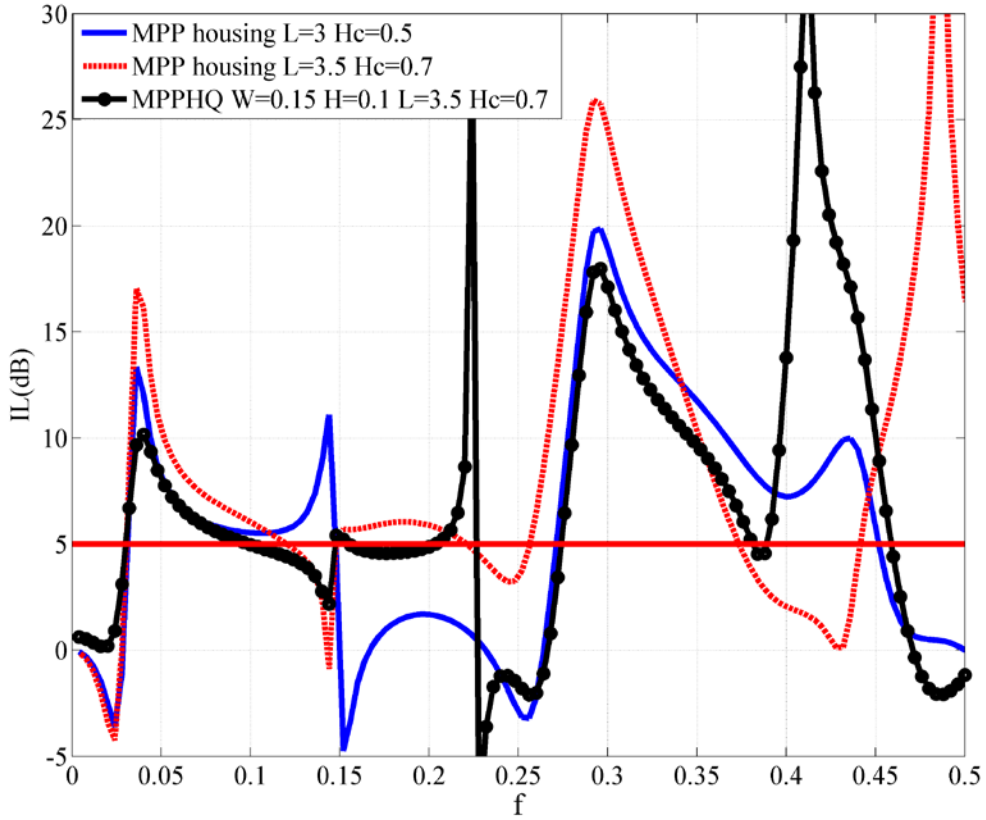

Figure 5.6: *IL* spectrums comparison between optimal MPP housing device and MPPHQ results

5.4 Experiment study

The experiment is carried out to validate the numerical simulation and the setup is the same as that in Chapter 4 of the *IL* measurement of MPP housing device. The experimental test rig is shown in Figure 5.7: (a) the CAD drawing of test rig and (b) the manufactured test rig. The test rig is divided into several parts which can be clearly identified in the CAD drawing: the main duct (purple components), the side branches for MPP (yellow components) and the hollow tube segment denoted as the combination of grey and red components. The red part is a rigid block and there is a gap between this red block and the grey wall

forming the hollow tube. The geometry of the tube can be varied through adding rigid plate covering on the outer surface of the rigid block or inner surface of the grey wall.

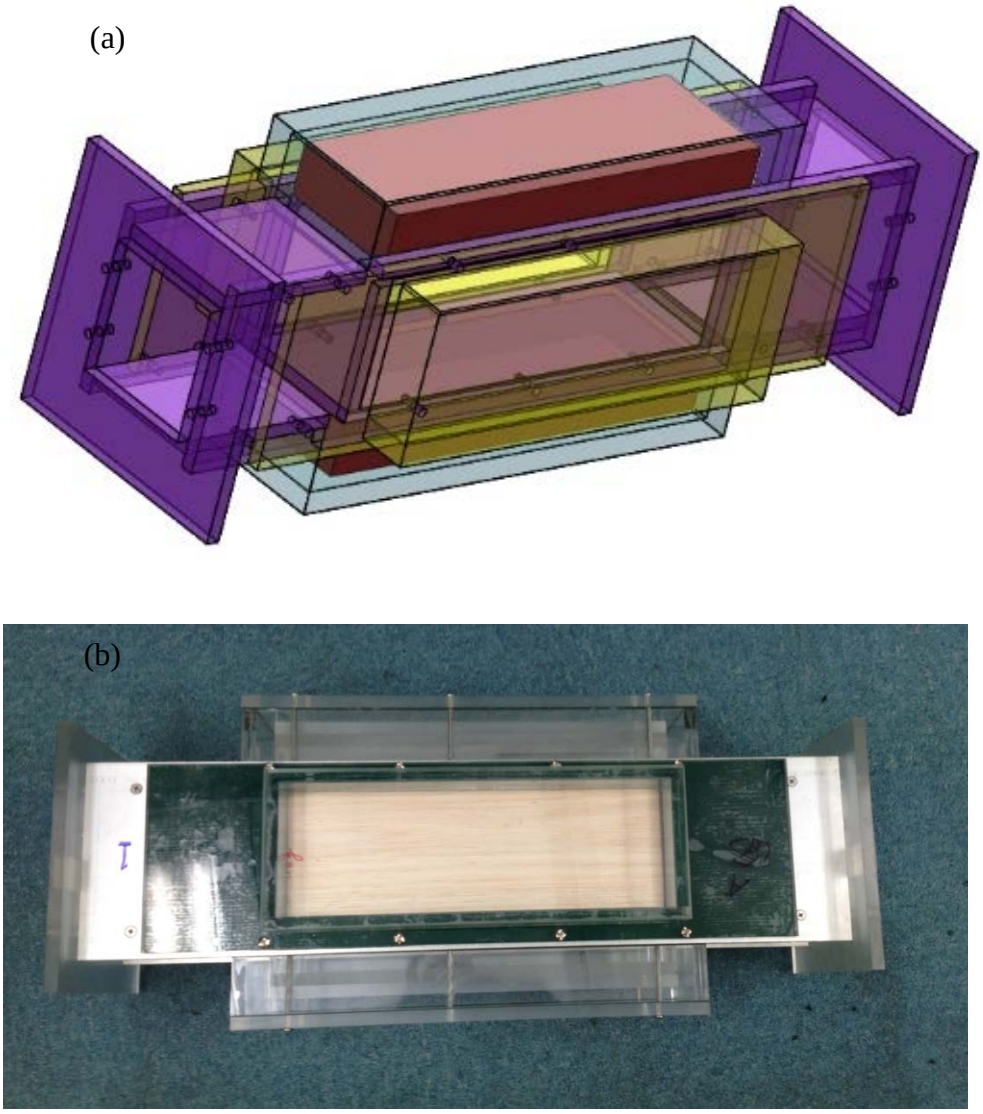

Figure 5.7: Test rig for the experiment: (a) the CAD drawing of test rig; (b) the manufactured test rig

Note that the dimension of the rigid block is the same as the MPP cavity for the aim of this design is to improve the device performance based on the previous MPP housing device and this tube segment is assumed to be installed just outside the wall of MPP cavity for the requirement of compact geometry. The action of

moving the tube segment to another side of the duct is just for the convenience of experiment. In the finalized MPPHQ device as shown in the Figure 5.7 (b), the dimension of the main duct is with a $100\,\text{mm}\ X\ 100\,\text{mm}$ cross section area and length of 610 mm. Two sides of main duct are installed with the side branch cavities with cavity length 300 mm and height 50 mm, with MPP covering on the surface (MPP properties: B=0.0032, m=0.98, σ=2.7, d^*=0.5 mm and t^*=1 mm). Another two sides are installed with the hollow tube segments. The dimension of rigid block is $320\,\text{mm}\ X\ 100\,\text{mm X}\ 60\,\text{mm}$, and there is a gap of 30 mm width between the rigid block and the outside rigid wall. The gap can be adjusted in the range of 5 mm to 30 mm according to the requirements. For the two sides that installed with the MPP, the material is aluminum for the convenience of manufacturing the slot for holding the MPP and fixing the backed cavities through screws. All other parts are made from 10 mm thick acrylic plastic plates, which can be considered to be acoustically rigid.

The experimental results are compared between the previous optimal MPP housing device (solid line with circles) and the fresh designed MPPHQ (dashed line) as shown in the Figure 5.8. The first row indicates the *IL* performance comparison from the raw data between the MPP housing device and the MPPHQ and the second row shows the results after dipole extraction (the details are explained in the Chapter 4). In both the two figures, by introducing the shallow hollow tube segment, the *IL* performance will be enhanced in the low frequency around 500 Hz to 800 Hz about 3 dB in average, and there is also improvement in the medium frequency range from 1300 Hz to 1600 Hz. By the extraction process, the *IL* curves become smoother and the effect of monopole component from the source is eliminated. The sharp drop existing in the raw data at around 1050 Hz will

disappear. As demonstrated in the Figure 3.10, the proposed MPP housing device will report different sound attenuation performance when the source is changed to a monopole from a dipole. The lower limit frequency in the experiment is 150 Hz due to the capability limitation of the small loudspeaker acting as a dipole source, and the upper limit is 1700 Hz which is the cut-on frequency of the duct.

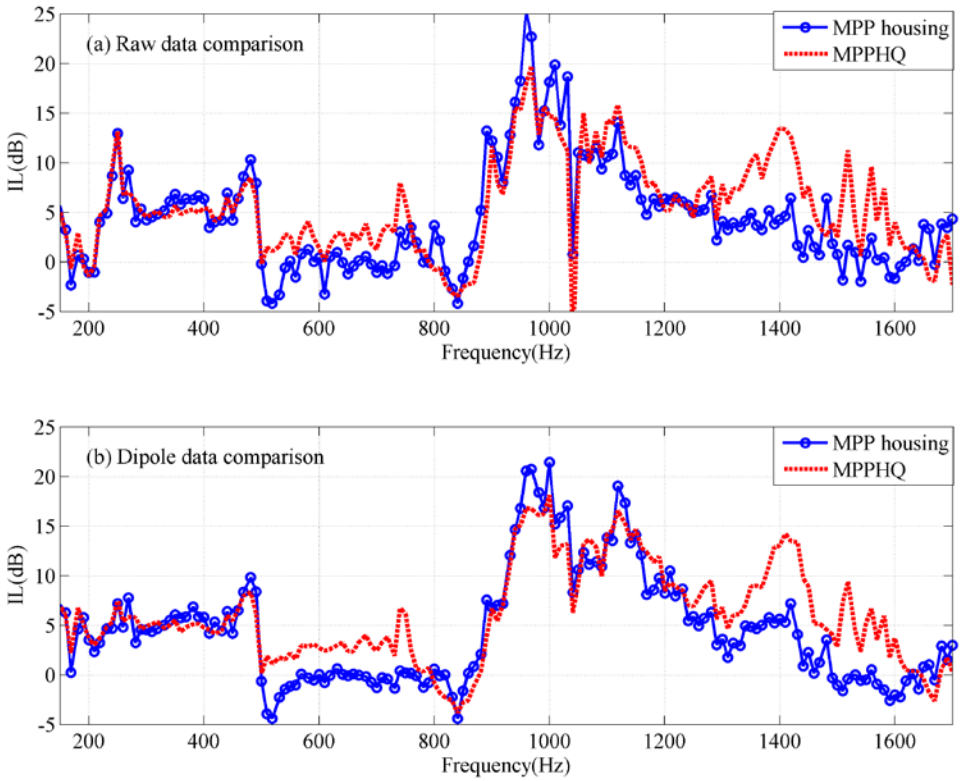

Figure 5.8: Experimental results comparison between MPP housing device and MPPHQ: solid line with circles represents the MPP housing device and dashed stands for the MPPHQ. (MPP properties: B=0.0032, m=0.98, σ=2.7, d^*=0.5 mm and t^*=1 mm; hollow tube parameters: W=0.15, H=0.1)

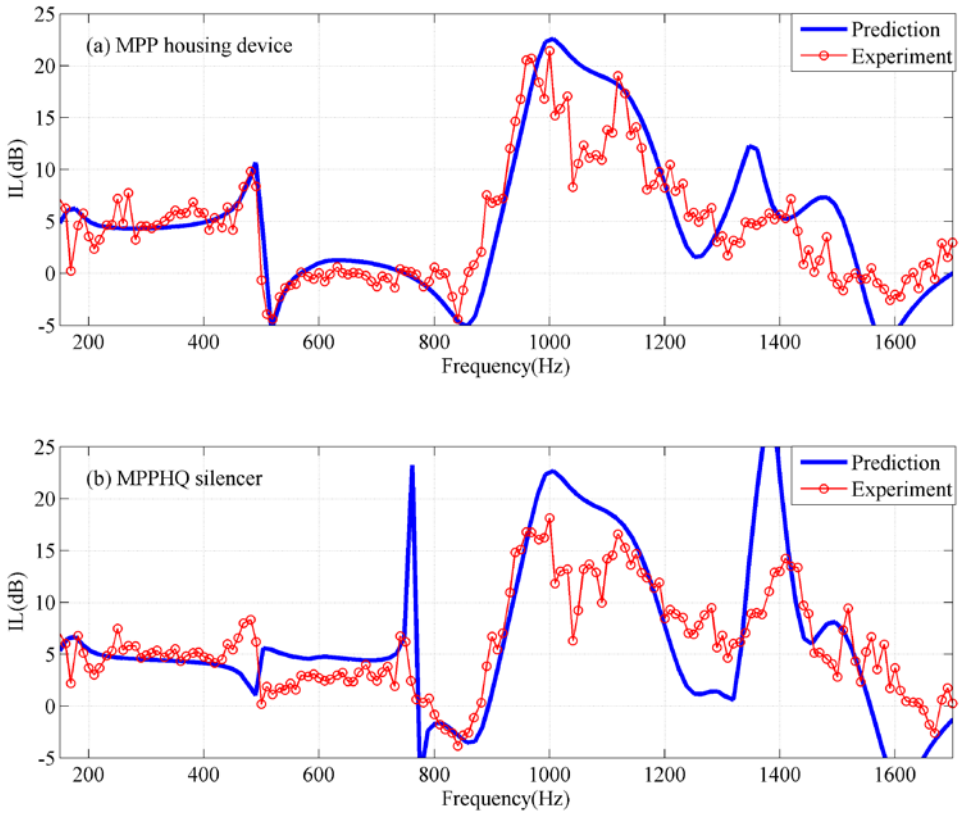

Figure 5.9: Validation of experimental results with numerical predictions: (a) MPP housing device and (b) MPP housing device integrated with hollow tube. The solid line is the predicted result and the line with circles stands for measurement

The results obtained from experiments are compared with the data from simulations for validation. Red line with circles represents housing device performance in experiments and blue solid line denotes prediction results. Both in the MPP housing device shown in Figure 5.9 (a) and MPPHQ in Figure 5.9 (b), the *IL* spectrum from the experiment generally matches with that of prediction. Although the *IL* of MPPHQ has not achieved 5 dB as predicted in the frequency range 500 Hz to 800 Hz, the result can still be utilized to validate the numerical prediction as there is a 3 dB noise attenuation to declare the function of fresh shallow tube.

5.5 Conclusions

Numerical simulations regarding to newly designed MPPHQ device have been conducted and the results have been validated through the experiments. Through analyzing numerical results, it is found device with parameter W=0.15 and H=0.1 would result in the optimal insertion loss performance which maintains the MPP housing device performance and has the capacity to improve the previous passband existing in the MPP housing device output. The update geometry still satisfies the requirement of a compact geometry requirement due to the limit space in the real applications. The numerical simulations have been validated through the experiments and there is a good agreement achieved. Thus the new design of MPPHQ housing device integrates the MPP housing device and the HQ tube nature segment can be beneficial to the industry products noise control.

Chapter 6 Investigation of cavity partition effect on the MPP housing device

6.1 Introduction

For the extensive application of MPP in noise control devices (Fuchs and Zha, 1997; Wu, 1997; Fuchs and Zha, 2006; Li *et al*., 2010; Allam and Abom, 2011; Wang *et al*., 2012; Park, 2013), a great many researchers have put their efforts to seek methods for widening the effective absorption bandwidth of MPP type devices. It is well known that the traditional MPP absorbers report resonance type absorption with narrow bandwidth due to the sound propagating only in the transverse direction inside the back cavities. To broaden the effective absorption bandwidth, a double (Maa, 1987) or a multi-layer MPPs (Lee and Chen, 2001; Lee and Kwon, 2004; Bravo *et al*., 2013) have been utilized, but such treatment will increase the size and weight of the absorber. Apart from multiple MPPs, reducing the size of perforation (Maa, 1998) or MPP with irregular cavity (Wang *et al*., 2010) can also be used to widen the effective frequency band. Particularly, Wang and Huang (2011) have tested the sound absorption performance of MPP absorber in a compound array with different cavity depths and obtained broadband sound absorption due to strong local resonance, and the MPP absorber array has been extended to a periodic array with oblique incidence in diffuse field (Wang *et al*., 2014).

The idea of such array of back cavities actually has a long history. Mani (1976) proposed the concept of the checkerboard liner first and showed experimentally that a circumferentially segmented liner could provide better attenuation performance than a uniform liner, recommending that a segmented liner both in axial and circumferential direction may have potential to further improve the liner performance. The working principle of performance improvement is the wave reflection and scattering happening at impedance discontinuities. Watson *et al*. (2004) found that the impedance variation of checkerboard liner would be more sensitive than that of uniform liner and indicated the optimum liner impedance depending on the structure. Jing *et al*. (2007) proposed a mechanism of multiple cavity resonance for broadening the absorption bandwidth of an MPP liner by partition which not only produced sound reflection as with the previous methods by means of scattering or impedance discontinuity, but also provided way to enhance acoustic energy dissipation. The basic idea is that, sound propagation occurs in both the transverse direction normal to the perforated panel and the longitudinal direction within the backing cavity. In this regard, the more resonances occur inside the MPP liner, the larger possibility is for the absorption peaks to close each other forming widened bandwidth. By inserting partition plates to the backing cavity to divide the single cavity into different size sub-cavities, more sound absorption peaks appear due to the coupling of the acoustic modes in different directions inside the sub-cavities and the multiple resonances are produced. Allam and Abom (2011) had also experimentally investigated the effect of uneven split in the outer chamber and concluded that the longest chamber length should be larger than half of the wave length to avoid the minima in the frequency range of interest. Lu *et al*. (2014) have developed a finite acoustic model to

investigate the characteristic of non-locally reacting acoustic liner and drawn that the resonance peaks of the liner could be tuned to the expected position to broaden the absorption bandwidth, with experiment validation.

The objective of current study is to develop a compact broadband device to control the ducted-fan noise at the source. Based on the optimal configuration of MPP housing device proposed in Chapter 3, a small hollow tube is introduced to tackle the passband drawback due to the cavity length in Chapter 5 but the total geometry size of the device is slightly enlarged. Thus the above mentioned partition techniques are applied in order to further improve the sound attenuation performance of the MPP housing device without any increase of housing size. From the study of the proposed MPP housing device to control different sound sources with dipole and monopole excitation in Chapter 3, it can be easily concluded that the MPP housing device will report different *IL* spectrums when the source nature is changed. Thus, the motivation of the following study is that, will the cavity partition effect keep the same when the sound source is changed?

In what follows, the proposed MPP housing device with incident sound wave excitation, housing a dipole source and housing a monopole source will be investigated both numerically and experimentally. The findings of this study would be beneficial to instruct the appropriate application of backing cavity partition technique according to different nature of sound sources.

6.2 Cavity partition effect of MPP housing device with Incident wave

The two-dimensional finite element model of the MPP device with backing cavities partitioned with incident sound wave is shown in Figure 6.1. The geometry is kept the same as the previous MPP housing device and consists of the main duct, two backed cavities and the MPP. The MPP is with length of L_c^* equal to the chamber with two ends clamped.

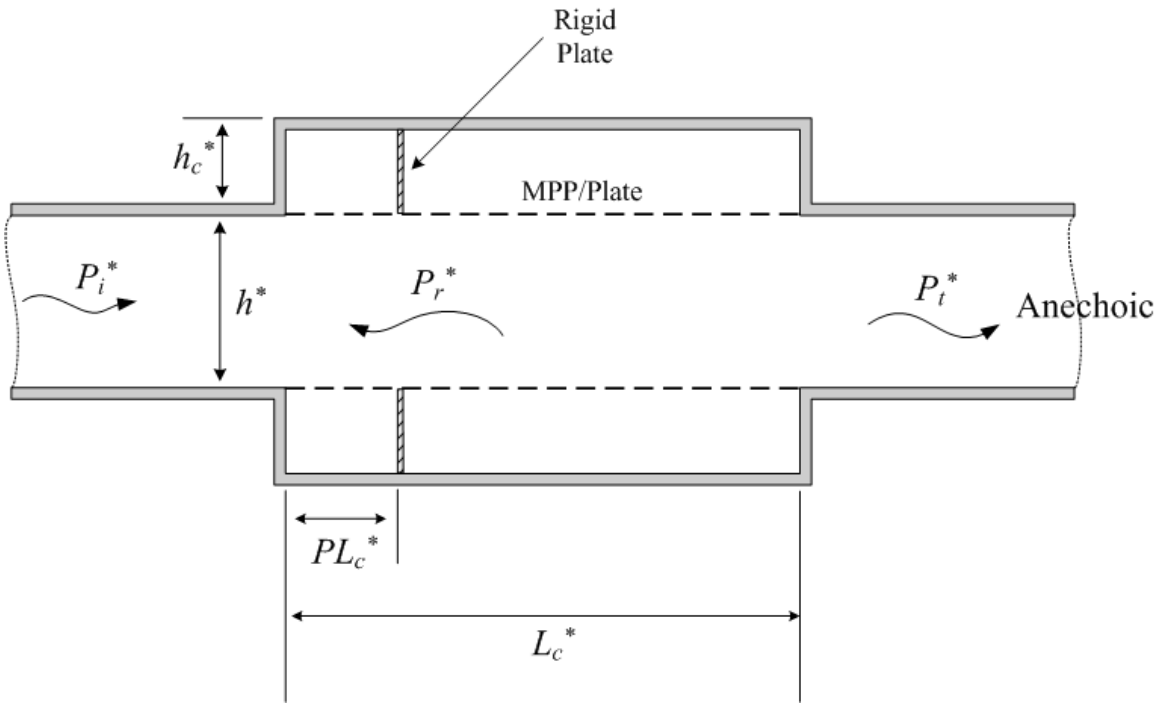

Figure 6.1: Schematic of MPP device with partition technique with incident wave excitation

The back cavity of the MPP housing device is to be divided into a number of non-uniform small cavities by inserting the rigid plates as shown in Figure 6.1. The current study is to investigate what the cavity partition effect on the MPP housing device would be, when the source nature is varied. Thus, only one rigid partition plate is utilized first to avoid the complex sound field coupling inside cavities by

multiple partitions or the partition plate integrated with perforations or even the partition plate not rigid with vibration. Apart from the rigid plate for partition, all other acoustic domains including the duct and back cavities and the boundary condition of vibrational plate are the same as proposed MPP housing device, so the details of the numerical modeling process will not be discussed in this Chapter. The following mainly focuses on the numerical and experimental results.

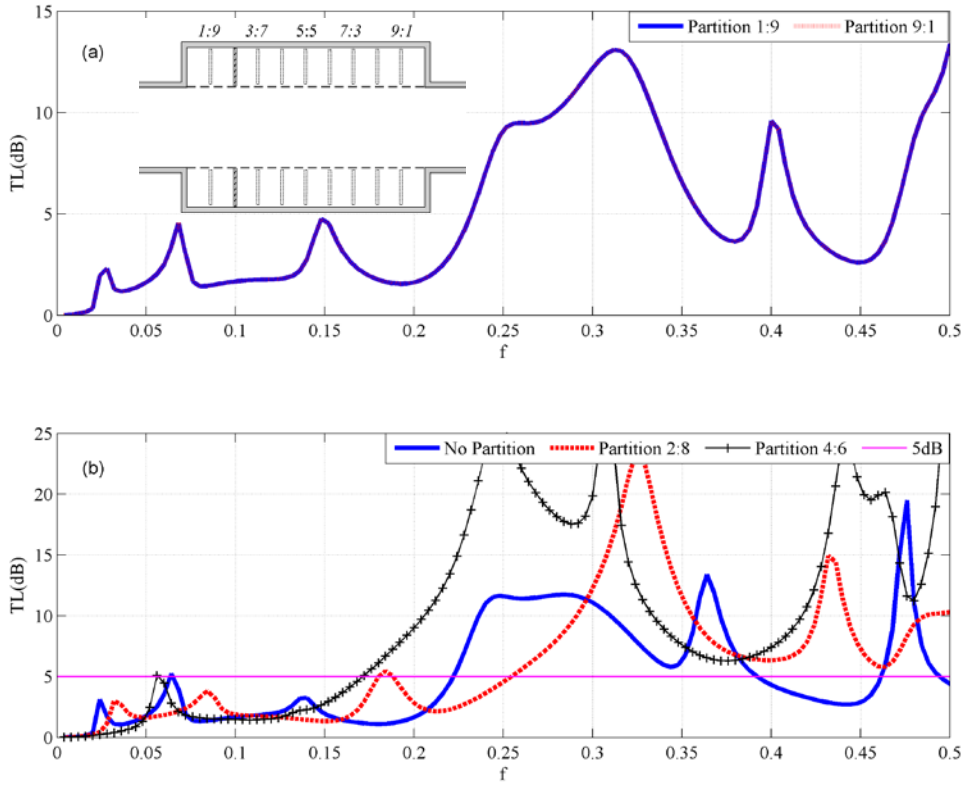

Figure 6.2: Numerical study of cavity partition effect: (a) Comparison between the device performance when the sub-cavities are 1:9 and 9:1; (b) Performance comparison among the no partition, 2:8 and 4:6

As illustrated in Figure 6.2 (a), the rigid plate for partition can be any position of the back cavity to divide the single cavity into two elements with equal or unequal length. When the partition plate is placed at 1:9 and 9:1 position, the *TL* spectrums

of the two cases are the same which indicate that with incident wave excitation, the cavity partition effect will be the same if the partition plate at upstream side of chamber (before position 5:5) and downstream side (after position 5:5) are symmetrically placed. Through the *TL* comparison among the non-partitioned MPP housing device, 2:8 partition and 4:6 partition cases shown as Figure 6.2 (b), the use of partition will improve the sound attenuation of MPP housing device in the high frequency regime $f > 0.4$ and the performance in the medium frequency range around $f=0.2$ can be further improved when the rigid plate is put at 4:6 position.

Optimization of the position of the partition plate is carried out to find the optimal location based on the cost function of the widest stopband in which the *TL* is larger than 5 dB. When the parameters of the MPP and the cavity size are kept constant, the optimal position in this case is 44:56 as shown in the Figure 6.3 (a). With no partition, the MPP housing device reporting a rather narrow bandwidth from $f=0.22$ to $f=0.39$. By introducing the partition at position of 44:56, both the medium frequency and high frequency performance have been raised up resulting in a broadband width from $f=0.16$ to $f=0.6$. The Figure 6.3 (1b) and Figure (1c) demonstrate the pressure distribution of non-partitioned MPP housing device and optimal partitioned MPP housing device at the frequency $f=0.42$ respectively, non-partitioned MPP housing device's trough point and peak for the partitioned one. And the Figure 6.3 (2b) and Figure (2c) show the intensity field of non-partitioned MPP housing device and optimal partitioned MPP housing device respectively at same frequency. Comparing Figure 6.3 (1c) and (1b), more sound energy will enter the cavity after the partition as the acoustic pressure in the cavity is much higher. Through the strong coupling between the different sound fields of the two sub-

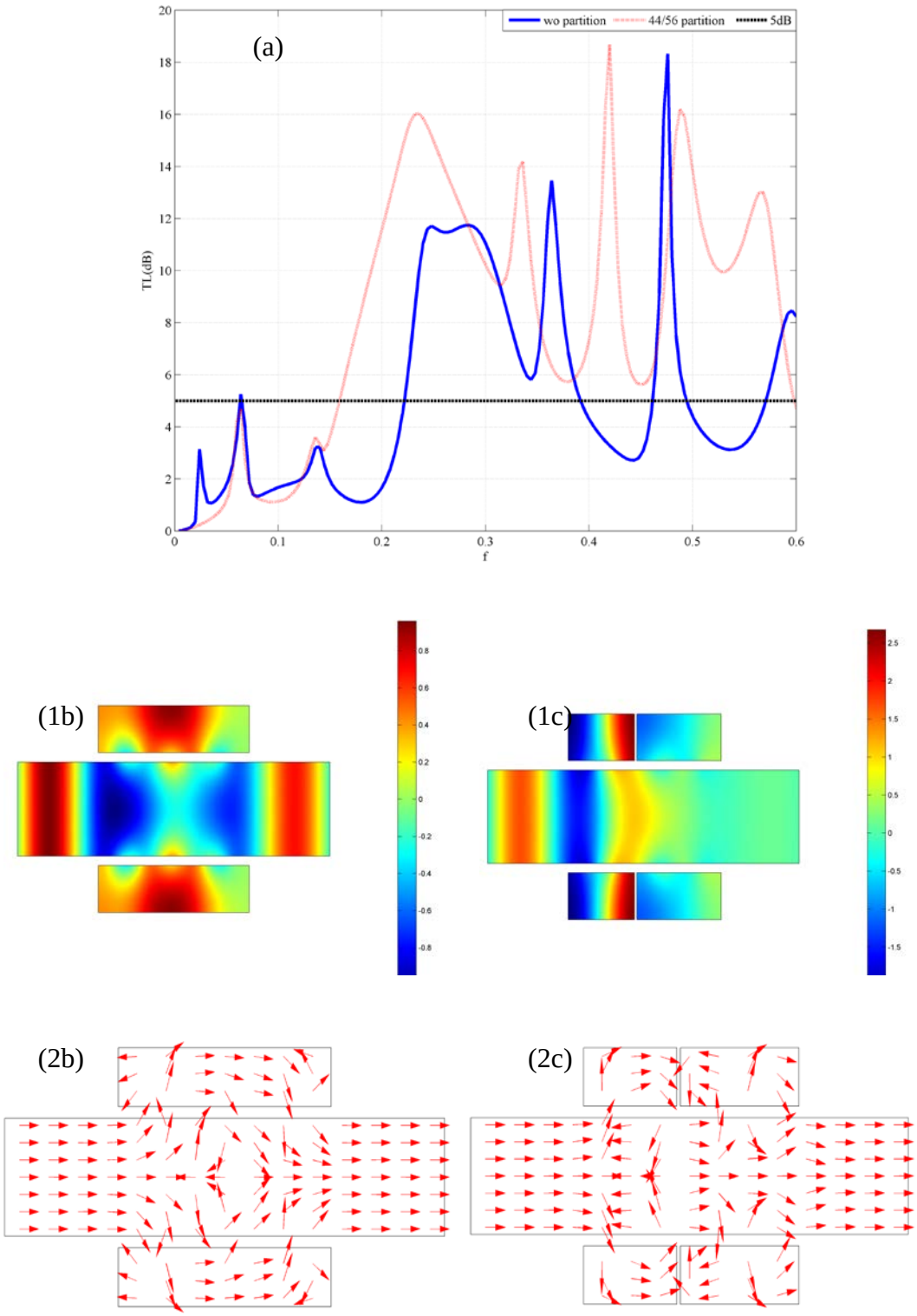

Figure 6.3: Performance comparison between the optimal partitioned MPP housing device and that without partition. (a) *TL* spectrum comparison; (b) Sound pressure contour and intensity field at f=0.42 of MPP housing device without partition and (c) partitioned MPP housing device

elements, the acoustic energy is greatly dissipated thus the acoustic pressure at the downstream is rather low resulting the *TL* peak. From the intensity fields depicted in Figure 6.3 (2b) and (2c), it can be easily found that strong acoustic coupling has happened near the field of rigid partition plate.

The experiments were carried out to verify the cavity partition effect on the MPP housing device with incident wave excitation. In the experiment, four microphones, two load methods were applied (Choy and Huang, 2002; Wang *et al*., 2012). The setup of the experiment is illustrated in Figure 6.4. The main duct is a square duct with 100 mm x 100 mm cross-section area, and the test section for MPP housing device is 300 mm with cavity height 50 mm.

Two pairs of microphones (B&K type 4187) are installed flush with the duct walls at the located position. The separation distance of microphone pairs is 80 mm in order to achieve measurement accuracy at low frequencies. Both the AD (NI. PCI-4452) and the DA (NI. PCI-M10-16E-1) convectors are controlled by a LABVIEW program, which is made to run through a range of testing frequencies from 30 to 1700 Hz in a loop with a frequency interval of 10 Hz. The output noise signal from the DA converter is passed to the loudspeaker via power amplifier (LAB 300). Because the loudspeaker is not quite effective at low frequencies, it is important to apply pure tone tests and discrete frequency approach is preferred. Signals collected by microphones pass through the conditioning amplifier (B&K 2691) and the AD convertor to the computer. For each set of data collection, two independent experiments under different downstream loading conditions are executed to

determine the *TL* of the tested MPP housing device, rigid end with a plate and anechoic end with absorption materials at the downstream end.

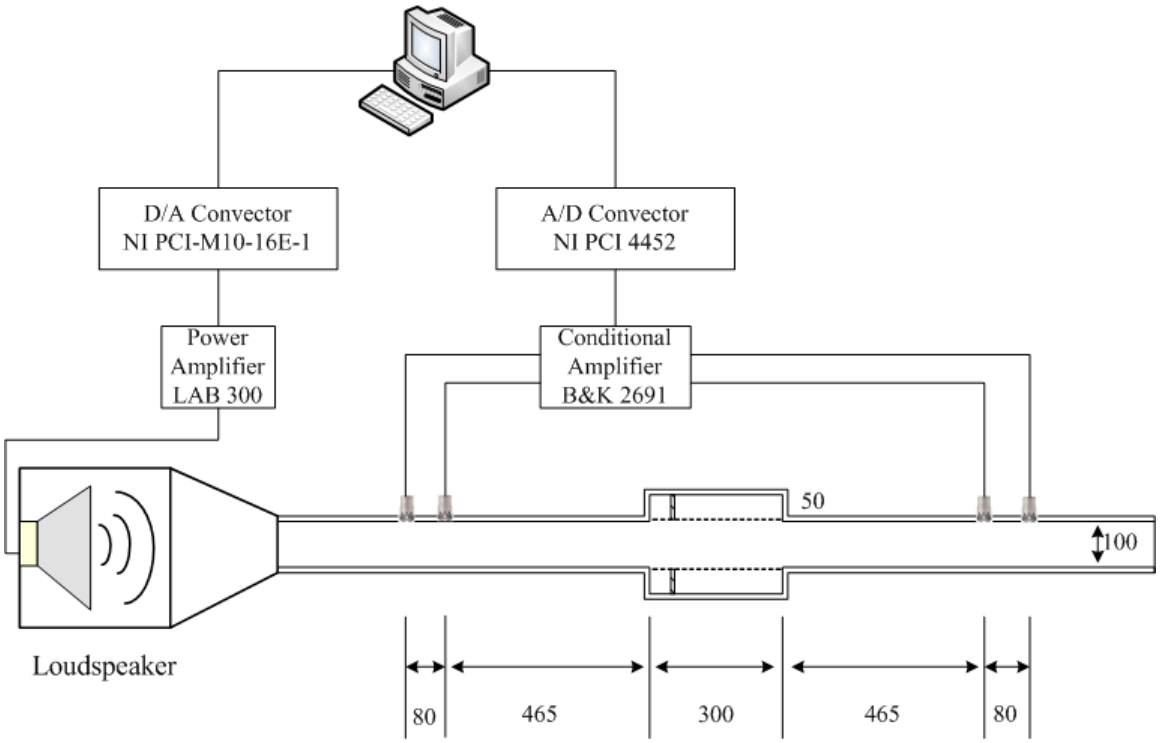

Figure 6.4: The setup of the measurement system

Although the MPP utilized in the experiment is not the optimal one, balsa wood with mass ratio m=0.98, bending stiffness B=0.032, hole size 0.5 mm and perforation 2.7%, the results can still be used to verify the cavity partition effect on the performance of MPP housing device. The experiment results are presented in Figure 6.5 with the comparison among the non-partitioned MPP housing device and that with 2:8 and 4:6 partition. The general trend of the cavity partition effect is that with partition, the *TL* performance of high frequency above 1200 Hz will be improved. The 2:8 partition case reports no significant pickup at the lower band limit around 870 Hz as in the non-partitioned device, but the 4:6 partition case will

push the lower band limit to lower than 500 Hz obtaining a broadband sound attenuation, which match well with the numerical prediction shown as Figure 6.2 (b).

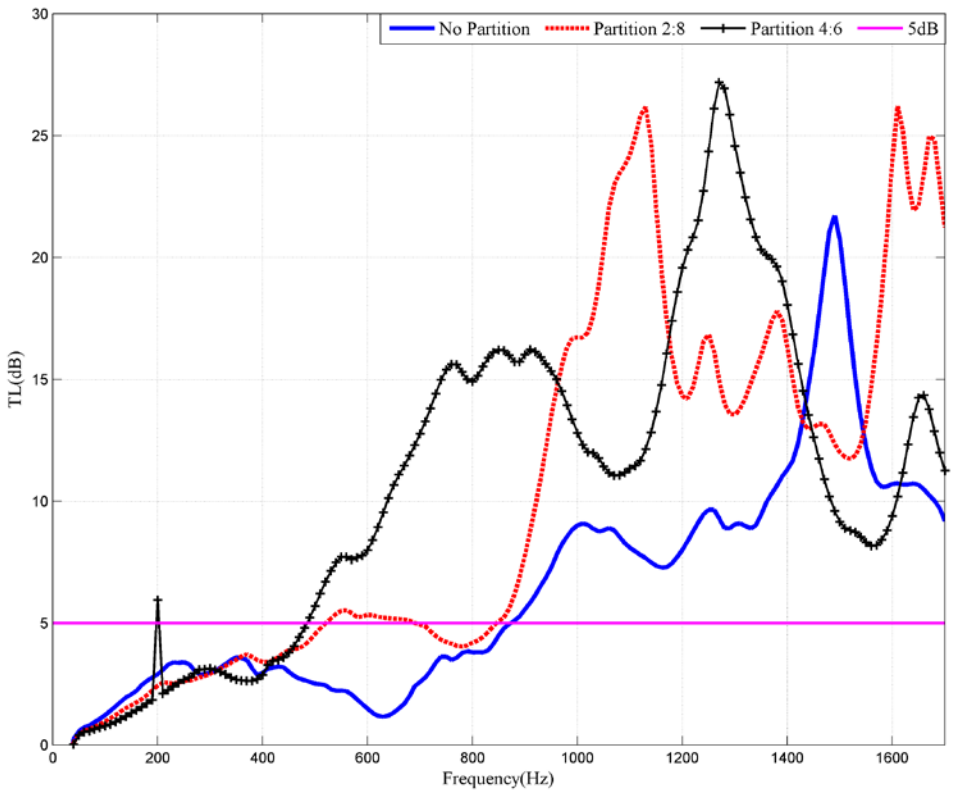

Figure 6.5: Experimental results of cavity partition effect with incident sound wave

The conclusions of cavity partition effect on the performance of MPP housing device with incident wave excitation are that, the application of partition will enhance the *TL* performance in the high frequency. With proper tuning, the sound attenuation in the low frequency range can also be achieved obtaining a broadened effective band in the target frequency range.

6.3 Cavity partition effect of MPP housing device with Dipole or Monopole source

To investigate the effect of partition in the case of dipole/monopole sound source, a two-dimensional finite element model is established as shown in Figure 6.6, the MPP housing device with different position of partition housing a dipole source. The geometry of the MPP housing device as well as the MPP properties are the same with proposed optimal configuration in Chapter 3 and the MPP housing device with incident wave excitation in Section 6.2. Note that the dipole source can be varied to a monopole and the source position can slightly shift to the upstream or downstream of the chamber.

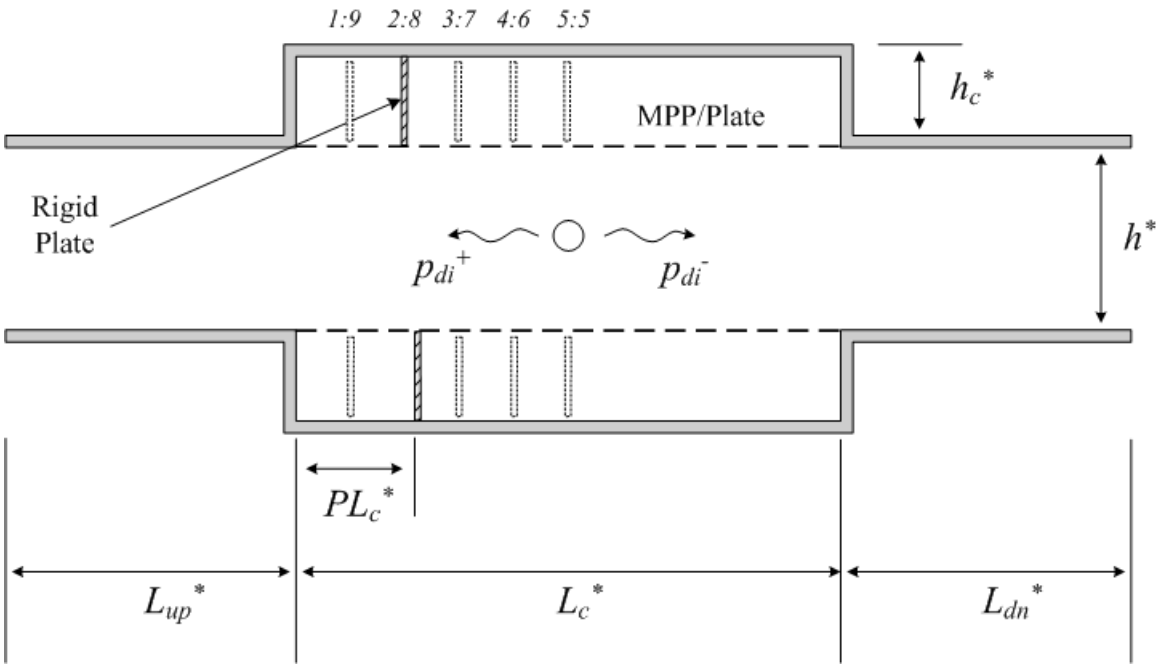

Figure 6.6: Schematic of MPP housing device with partition technique housing a dipole source

The numerical investigation results of the partitioned MPP housing device with the dipole sound source in the center are shown as Figure 6.7 (a). With sub-cavities

length ration of 1:9, the low frequency effective band will be widened as the upper limit around f=0.13 is pushed to f=0.15. However, the performance of medium frequency range [0.25 0.32] will deteriorate although the amplitude of *IL* will be increased above the frequency 0.32. With partition ratio of 2:8, the bandwidth of low frequency range is rather broad from 0.04 to 0.18, but the previous effective band existing in non-partitioned MPP housing device in which the *IL* is larger than 5 dB in the medium frequency is disappeared. When the partition ratio is further moved to 5:5, which is the center of the cavity, the sound attenuation performance in the low frequency is totally destroyed with only one effective band in the medium frequency from 0.2 to 0.46. This phenomenon indicates that the position of the partition plate is sensitive to the device performance when the source is with a dipole nature.

To further investigate the relationship between the dipole nature sound source and the position of the partition plate, the dipole sound source is slightly moved to the upstream (the distance of shifting is 10% of the cavity length, $0.1L_c$) as demonstrated in Figure 6.7 (b). The vertical dashed line represents that the cavity can be divided into two sections with ratio of 8:2 and the dipole source is located at the center of longer part as the shift distance is $0.1L_c$. The numerical results point out that only if the partition plate placed at the 8:2 position can obtain improvement of sound attenuation both in low frequency and medium frequency compared with the non-partitioned MPP housing device. From the Figure 6.7 (b), with an 8:2 position partition, the low frequency sound attenuation band is widened, as the upper limit is increased and the amplitude of *IL* in medium frequency is raised up with same bandwidth. If the partition plate is closer to the dipole source,

that is, at the position of 5:5, the low frequency performance is undermined again as the previous case of dipole source in the center with partition of 5:5.

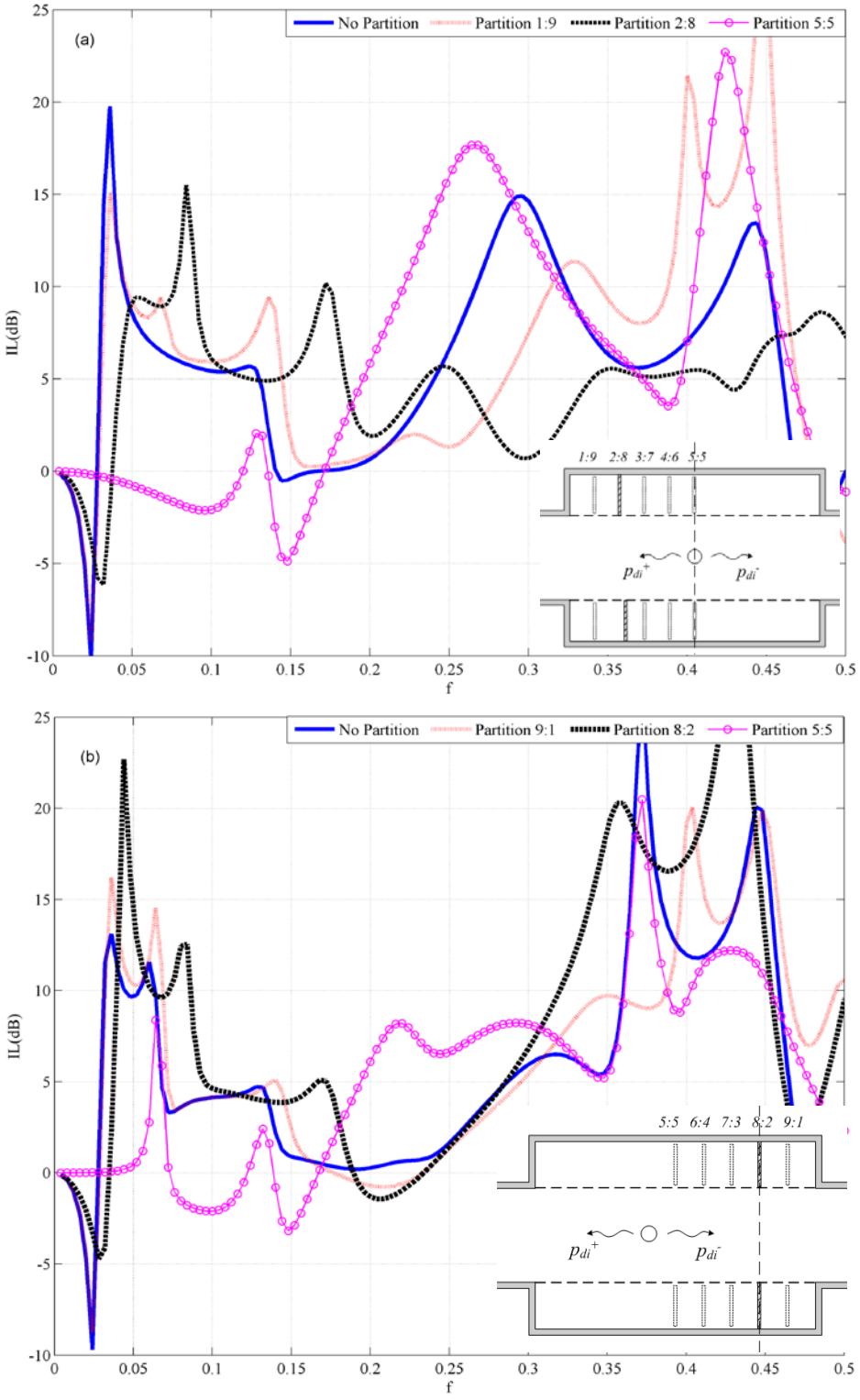

Figure 6.7: Cavity partition effect study when (a) the dipole source is at the chamber center and (b) the dipole source is not at the center

Experiments are also carried out with a loudspeaker in the center of MPP housing device to simulate the dipole sound source same as the strategy in Chapter 3. The experiment results are depicted in Figure 6.8. With a 1:9 partition shown as the dotted line and 2:8 partition in dashed line, the upper limit of 480 Hz is slightly shifted to higher frequency and the medium frequency performance will be weakened as the amplitude of *IL* will be lower. These two phenomena match well with the prediction trend. However, in the prediction with the partition of 1:9 and 2:8, the amplitude of sound attenuation of the device can be maintained with only change of bandwidth while there is a drop of *IL* existing in the low frequency range from 150 Hz to 400 Hz in the experiments. For the 5:5 partition case, the low frequency performance becomes worse while the medium frequency noise reduction behavior is improved same as the prediction.

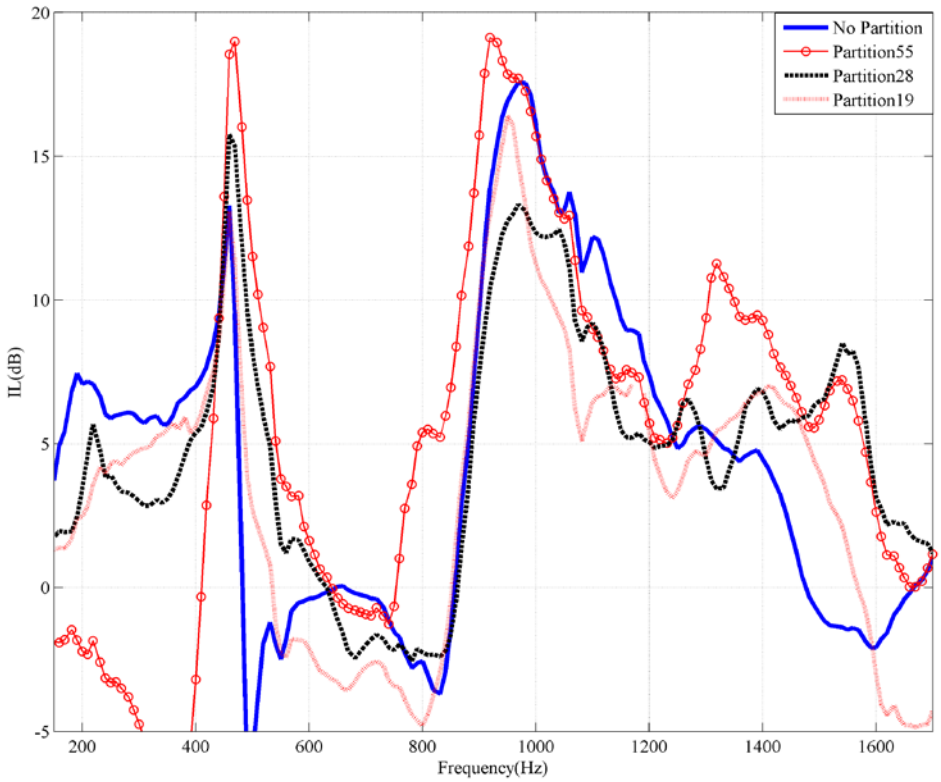

Figure 6.8: Experimental investigation of partition effect with dipole sound source at the center

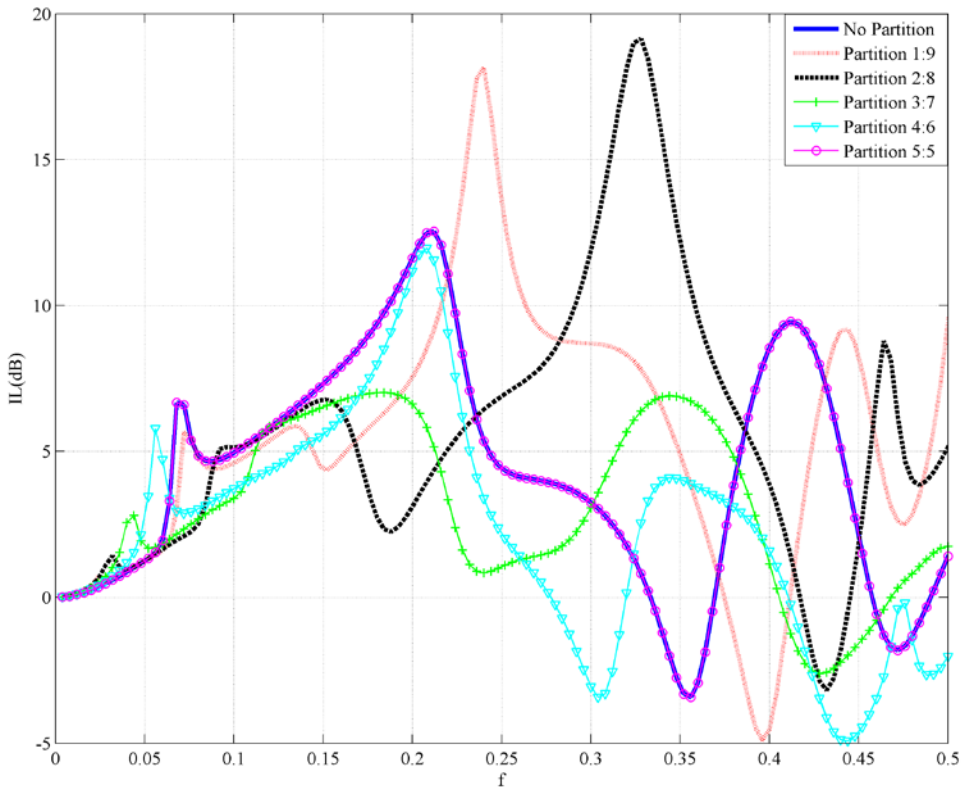

Figure 6.9: Cavity partition effect study of MPP housing device housing a monopole source at the center

When the sound source in the center is changed to a monopole, there is only one effective band from low to medium frequency shown as Figure 6.9 same as the study in Chapter 3. The cavity partition effect is investigated by inserting the rigid plate at different positions from 1:9 to 5:5. Generally speaking, by the application of partition, the *IL* performance can be improved in particular frequency region and partition at 1:9 reports the best outcome as the bandwidth is widest from 0.07 to 0.35 with little drop at f=0.15. Although the 2:8 partition case further extends the upper frequency to f=0.4, the trough point around f=0.19 decreases sharply and the lower limit has grown to f=0.09. The special point is that, when the partition plate is located at the center of cavity which is also the position of the source, the *IL* performance is actually the same as that of non-partitioned one shown as the solid

line and line with circles. It gives the warning that, in the monopole source case, it is useless to place the partition at the position of source when the source is at the center.

6.4 Conclusion

This part of study mainly focuses on the effect of cavity partition on the noise attenuation of the proposed MPP housing device when the nature of sound source is varied. In the incident wave excitation case, the application of partition will enhance the *TL* performance in the high frequency and broadband sound attenuation in both low and medium frequency can be achieved through proper tuning.

When the MPP housing device is used to control a dipole sound source and the source is located at the center, the inserting of partition plate will destroy the previous performance of proposed non-partitioned MPP housing device in high or low frequency depending on the position of plate. And if the plate is placed at exactly the position of source, the low frequency effective band disappears. When the source is slightly shifted from the center, the optimal position of partition plate is the demarcation point that in the segment of source side, the source is at the center of this special part. Thus, the role of the dipole source nature can be maximally maintained reporting both enhancement in the low and medium frequency of noise attenuation.

In the monopole source situation, the effect of partition is similar to the incident wave excitation case. Through the application of partition plate, the *IL* performance could be enhanced in certain frequency range and by proper tuning, a broad bandwidth can be achieved. However, the warning is that, due to the nature of monopole source, the placement of partition plate at the source position resulting equal length of two sub-cavities is no use, for the *IL* spectrum is the same as non-partitioned case.

Chapter 7 Conclusions and recommendations

7.1 Conclusions

The features and mechanism of sound sources inside the domestic product of ducted-fan such as hairdryer has been studied extensively. It involves the aerodynamics and structure vibration. Based on the noise source identification, the feasibility of developing a more effective silencing device with vibrating micro-perforated panel to control two different kinds of noise sources in the duct has been investigated with sound quality concerns, which is the dominant part of current study. The configuration of the device shares the feature of plate silencer or micro-perforated panel silencer but the working principle to reduce noise and its application are totally different. It is proved that such micro-perforated panel housing can mitigate the fan noise radiation in a duct with low aspect ratio effectively. The fan is considered as dipole source while the motor can be regarded as monopole source. The coupling among the dipole or monopole source, acoustic loading attributed to the backed cavity and the micro-perforated panel has been investigated. The performance of such housing device has been studied theoretically, numerically and experimentally. The physics behind having noise abatement has also been explored in detail, numerically and analytically.

In order to understand the characteristics of sound sources inside real product of ducted-fan system such as hairdryer, a series of experiments have been carried out

to identify the noise sources and investigate the corresponding sound field characteristics. Through the acoustic field measurement, the dominant noise is ranged from 750 Hz to 850 Hz that can be regarded as the low frequency region. By using the computational fluid dynamic (CFD) study, the maximum vortex is found to occur at the tip clearance region and the vacancy volume locating at the inlet side. They highly influence the velocity variation in each region of the duct. In order to change the strength of vortices and the acoustic pressure perturbations at the inlet of the hairdryer, different kinds of materials with different roughness properties have been tested. When 1 mm P60 type sandpaper with average particle diameter of 265 μm is treated on the inlet surface of the duct or some rubbers are used to fill the air gap at the inlet, the noise at low frequencies region at around 800 Hz is diminished. However, there is a trade-off enhancing of the noise level at blade passage frequency of 2200 Hz. The physics behind can be explained by the aerodynamics measurement. The particle image velocimetry (PIV) test results show that the rough surface can provide a more uniform inlet flow and noise at the low frequencies can be reduced. Concerning the noise at the range of first blade passage frequency of 2200 Hz, a noise control method is developed in the current studies.

A micro-perforated panel (MPP) housing device enclosing a dipole source in short duct with compact geometry is developed. The in-depth understanding of vibro-acoustic coupling between the vibrating MPP and the sound fields of a duct and backed cavities with a non-uniform dipole sound source excitation is implemented through the establishment of a theoretical model validated by finite element simulation in the first step. The noise abatement mechanism has been investigated

through the modal analysis, sound source radiation ability and sound intensity field study, and concluded that the panel vibration with the second and fourth modes dominate radiates sound waves to the duct interacting with the direct source radiation and such interference undergoes sound cancellation. Together with the absorption supplemented by the perforations, the optimal result can be obtained with configuration of L_c=3, H_c=0.5, B=0.0014, m=0.1, σ=2.7 and d^*=0.1 mm, and the sound suppression can achieve 70% in the desired low frequency range from f=0.03 to f=0.14 and medium frequency f=0.24 to f=0.485. When the source is changed to a monopole, the proposed MPP housing device can only work effectively in one frequency range from low to medium frequency f=0.06 to f=0.2.

The proposed 2D theoretical model of micro-perforated panel housing (MPP housing) device has also been validated by experiment and good agreement between the measured and predicted results has been achieved. The MPP housing device with a compact geometry of expansion ratio 2 can achieve larger than 5 dB insertion loss with wide frequency range at the low and medium frequency range to cover the first two BPF noises of ducted-fans with corresponding rotation speed. During the experimental validation, the white noise is generated by a small speaker which simulates a dipole sound source inside the duct. By using the proposed MPP housing, the loudness is signaficantly decreased, about 0.3 *sone* from 150 Hz to 500 Hz region as well as in the medium frequency from 700 Hz to 1400 Hz. The MPP housing device has been successfully applied on the hairdryer to control the BPF noise at 2200 Hz after the elimination of low frequency broadband unsteady inlet flow noise by rough surface at the inlet. The total sound pressure level can be lower about 2 dB with the MPP housing device geometry of length 90 mm, width 20 mm and cavity height 20 mm which satisfy the requirement of compact

geometry from the manufacturer. The loudness will be 10% lower from 800 Hz to 3000 Hz by the utilization of MPP housing device, covering the two dominant peak regions existing in loudness curve of hairdryer with smooth enclosure provided by Kenford Company. In addition, the sharpness of the product will also be lower, making the product sound not that annoying. The MPP housing device is designed to control the ducted-fan noise in limit space at or near the source position. The utilization on the hairdryer is successful but its usage is not limit to hairdryer. It can also be utilized to control the noise of hood in the kitchen, air-pump in the construction site, large-machineries like turbo-fan engine, and so on.

The proposed MPP housing device is further integrated with a non-uniform section hollow tube to enhance the sound attenuation performance at the passband region caused by the cavity length. Numerical model has been established and it is found that with rather narrow hollow segment of side width W = 0.15 and upper width H=0.1, optimal insertion loss performance can be achieved which maintains the performance of proposed MPP housing device and tackles the previous passband drawback existing in the MPP housing device output. The geometry of the hybrid MPPHQ housing device remains compact and the model has been validated through the experiment.

Finally, the cavity partition effect on the noise attenuation of MPP housing device has been examined numerically and experimentally with different nature of sound sources. The partition can enhance the *TL* performance in the high frequencies and widen the bandwidth when the partition is adjusted in an appropriate position. For the proposed MPP housing device controlling a dipole sound source, the performance of noise reduction will be deteriorated by using the partitioned cavity.

On the other hand, when the source is slightly shifted from the center of whole cavity but it is located at the centre of one of the segment, enhancement of noise attenuation in both the low and medium frequency can be obtained. In the monopole source case, the effect of partition is similar to the incident wave as the *IL* performance could be enhanced in certain frequency range. However, the warning is that, when the source is at the center of the chamber it is useless to partition the cavity exactly at the center.

7.2 Recommendations for future study

Briefly summarizing the main work of this thesis, the first part focuses on noise source identification of product of hairdryer with fan installed in the duct. And the other part focuses on the development of MPP housing device to control sound source radiation with sound quality improvement. The noise abatement mechanism has been deeply investigated and the MPP housing device has been successfully applied onto domestic product of hairdryer. And the performance of MPP housing device has been further improved by introducing a shallow hollow tube and partition in backing cavities. Based on the present study, future work can be carried out.

1. Through identification of noise sources, the unsteady inlet flow results in a low frequency broadband noise and can be eliminated by treating the surface of inlet duct surface by roughness. However, the relationship among the broadband noise and the speed of inlet flow, configuration of inlet, the roughness of the inlet surface is still not clear enough. Systematic experiments could be carried with more simple structure with flow passing through to investigate the detail mechanism of the

unsteady inlet flow noise generation and to give instructions to the control of such flow-induced noise.

2. In the study of cavity partition effect investigation of MPP housing device, only the numerical model has been established and there is strong coupling observed near the rigid partition plate. The physics behind is not that distinct especially for the dipole and monopole source in the center. Thus it is necessary to build a mathematical model to investigate the near field coupling and help the deep understanding of causes of weaken or enhance effect when the partition is located at different positions.

3. To investigate the cavity partition effect on the MPP housing device with variation of the nature of source, only one rigid partition plate is utilized in the current study. It is found that the sound attenuation performance of the MPP housing device can be enhanced by proper tuning location of the partition with incident wave and monopole sound source. In the dipole source situation, the attenuation performance can also be enhanced when the source is located at the centre of one segment, which is one segment of the partitioned cavity. However, it is necessary to study the effect of multi-partitioned cavity with different nature of sound sources. It is expected that, through proper internal configuration, the MPP housing device can contribute broadband sound attenuation, especially for the dipole sound source, for the noise attenuation mechanism is totally different from the impedance discontinuity or multiple cavity resonance mechanism.

References

Abrego, A.I. and Bulaga, R.W. (2002). "Performance Study of a Ducted Fan System," *American Helicopter Society Aerodynamics, Acoustics, and Test and Evaluation Technical Specialists Meeting*, San Francisco, CA.

Allam, S. and Abom, M. (2011). "A new type of muffler based on micro perforated tubes,"*Journal of Vibration and Acoustics*, **133**(3), 031005.

Allard, J.I. (1993). *Propagation of Sound in Porous Media Modelling Sound Absorption Material*, Elsevier Applied Science, England.

Asdrubali, F. and Pispola, G. (2007). "Properties of transparent sound-absorbing panels for use in noise barriers," *the Journal of the Acoustical Society of America*, **121**, 214–221.

Atig,M., Dalmont,J.P. and Gilbert,J.(2004). "Termination impedance of open ended cylindrical tubes at high sound pressure level," *C. R. Acad. Sci. Paris, Series II*, 299-304.

Bolt, R.H. (1947). "On the design of perforated facings for acoustic materials," *the Journal of the Acoustical Society of America*, **19**(5), 917-921.

Bravo, T., Maury, C. and Pinhede, C. (2013). "Enhancing sound absorption and transmission through flexible multi-layer micro-perforated structures," *Journal of the Acoustical Society of America*, **134**, 3663–3673.

Brown, S. (1964). "Acoustic design of broadcasting studios," *Journal of Sound and Vibration*, **1**, 239-257.

Chanaud, R.C. (1994). "Effects of geometry on the resonance frequency of Helmholtz resonators,"*Journal of Sound and Vibration*, **178**(3), 337–348.

Chanaud, R.C. (1997). "Effects of geometry on the resonance frequency of Helmholtz resonators, part II,"*Journal of Sound and Vibration*, **204**(5), 829–834.

Chen, K., Paurobally, R., Pan, J. and Qiu, X.J. (2015). "Improving active control of fan noise with automatic spectral reshaping for reference signal," *Applied Acoustics*, **87**, 142-152.

Cheng, L., Li, Y.Y. and Gao, J.X. (2005). "Energy transmission in a mechanically-linked double-wall structure coupled to an acoustic enclosure," *the Journal of the Acoustical Society of America*, **117**(5), 2742–2751.

Chiu, M.C. and Chang, Y.C. (2008). "Numerical studies on venting system with multi-chamber perforated mufflers by GA optimization," *Applied Acoustics*, **69**(11), 1017–1037.

Choy, Y.S. and Huang, L. (2002). "Experimental studies of a drum-like silencer," *the Journal of the Acoustical Society of America*, **112**, 2026-2035.

Choy, Y.S. and Huang, L. (2003). "Drum silencer with shallow cavity filled with helium," *the Journal of the Acoustical Society of America*, **114**, 1477-1486.

Choy, Y.S. and Huang, L. (2005). "Effect of mean flow on the drum-like silencer," *the Journal of the Acoustical Society of America*, **118**, 3077-3085.

Choy, Y.S., Liu, Y., Cheung, H.Y., Xi, Q. and Lau, K.T. (2012). "Development of composite plate for compact silencer design," *Journal of Sound and Vibration*, **331,** 2348-2364.

Dickey, N.S., Selamet, A. and Novak, J.M. (1998). "Multi-pass perforated tube silencers: A computational approach," *Journal of Sound and Vibration*, **211**(3), 435–447.

Doak, P.E. (1973). "Excitation, transmission and radiation of sound from source distributions in hard-walled ducts of finite length (I): The effects of duct cross-section geometry and source distribution space-time pattern,"*Journal of sound and vibration*, **31**, 1–72.

Doolan, C.J. (2008). "A Review of Airfoil Trailing Edge Noise and Its Prediction," *Acoustics Australia*, **36**, 1-7.

Drotleff, H. and Zhou, X. (2001). "Attractive room acoustic design for multi-purpose halls," *Acta Acustica united with Acustica*, **87**, 500-504.

Fastl, H. and Zwicker, E. (2007). *Psychoacoustics, Facts and Models*. Springer, Berlin, New York.

Ffowcs Williams, J.E. and Hall, L.H. (1970). "Aerodynamic sound generation by turbulent flow in the vicinity of a scattering half-plane," *Journal of Fluid Mechanics*, **40**, 657-670.

Ford, R.D. and Mccormick, M.A. (1969). "Panel sound absorbers," *Journal of Sound and Vibration*, **10**, 411-423.

Fuchs, H.V. and Zha, X. (1997). "Acrylic-glass sound absorbers in the plenum of the Deutscher Bundestag," *Applied Acoustics*, **51**(2), 211–217.

Fuchs, H.V. and Zha, X. (2006). "Micro-perforated structures as sound absorbers – a review and outlook," *Acta Acustica United with Acustica*, **92**, 139–146.

Gerhold, C.H. (1997). "Active control of fan-generated tone noise," *AIAA Journal*, **35** (1), 17-22.

Guo, Y., Allam, S. and Abom, M. (2008). "Micro-perforated plate for vehicle applications," *Proceedings of the 2008 Congress and exposition of noise control engineering*, Inter-Noise 2008, Shanghai, China.

Gutin, L. (1936). "On the sound field of a rotating propeller," *National Advisory Committee for Aeronautics*, Technical Memorandum 1195**,** 899-909.

Hansen, C.H. (1997). "Active noise control - from laboratory to industrial implementation," *Proceedings of Noise-Con 97*, Pennsylvania State University.

Hansen, C.H. (2004). "Current and future industrial applications of active noise control," *Proceedings of the Active 04*, Virginia, USA.

Herschel, J.F.W. (1833). "On the absorption of light by coloured media, viewed in connexion with the undulatory theory," *Philosophical Magazine and Journal of Science*, **3**, 401-412.

Horoshenkov, K.V. and Sakagami, K. (1998). "Acoustic response of a thin poroelastic plate," *in Proceedings of the 16th International Congress on Acoustics*, Seattle.

Horoshenkov, K.V. and Sakagami, K. (2001). "A method to calculate the acoustic response of a thin, baffled, simply supported poroelastic plate," *the Journal of the Acoustical Society of America*, **110**, 904-917.

Howe, M.S. (1978). "A review of the theory of trailing edge noise," *Journal of Sound and Vibration*, **61**, 437–465.

Huang, L. (1999). "A theory of passive duct noise control by flexible panels," *the Journal of the Acoustical Society of America*, **106**, 1801-1809.

Huang, L. (2002). "Modal analysis of a drumlike silencer," *the Journal of the Acoustical Society of America*, **112**, 2014–2025.

Huang, L. (2004). "Parametric studies of a drum-like silencer," *Journal of Sound and Vibration*, **269,** 467-488.

Huang, L. (2006). "Broadband sound reflection by plates covering side-branch cavities in a duct," *the Journal of the Acoustical Society of America*, **119**, 2628-2638.

Huang, L. and Choy, Y.S. (2005). "Vibroacoustics of three-dimensional drum silencer," *the Journal of the Acoustical Society of America*, **118**, 2313-2320.

Huang, L., Ma, X. and Feng, L.G. (2010). "Suppression of broadband noise radiated by a low-speed fan in a duct," *the Journal of the Acoustical Society of America*, **128**, 152-163.

Ih, J.G. and Lee, B.H. (1985). "Analysis of higher-order mode effects in the circular expansion chamber with mean flow," *the Journal of the Acoustical Society of America*, **77**, 1377–1388.

Ingard, K.U. (1994). *Note on Sound Absorption Technology*, Noise Control Foundation, USA.

Ingard, U. (1953). "On the theory and design of acoustic resonators," *the Journal of the Acoustical Society of America*, **25**, 1037–1061.

ISO 226 (2003). "Acoustics—Normal Equal-Loudness Level Contours, " International Organization for Standardization: Geneva, Switzerland.

ISO 532 (1975). "Method for calculating loudness level," International Organization for Standardization: Geneva, Switzerland.

Ji, Z.L. (2010). "Boundary element acoustic analysis of hybrid expansion chamber silencers with perforated facing," *Engineering Analysis with Boundary Elements*, **34**(7), 690-696.

Jing, X.D., Wang, X.Y. and Sun, X.F. (2007). "Broadband Acoustic Liner Based on the Mechanism of Multiple Cavity Resonance," *AIAA Journal*, **45**(10), 2429–2437.

Kang, J. and Fuchs, H.V. (1999). "Predicting the absorption of open weave textiles and micro-perforated membranes backed by an air space," *Journal of Sound and Vibration*, **220**(5), 905–920.

Karstadt, S., Hess, M., Matyschok, B. and Pelz, P.F. (2010). "The Influence of Tip Clearance on the Acoustic and Aerodynamic Characteristics of Fans," *Proceedings of ASME Turbo Expo 2010: Axial Flow Fan and Compressor Aerodynamics Design methods, and CFD Modeling for Turbo-machinery*, Glasgow, UK.

Kim, H.S., Hong, J.S. and Oh, J.E. (1998). "Active noise control with active muffler in automotive exhaust systems," *Noise Control Engineering Journal*, **41**(2), 178-183.

Kostek, T.M. and Franchek, M.A. (2000). "Hybrid Noise Control in Ducts," *Journal of Sound and Vibration*, **237**(1), 81-100.

Lee, D.H. and Kwon, Y.P. (2004). "Estimation of the absorption performance of multiple layer perforated panel systems by transfer matrix method," *Journal of Sound and Vibration*, **278**, 847-860.

Lee, F.C. and Chen, W.H. (2001). "Acoustic transmission analysis of multi-layer absorbers," *Journal of Sound and Vibration*, **248**(4), 621–634.

Li, D., Cheng, L., Yu, G.H. and Vipperman, J.S. (2007). "Noise control in enclosures: Modeling and experiments with T-shaped acoustic resonators," *the Journal of the Acoustical Society of America*, **122**(7), 2615-2625.

Li, G. and Mechefske, C.K. (2010). "A comprehensive experimental study of micro-perforated panel acoustic absorbers in MRI scanners," *Magnetic Resonance Materials in Physics, Biology and Medicine*, **23**, 177–185.

Liu, Y., Choy, Y.S., Huang, L. and Cheng, L. (2012). "Noise suppression of a dipole source by tensioned membrane with side-branch cavities," *the Journal of the Acoustic Society of America*, **132**(3**)**, 1392–1402.

Longhouse, R. E. (1976). "Noise mechanism separation and design considerations for low tip-speed, axial-flow fans," *Journal of Sound and Vibration*, **48**, 461-474.

Lu, Z.B., Jing, X.D., Sun, X.F. and Dai, X.W. (2014). "An investigation on the characteristics of a non-locally reacting acoustic liner," *Journal of Vibration and Control*.

Lueg, P. (1938). United States patent 2,043,416.

Maa, D.Y. (1975). "Theory and design of microperforated panel sound absorbing construction (in Chinese)," *Scientia Sinica*, **18,** 55–71.

Maa, D.Y. (1987). "Micorperforated Panel wide-band absorbers," *Noise Control Engineering Journal*, **29,** 77–84.

Maa, D.Y. (1998). "Potential of microperforated panel absorber," *the Journal of the Acoustical Society of America*, **104**, 2861–2866.

MacGillivray, J.R., Lauchle, G.C. and Swanson, D.C. (1995). "Active control of axial flow fan noise," *the Journal of the Acoustical Society of America*, **98**, 2885.

Mani, R. (1976). "Acoustic Duct with Peripherally Segmented Acoustic Treatment," United States patent 3,937,590.

Mechel, F.P., and Ver, I.L. (1992). *Noise and Vibration Control Engineering: Principles and Applications*, Wiley, New York, Chapter 8.

Munjal, M.L. (1987). *Acoustics of ducts and mufflers with application to exhaust ventilation system design*, Wiley, New York.

Munjal, M.L. (2014). *Acoustics of Ducts and Mufflers*, John Wiley and Sons, UK.

Nauhaus, L., Schulz, J., Neise, W., and Moser, M. (2003). "Active control of the aerodynamic performance and tonal noise of axial trubomachines," *Proceedings of the Institution of Mechanical Engineers Part A: Journal of Power and Energy*, **217**(4), 375-383.

Park, S.H. (2013). "A design method of micro-perforated panel absorber at high sound pressure environment in launcher fairings," *Journal of Sound and Vibration*, **332**, 521–535.

Quincke, G. (1866). "Ueber interferenzapparate fur schallwellen," *Annalen der Physik und Chemie*, **128**, 177-192.

Quinlan, D.A. (1992). "Application of active control to axial flow fans," *Noise Control Engineering Journal*, **39**, 95-101.

Rayleigh, J.W.S. (1945). *The Theory of Sound*, Dover, New York.

Rodarte, E. and Miller, N.R. (2001). *Flow Induced Noise in Heat Exchangers*, University of Illinois, Champaign.

Russell, D.A., Junell, J. and Ludwigsen, D.O. (2013). "Vector acoustic intensity around a tuning fork," *American Journal of Physics*, **81**(2), 99-103.

Sakagami, K., Kiyama, M., Morimoto, M. and Takahashi, D. (1996). "Sound absorption of a cavity-backed membrane: a step towards design method for membrane-type absorbers," *Applied Acoustics*, **49**, 237-247.

Sakagami, K., Morimoto, M. and Koike, W. (2006). "A numerical study of double-leaf micro-perforated panel absorbers," *Applied Acoustics*, **67**(7), 609-619.

Sakagami, K., Nakamori, T., Morimoto, M. and Yairi, M. (2009). "Double-leaf micro-perforated panel space absorber: A revised theory and detailed analysis," *Applied Acoustics*, **70**(5), 703–709.

Squicciarini, G., Thompson, D.J. and Corradi, R. (2014). "The effect of different combinations of boundary conditions on the average radiation efficiency of rectangular plates," *Journal of Sound and Vibration*, **333**(17), 3931–3948.

Stewart, G.W. (1928). "The theory of the Herschel-Quincke tube," *Physical Review*, **31**,
696-698.

Selamet, A., Dickey, N.S. and Novak, J.M. (1994). "The Hershcel-Quincke tube: a theoretical, computational, and experimental investigation," *the Journal of the Acoustical Society of America*, **96**(5), 3177-3185.

Selamet, A. and Ji, Z.L. (1999). "Acoustic attenuation performance of circular expansion chambers with extended inlet/outlet," *Journal of Sound and Vibration*, **223**(2), 197–212.

Selamet, A. and Lee, I. (2003). "Helmholtz resonator with extended neck," *the Journal of the Acoustical Society of America*, **113**(4), 1975–1985.

Selamet, A. and Radavich, P.M. (1997). "The effect of length on the acoustic attenuation performance of concentric chambers: an analytical, numerical and experimental investigation," *Journal of Sound and Vibration*, **201**(4), 407–426.

Selamet, A., Xu, M.B., Lee, I.-J. and Huff, N.T. (2005). "Helmholtz resonator lined with absorbing material," *the Journal of the Acoustical Society of America*, **117**, 725–733.

Seo, S.H. and Kim, Y.H. (2005). "Silence design by using array resonators for low frequency band noise reduction," *the Journal of the Acoustical Society of America*, **118**(4), 2332–2338.

Takahashi, D., Sakagami, K. and Morimoto, M. (1996). "Acoustic properties of permeable membranes," *the Journal of the Acoustical Society of America*, **99**(5), 3003–3009.

Takahashi, D. and Tanaka, M. (2002). "Flexural vibration of perforated plated and porous elastic materials under acoustic loading," *the Journal of the Acoustical Society of America*, **112**(4), 1456–1464.

Tang, S.K. (2005). "On Helmholtz resonators with tapered necks," *Journal of Sound and Vibration*, **279**, 1085–1096.

Tang, S.K., Ng, C.H. and lam, E.Y.L. (2012). "Experimental investigation of the sound absorption performance of compartmented Helmholtz resonators," *Applied Acoustics*, **73**, 969–976.

Trunzo, R., Lakshminarayana, B. and Thompson, D.E. (1981). "Nature of inlet turbulence and strut flow disturbances and their effect on turbomachinery rotor noise," *Journal of Sound and Vibration*, **76**(2), 233-259.

Tyler, J.M. and Sofrin, T.G. (1962). "Axial flow compressor noise studies," *SAE Transactions*, **70**, 309-332.

von Bismarck, G. (1974). "Sharpness as an attribute of the timbre of steady sounds, " *Acta Acustica united with Acustica*, **30**, 159–172.

Wang, C.Q., Cheng, L. and Huang, L. (2008)."Realization of a broadband low-frequency plate silencer using sandwich plates," *Journal of Sound and Vibration*, **318**, 792-808.

Wang, C.Q., Cheng, L., Pan, J. and Yu, G.H. (2010). "Sound absorption of a micro-perforated panel backed by an irregular-shaped cavity," *the Journal of the Acoustical Society of America*, **127**(1), 238–246.

Wang, C.Q., Han J. and Huang, L. (2007). "Optimization of a clamped plate silencer," *the Journal of the Acoustical Society of America*, **121**(2), 949-960.

Wang, C.Q., and Huang, L. (2008). "Analysis of absorption and reflection mechanisms in a three-dimensional plate silencer," the *Journal of the Acoustical Society of America*, **313**, 510-524.

Wang, C.Q., and Huang, L. (2011). "On the acoustic properties of parallel arrangement of multiple micro-perforated panel absorbers with different cavity depths," *the Journal of the Acoustical Society of America*, **130**(1), 208–218.

Wang, C.Q., Huang, L. and Zhang, Y.M. (2014). "Oblique incidence sound absorption of parallel arrangement of multiple micro-perforated panel absorbers in a periodic pattern," *Journal of Sound and Vibration*, **333**(25), 6828–6842.

Wang, J. and Huang, L. (2006). "Active control of drag noise from a small axial flow fan," *the Journal of the Acoustical Society of America,* **120** (1), 192-203.

Wang, X.N., Choy, Y.S. and Cheng, L. (2012). "Hybrid noise control in a duct using a light micro-perforated plate," *the Journal of the Acoustical Society of America*, **132**(6), 3778–3787.

Watson, W.R., Robinson, J.H., Jones, M.G. and Parrott, T.L. (2004). Computational study of optimum and off-design performance of checkerboard liners," *Proceeding of the 10th AIAA/CEAS Aeroacoustics Conference & Exhibit*, AIAA Paper, 2004- 3030

Wong, Y.J., Paurobally, R. and Pan, J. (2003). "Hybrid active and passive control of fan noise," *Applied Acoustics*, **64**, 885-901.

Wu, C.J., Wang, X.J. and Tang, H.B. (2008). "Transmission loss prediction on a single-inlet/double-outlet cylindrical expansion-chamber muffler by using the modal meshing approach," *Applied Acoustics*, **69**(2), 173-178.

Wu, M.Q. (1997). "Micro-perforated panels for duct silencing," *Noise Control Engineering Journal*, **45**, 69–77.

Xu, M.B., Selamet, A. and Kim, H. (2010). "Dual Helmholtz resonator," *Applied Acoustics*, **71**, 822–829.

Yu, X. and Cheng, L. (2015). "Duct noise attenuation using reactive silencer with various internal configurations," *Journal of Sound and Vibration*, **335**, 229-244.

Zhang, Z.M. and Gu, X.T. (1998). "The theoretical and application study on a double layer microperforated sound absorption structure," *Journal of Sound and Vibration*, **215**(3), 399-405.